MECHANOBIOLOGY OF THE AORTIC VALVE INTERSTITIAL CELL

by

William David Merryman, II

Bachelor of Science, Engineering Science, University of Tennessee, 2001

Master of Science, Engineering Science, University of Tennessee, 2002

Submitted to the Graduate Faculty of
School of Engineering in partial fulfillment
of the requirements for the degree of
Doctor of Philosophy

University of Pittsburgh

2007

UNIVERSITY OF PITTSBURGH

SCHOOL OF ENGINEERING

This dissertation was presented

by

William David Merryman, II

It was defended on

June 13, 2007

and approved by

Hai Lin, Assistant Professor, Department of Bioengineering

Philip Leduc, Assistant Professor, Department of Mechanical Engineering,
Carnegie Mellon University

Sanjeev G. Shroff, Professor, Department of Bioengineering

Frederick J. Schoen, Professor, Department of Pathology, Harvard Medical School

Michael S. Sacks, Professor, Department of Bioengineering
Dissertation Director

MECHANOBIOLOGY OF THE AORTIC VALVE INTERSTITIAL CELL

William David Merryman, II, PhD

University of Pittsburgh, 2007

The aortic valve (AV) is essentially a passive organ that permits unidirectional blood flow from the left ventricle to the systemic circulation and prohibits regurgitant flow during diastole. The extracellular matrix (ECM) of the AV leaflet is tri-layered with type I collagen making up the fibrosa layer (aortic side), glycosaminoglycans constituting the middle spongiosa layer, and elastin fibers largely in the ventricularis layer. Each component of the ECM is synthesized, enzymatically degraded, and maintained by the resident population of interstitial cells (AVICs) dispersed throughout the leaflet. The AVICs have been recognized as a heterogeneous mix of cells which include fibroblasts, smooth muscle cells, and myofibroblasts, which have characteristics of both fibroblasts and smooth muscle cells but are unique from each.

The hypothesis of this dissertation is that the phenotype and function of the AVIC is predicated on the mechanical environment in which it resides, and during times of activated remodeling (increased myofibroblasts), the mechanobiological response of the AVIC may be contributor to changes in valvular tissue integrity. To test this hypothesis, we examine 1) the mechanical properties of the AVIC and the correlation to biosynthesis, 2) the strong connectivity of the AVIC to the ECM which is demonstrated by the AVICs ability to generate tissue-level forces due to contraction, 3) potential tissue remodeling capabilities of the AVIC via collagen gel contraction, 4) the micromechanics of the AVIC to increasing strain levels, and 5) synergistic response of the *in situ* AVIC to TGF-β1 and cyclic strain.

Results from this work highlight the mechanobiological properties of the AVIC myofibroblast phenotype and its role in valvular tissue homeostasis, remodeling, and dysfunction. Moreover, these results demonstrate the unexamined mechanical properties of the AVIC and the strong correlate with ECM biosynthesis. As the AVIC is situated in a tissue with large strains and varying modes of deformation, the mechanical properties of the cell are likely prominent in their function. We believe that these results will add to the growing body of AVIC literature and further believe that our focus on the AVIC micro-mechanical environment will be very relevant to understanding the mechanobiologic function of the AVIC.

TABLE OF CONTENTS

LIST OF TABLES

LIST OF FIGURES

PREFACE

I would like to thank the Department of Bioengineering at the University of Pittsburgh and the wonderful leadership by its chair, Dr. Harvey S. Borovetz. I would like to thank the fruitful and enjoyable collaborations that have guided much of the work within this Dissertation. Particularly, I would like to thank Drs. Farshid Guilak, Frederick J. Schoen, and Richard A. Hopkins. Additionally, I would like to thank the members of this Dissertation committee for their comments and contributions to this work. I thank Howard Lukoff for the countless ELISAs he preformed for this work. Finally, I would like to thank Dr. Michael S. Sacks for the opportunity to work in a fast-paced, academic research environment and additionally for his guidance and mentoring during the past four and half years.

I would like to thank my lab mates for the friendships that have been forged during the grueling task that is the completion of a PhD. I have enjoyed all our conversations and laughs over the years and wish you all success in future endeavors, be they academic or otherwise. In no particular order, and just so they can say they were mentioned here, I would like to thank Jon Grashow, George Engelmayr, David Schmidt, Todd Courtney, Becca Long, and John Stella.

There are two quotations below that I have always loved and thought very wise. After finishing this degree, I can now say that I see their wisdom in a whole new light.

"We shall not cease from exploration,
and the end of all our exploring
will be to arrive where we started
and know the place for the first time."
-T. S. Eliot

"Education without values,
as useful as it is,
seems rather to make man a more clever devil."
-C. S. Lewis

Lastly, and by far, most importantly, I thank and love with all that I am, my wife, Erin, and my daughter, Quinn. I thank you for all the support that you have given me during the completion of this degree. Know that every minute that I spent working on this was for *our* family and future, and that during each and every minute I was thinking of you. In every sense that I can mean it, this is *our* PhD. Thank you both…for everything.

ACRONYMS

HV	heart valve
VIC	valve interstitial cell
AV	aortic valve
AVIC	aortic valve interstitial cell
MV	mitral valve
MVIC	mitral valve interstitial cell
PV	pulmonary valve
PVIC	pulmonary valve interstitial cell
TV	tricuspid valve
TVIC	tricuspid valve interstitial cell
TVP	transvalvular pressure
VEC	valvular endothelial cell
CSK	cytoskeleton
SMA	α-smooth muscle actin
Hsp47	heat shock protein 47
CICP	type I collagen c-terminal propeptide
TGF-β1	transforming growth factor β1
WC	with curvature

AC	against curvature
SALS	small angle light scattering
DMEM	Dulbecco’s modified eagle medium
FBS	fetal bovine serum
ECM	extracellular matrix
AFM	atomic force microscopy
SLS	standard linear solid
TEM	transmission electron microscopy
ANOVA	analysis of variation
KCl	potassium chloride
ELISA	enzyme-linked immunosorbent assay

1.0 INTRODUCTION

1.1 THE MAMMALIAN HEART AND HEART VALVES

Mammalian hearts are composed of four chambers which fill alternately to deliver blood to both the lungs for oxygenation and the systemic circulation and organs for metabolic nutrition and exchange (**Figure 1**). In the normal cardiac cycle, oxygen depleted blood returns to the right side of the heart and is pumped to the lungs for carbon dioxide-oxygen exchange. From there, the now oxygen-rich blood is returned to the left side of the heart in order to be pumped to the systemic circulation. Each side of the heart employs a dual-chamber pumping mechanism which is necessary to allow the chambers of the heart to fill while not pumping blood during the cardiac cycle. These chambers are called the atrium and the ventricle. The atrium delivers blood to the ventricle, which in turn delivers blood to either the lungs or systemic circulation.

In the most general terms, heart valves (HVs) are thin, planar membranes that are positioned in the mammalian heart such that blood flow progresses in the forward direction only. They are necessary for the heart to function properly as a pump with chambers that fill alternately. Mammalian hearts have four HVs: tricuspid valve (TV); pulmonary valve (PV); mitral valve (MV); and aortic valve (AV) (**Figure 2**). The TV and MV are termed atrioventricular valves as they lie between the atrium and ventricle on both the right and left sides of the heart, respectively. The PV and AV are termed semilunar valves, due to the halfmoon shape of their leaflets or cusps, and lie between the ventricle and the great vessel from which their name derives.

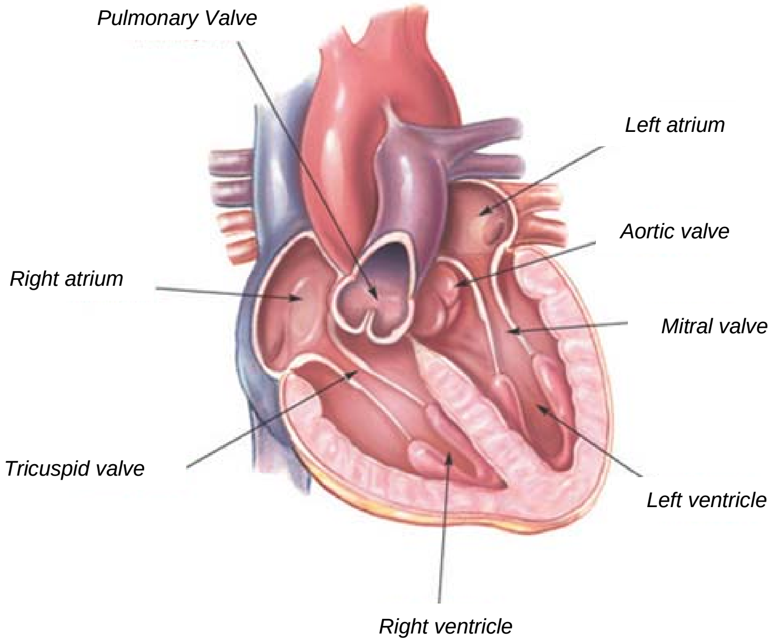

Figure 1. Anatomy of the mammalian heart (**www.edwards.com**).

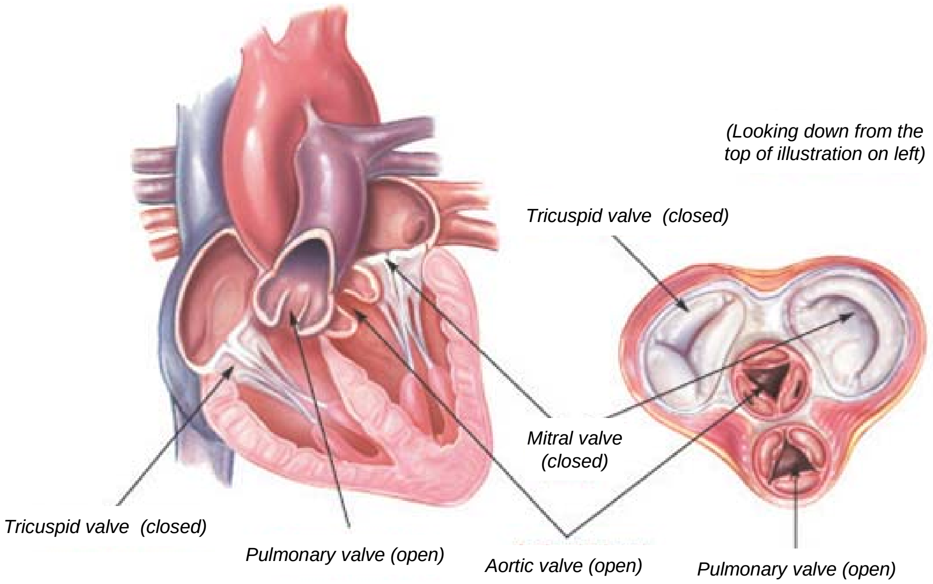

Figure 2. Location of the four heart valves (**www.edwards.com**).

HVs are essentially passive mechanical structures that are driven to open and close by the inertial forces from the surrounding blood during the two functional heart cycles (**Figure 3**). During diastole, when the right and left ventricles are filling, the TV and the MV are open to allow blood to pass from the atriums into the ventricles. To keep pressure in the ventricles low enough to allow low pressure filling from the atriums, the PV and AV are closed during diastole. Once the ventricles are full, they contract opening the semilunar valves (AV and PV), ejecting the blood into the great vessels. To prevent retrograde blood flow into the atriums, the MV and TV close during systole. This two-cycle mechanism is essential for two reasons: 1) it allows the heart generate contractile forces sufficient to propel the blood to both the lungs and the systemic circulation; 2) it allows the myocardial muscle tissue of the heart to receive the necessary metabolic nutrients it needs during diastole.

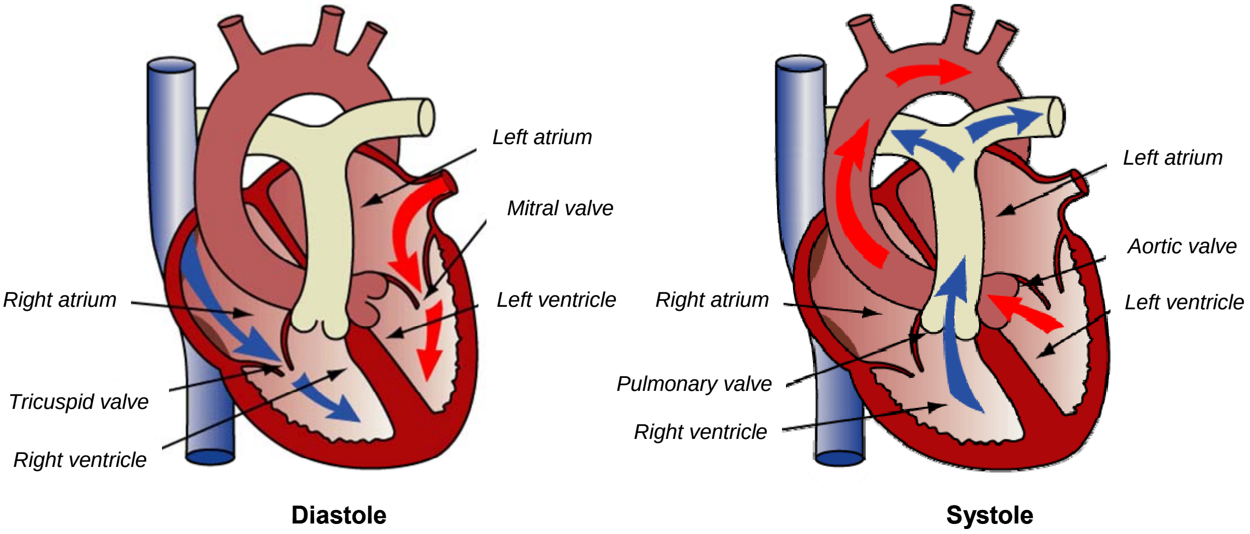

Figure 3. Two stages of heart function: diastole and systole (www.sjm.com/resources).

1.2 HEART VALVE PHYSIOLOGY AND TISSUE LEVEL BIOMECHANICS

1.2.1 Heart Valve Hemodynamics

The mechanisms ensuring the proper function of the heart valves are essentially controlled by the surrounding hemodynamic environment. Understanding the interactions between the heart valves and their dynamic fluid environment is thus critical to better understand normal valve function and disease progression. Although the four heart valves present different anatomies, and different opening/closing characteristics, they all function to allow the unidirectional flow of blood while maximizing flow rate and minimizing resistance to flow. Thus, in the following, AV hemodynamics are focused on as an example for all the heart valves.

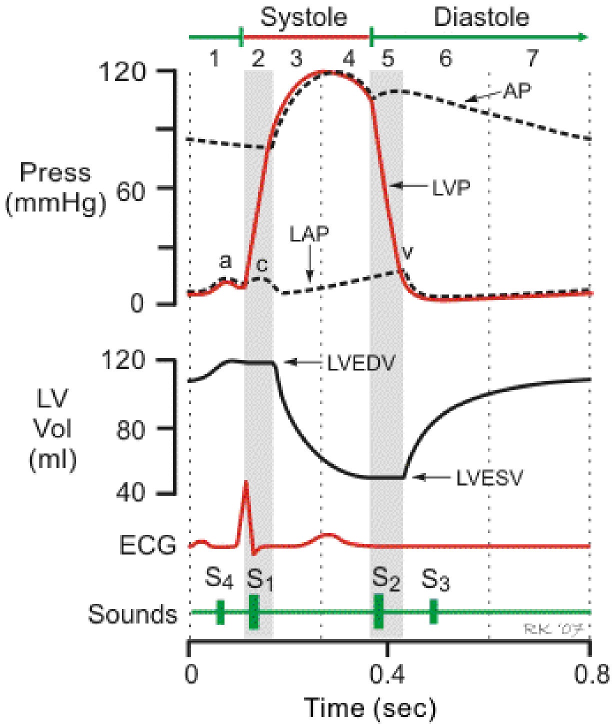

Figure 4. Diagram of the normal cardiac cycle. During systole, aortic pressure (AP) rises with the opening of the AV due to increased pressure in the left ventricle (LVP). During systole, the AV closes and AP is approximately 90-100 mmHg, which is imposed on the closed AV during this portion of the cardiac cycle. (www.cyphysiology.com.)

The AV opens during systole when the ventricle is contracting and then closes during diastole as the ventricle relaxes (**Figure 4**). In healthy individuals, blood flows through the AV accelerating to a peak value of 1.35 ± 0.35 m/s [1]. The valve closes near the end of the deceleration phase of systole with very little reverse flow through the valve. The axial pressure difference causes the low inertia flow in the developing boundary layer along the aortic wall to decelerate then to reverse direction resulting in vortices in the sinuses behind the aortic valve leaflets [2]. This action forces the belly of the leaflets away from the aortic wall and toward the closed position. When this force is coupled with the vortices that push the leaflet tips toward the closed position, a very efficient and fast closure is obtained. *In vitro* studies have shown that the axial pressure difference alone is sufficient to close the valve [2]. Thus, without the vortices in the sinuses, the valve still closes, but its closure is not as efficient as when the vortices are present.

The velocity profile at the level of the AV annulus is relatively flat. However there is a slight skew towards the septal wall (less than 10% of the center-line velocity) caused by the orientation of the AV relative to the long axis of the left ventricle [3]. The flow patterns just downstream of the AV are of particular interest because of their complexity and relationship to arterial disease. Highly skewed velocity profiles and corresponding helical flow patterns have been observed in the human aortic arch using magnetic resonance phase velocity mapping [3].

A complex CFD model was recently developed to simulate the flow through a trileaflet semi-lunar heart valve by Ajit Yoganathan's research group at the Georgia Institute of Technology. The kinematics of the valve was prescribed and the unsteady flow solution was computed for the case of a peak systole Reynolds number of 3000 (**Figure 5**). The accelerating flow phase is dominated by the instability of the shear layers emanating from the leaflets, which gives rise to complex vortex shedding. The flow predictions provide evidence of the drastic difference between the hemodynamic stresses experienced by the aortic and ventricular sides.

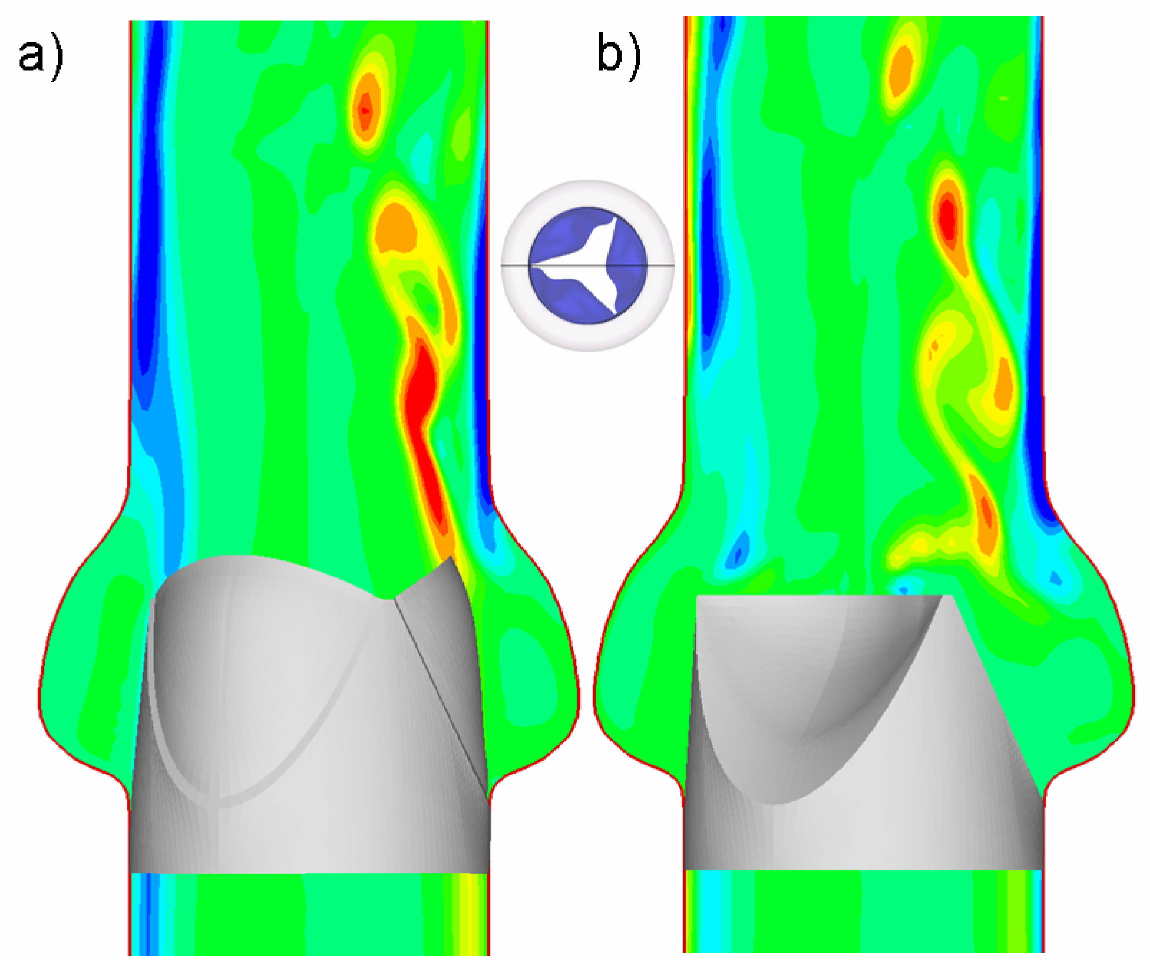

Figure 5. Numerical simulation of unsteady, pulsatile flow in a trileaflet prosthetic heart valve. Contours of the out-of-plane vorticity are shown at two instants during the cardiac cycle: a) fully open phase; and b) closing phase.

The limiting streamlines (i.e., lines tangent to the shear stress vector field) and the shear stress magnitude at two instants in time are shown on both the aortic and ventricular sides of the leaflets (**Figure 6**). The ventricular stress field during the open phase suggests a fairly smooth, straight, accelerating flow, which is consistent with the favorable pressure gradient experienced by the flow as it is pushed by the contracting ventricle to pass through the leaflets. On the aortic side, however, the rapid cross-sectional area expansion in the sinus region imposes an adverse streamwise pressure gradient that gives rise to a very complex and disorganized flow. The stress field undergoes rapid changes as soon as the leaflets begin to close. On the ventricular side, the flow during the closing phase remains fairly straight, albeit less orderly than during opening. In addition to the drastically different flow patterns on the two sides of each leaflet, the computations also suggest significant differences in the magnitude of the shear stress field. In general the aortic side is characterized by lower magnitudes but more complex patterns in the shear stress vector field than the ventricular side.

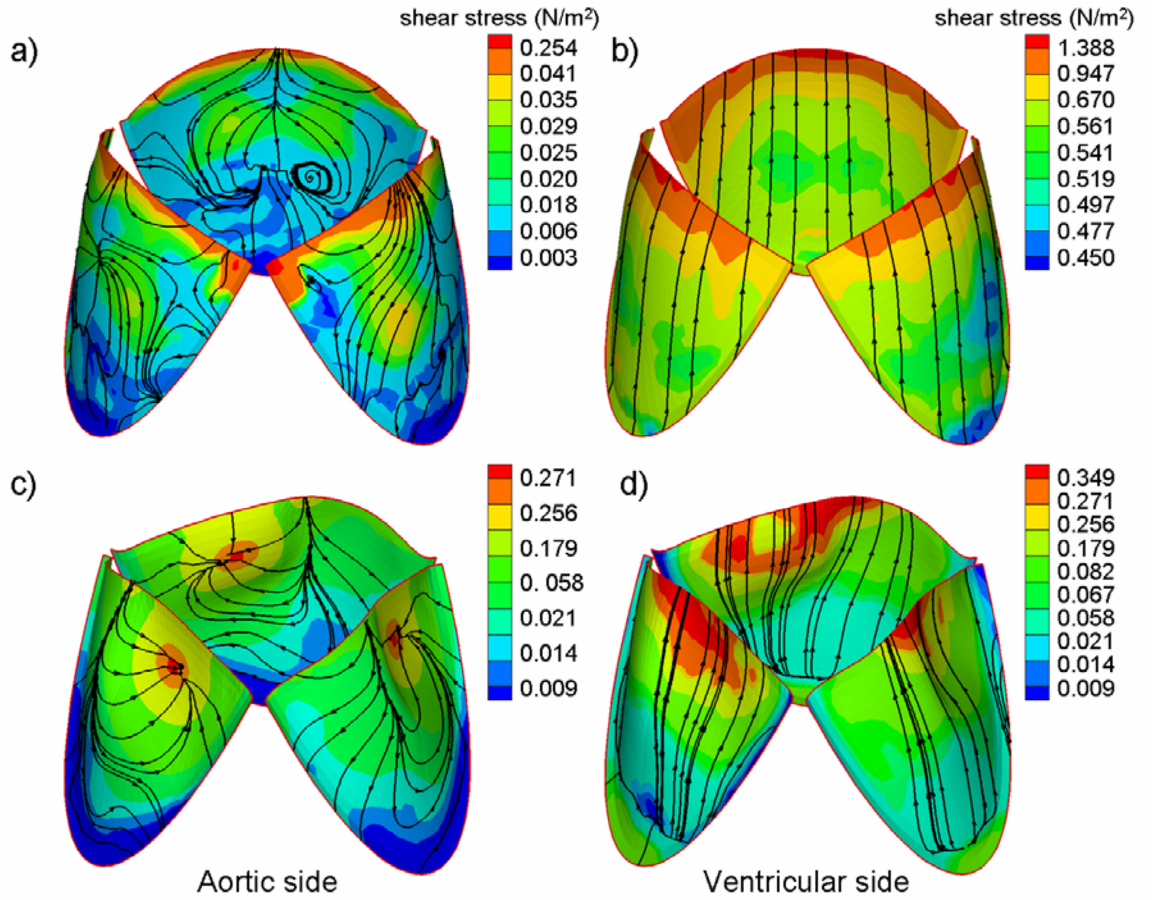

Figure 6. Instantaneous friction streamline and shear stress magnitude plots on the aortic (a and c) and ventricular (b and d) sides of the leaflets during the fully open (a and b) and early closing (c and d) phases of the cardiac cycle.

1.2.2 Dynamic Leaflet Strains

Accurate diagnosis and treatment of valve disease, along with the development of improved surgical strategies/techniques, requires a complete understanding of normal valve dynamics. As an example, investigators have undertaken the task of studying mitral valve (MV) dynamics and left ventricular fluid mechanics [2, 4-9]. However, due to the complexity of valve anatomy, it is difficult to theoretically [10] or computationally [11-13] determine the functional role and importance of each individual component. Moreover, these simulations are currently difficult to fully validate *in vivo* with available imaging technologies.

Many approaches have been taken to attempt to quantify valvular dynamics. Early work by Thubrikar et al used biplane fluoroscopy to determine dynamic valve function. [14-16]. These experiments involved lead markers sutured onto the valve leaflets. Thubrikar reported that leaflet radial length does not change significantly during maximum flow. Instead he observed when the leaflet closes and coapt under increasing pressure, the radial length increases during diastole [17]. Thubrikar used two markers at the basal and belly region of the leaflet, which did not cover the free edge. Further, two markers only allowed straight distance measurements, and did not follow leaflet surface. More recently high resolution approaches, such as biplane x-ray imaging, demonstrated significant regional complexities in valve motion and strain [18]. However, in these studies the number of markers used was small so that the spatial resolution was insufficient for detailed surface strain studies. This is considered critical as the high degree of structural and mechanical heterogeneity in heart valve leaflets [19-21] suggest an equally complex regional strain response over the cardiac cyclic.

1.2.3 Biomechanical Descriptors of Heart Valve Leaflets

Mechanically, the native semilunar valve leaflets undergo similar passive loading regimes: flexure during opening and closing, shear stress from flowing blood when opened, and planar tension when closed. The atrioventricular valves are more complicated due to their asymmetrical shape and the tethering effect of the chordae tendinae. Aortic and pulmonary valve leaflets have an evolved, specialized architecture that allows for efficient opening and closing with slight pressure gradients while also withstanding large transvalvular pressures when apposed during closure. Additionally, the leaflets have a tri-layered structure, which is composed predominantly of fibrillar collagen (fibrosa layer), glycosaminoglycans (spongiosa), and elastin (ventricularis). It is the structural arrangement of the aligned fibrillar collagen network that largely defines the mechanics of the leaflet.

Interestingly, the ultimate tensile strength of human aortic and pulmonary valve leaflets are very similar (1460 and 1450 kPa, respectively) [22] though they must support vastly different transvalvular pressures (10 mmHg for the pulmonary and 80 mmHg for the aortic) [23]. While uniaxial testing of native leaflets is useful for failure strength measurements, this information does not complete our understanding of the tissue biomechanics, in that they rarely fail catastrophically. Of greater concern is their ability to remain sufficiently compliant and coapted when apposed, which is a bi-directional response. Because of these considerations, native leaflet response to diastolic pressure is best examined mechanically by biaxial testing of the belly region of the leaflets [19, 24-26]. It is well known that collagen fibers can withstand high tensile forces, but have low torsional and flexural stiffness. Thus, directions in which the fibers are oriented can be identified with the directions in which the tissue is able to withstand the greatest tensile stresses. This is especially the case for in the study of the structure of the AV, which is uniquely suited for efficient transmission of mechanical stresses with the minimal use of material.

To quantify the gross fiber architecture of the valve leaflet, we used small angle light scattering (SALS) [27]. In SALS, laser light is passed through a tissue specimen and the spatial intensity distribution of the resulting scattered light represents the sum of all structural information within the light beam envelope. To simulate changes to aortic valve leaflet structure with increasing trans-valvular pressure, fresh porcine aortic valves were fixed at trans-valvular pressures ranging from 0 mmHg to 90 mmHg. Overall, increasing trans-valvular pressure induced the greatest changes in fiber alignment between 0 and 1 mmHg, and past 4 mmHg there was no detectable change in fiber alignment.

Thus, we can see that for the AV much of the observed change in collagen structure is due to straightening of the collagen fibers. This is a finely tuned affair; straightening must occur at the right strain level and at the right rate to facilitate coaptation, yet not allow excessive tissue deformations that may lead to regurgitation. Further evidence of adaptation is the unique structure of the commissure region, which approximately corresponds to the coaptation region. The coaptation region is under no trans-valvular pressure, but is loaded instead in a uniaxial-like manner due to tethering forces generated at the attachment of the commissures to the aortic root. Unlike the biaxially loaded belly region, the uniaxial loading of the commissures would tend to make their structure more highly aligned, i.e. more like a tendon. Like tendons, a highly aligned fiber network would have a very short transition region from low to high stiffness, as evidenced by rapid fiber uncrimping with stress. The highly aligned nature of the commissure region at unloaded state and the more rapid realignment with transvalvular pressure in the commissure regions are consistent with the pre-transition strain level behavior of tendon-like materials.

The ability of heart valve leaflets to open and close efficiently 3 x 10^9 times during a person's lifetime is also of great importance, and this motion is directly related to the bending stiffness of the tissue. Additionally, the bending stiffness of the leaflets can be used to assess damage mechanisms associated with calcification and flexural fatigue [28, 29]. Bending tests are highly sensitive at low stress-strain values, and when combined with specialized imaging techniques and histology, allow investigators to probe the individual layers of a leaflet tissue. The sum of these analyses serves to describe the gross mechanical response resulting from the fibrous architecture of native heart valve leaflets. Finally, experimental results not only provide quantitative data for use in setting engineered tissue goals, but also allow for the development and implementation of constitutive models [30, 31] which, when properly formulated and validated, can vastly expand the scope of variables that can be perturbed through analytical and numerical simulations.

1.2.4 Tissue Preparation for Biomechanical Testing of Heart Valve Leaflets

Performing biomechanical analysis is largely dependent upon the size of the sample specimen, particularly regarding the ability to grip and apply mechanical loads to the tissue. Because of size limitations and our interest in bioprosthetic heart valve biomechanics, the majority of our native valvular research has dealt with porcine AV leaflets. Leaflets are excised from the valve by cutting along the basal attachment. Typically, a square specimen (10mm x 10mm) from the central belly region of the leaflet is removed. Depending on what exactly is being analyzed, the specimen can be run through the following series of tests in sequential order: flexure testing, biaxial testing, and SALS analysis (**Figure 7**). This sequence is important due to the application of markers with cyanoacrylate that would alter mechanical response if leaflets were tested otherwise (i.e. biaxial before flexure).

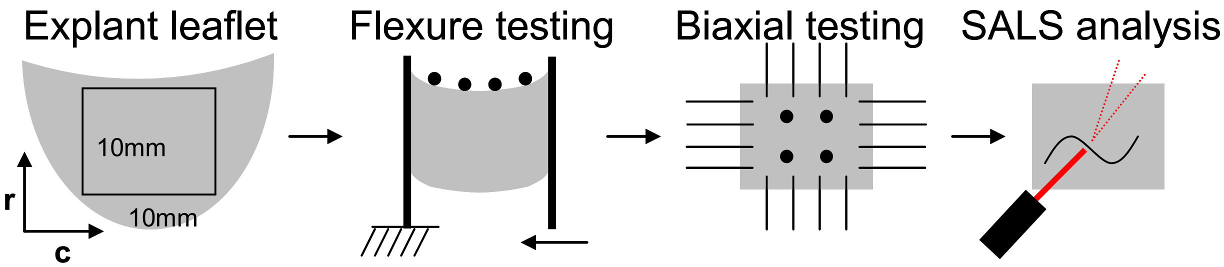

Figure 7. Schematic of biomechanical analyses of heart valve leaflets. Proceeding form the left to the right, the leaflet is excised, tested under flexure, tested biaxially, and then analyzed with SALS. The small black circles represent applied markers used for strain determination.

1.2.5 Flexure Testing of Heart Valve Leaflets

Loads to achieve flexure are applied by stationary and translatable arms that are coupled to the ends of the tissue by short metal sleeves (attached by cyanoacrylate) that slide onto the arms of the bending device [28, 32, 33]. The translatable arm is a deformable bar that was previously calibrated to determine loads from deflection. Markers are attached to top of the tissue nearest the free edge. Specimen deflection is recorded with a CCD camera and real-time, resulting moment, M (mN*mm), and change-in-curvature, Δκ (mm^{-1}), values are determined at small time increments with a custom program by tracking the marker and bending bar positions. The applied moment versus the change-in-curvature is related by the Bernoulli-Euler moment-curvature equation, $M=E_{eff} I \Delta\kappa$, where $E_{eff} I$, termed flexural rigidity, corresponds to the slope of M-Δκ curve, with I as the second moment of inertia calculated as $I={}^{1}/_{12}t^{3}w$. The terms t and w are the thickness and width of the sample, respectively. The physical meaning of E_{eff} is the instantaneous effective stiffness for a given Δκ, and is analogous to Young's modulus from uniaxial tension testing.

Flexure of soft biological materials offers two distinct advantages over uniaxial mechanical testing: 1) the ability to discern slight changes in stiffness at low-stress strain levels that would not be appreciable in tension and 2) the ability to assess individual layers of multi-layered structures. Because of these advantages, flexure is ideal for analyzing slight changes to leaflet layer properties due to structural damage, cellular contraction, and ECM biosynthesis.

1.2.6 Biaxial Testing of Heart Valve Leaflets

Biaxial testing of native and bioprosthetic leaflets has been described extensively in previous publications [19, 34-36]. Briefly, tissue deformations are measured by monitoring the movements of four small graphite particles which are attached to the center of the specimen in a square configuration. Sutures (four per side) are attached to the sample to apply loads and are coupled to the actuating arm of the device via pulleys to allow equal stress distribution at each suture point. Additionally, it is essential to allow freedom for strain in the orthogonal direction during biaxial testing and this suturing method accomplishes this by not rigidly fixing each side of the tissue [37]. When compared to the reference state, these marker movements reveal the resulting orthogonal strains and in-plane shear from applied loads, which are simultaneously monitored with sensitive load cells. Typically, loads are applied in a quasi-static fashion which is not physiological for leaflets; therefore, we recently built a system that was capable of applying and tracking high-speed physiologic strain rates (500-1000%/sec) [38, 39]. Both systems reveal the orthogonal, coupled stress-strain response which is of paramount importance for anisotropic planar tissues such as leaflets.

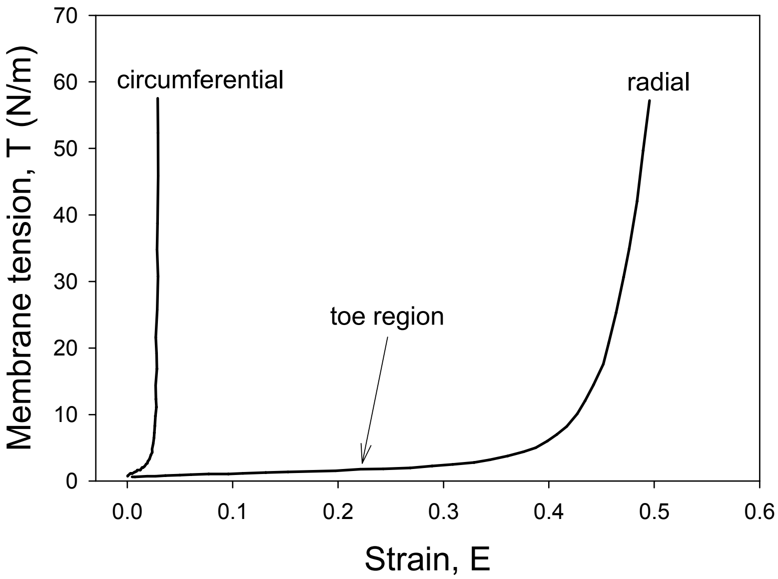

Figure 8. Biaxial response of a native porcine aortic leaflet. Note the anisotropic response of the tissue. 60 N/m membrane tension corresponds to in vivo diastolic pressures at rest.

As mentioned above, native AV and PV have an aligned and organized collagen architecture that is primarily oriented in the circumferential direction of the leaflet. This fibrous architecture largely defines the response to biaxial tension. As in other collagenous tissues with some degree of orientation, native leaflets have distinct responses in the circumferential and radial directions (**Figure 8**). At the beginning of the biaxial test, the collagen fibers become uncrimped in the circumferential direction and exhibit a sharp rise in tension with little increasing strain. This is not surprising since the robust collagen fibers are supporting the applied load and are straightened and taut. Radially, there is a much more gradual response since this axis has fewer aligned fibers. Initially, there is a large toe region where strain increases with little appreciable stress. Then there is a transition leading to a rise in stress where the tissue reaches maximum extensibility. The high compliance exhibited in this initial radial direction toe region allows the leaflet to stretch and remain coapted during diastole. Conversely, the stiff circumferential direction is necessary to support the large transvalvular pressure imposed on the tissue. These distinct directional responses are crucial for proper valve function and must be of the highest priority when analyzing engineering constructs.

1.2.7 Analysis of the Collagen Architecture of Heart Valve Leaflets

SALS is an effective technique for the microstructural analysis of planar fibrous connective tissues, and we have used it previously for mapping the architecture of leaflets from normal, pressure fixed, and explanted bioprosthetic valves [20, 27, 40]. Briefly, a continuous unpolarized wave laser is passed through the tissue, which scatters light according to the internal planar fiber structure. The resulting angular distribution of scattered light intensity about the laser axis represents the distribution of fiber angles within the beam envelope at the current tissue location. Gathered information includes: 1) preferred fiber direction, 2) distribution skew, and 3) orientation index, which represents 50% of the total number of fibers.

The mechanical response of the native semilunar leaflets is highly dependent on the state of the aligned collagen network, and while biaxial testing demonstrates this response, it does not reveal local variations in the architecture. Therefore, to identify regions of interest, SALS has been utilized to probe areas of collagen disruption and damage [40]. Additionally, SALS has been used to assess exactly how the AV collagen fibers rotate due to applied transvalvular pressure [20]. It can be seen that increasing pressure on the leaflet induced the greatest changes in fiber alignment between 0 and 4 mmHg, with no further change past 4 mmHg (**Figure 9**).

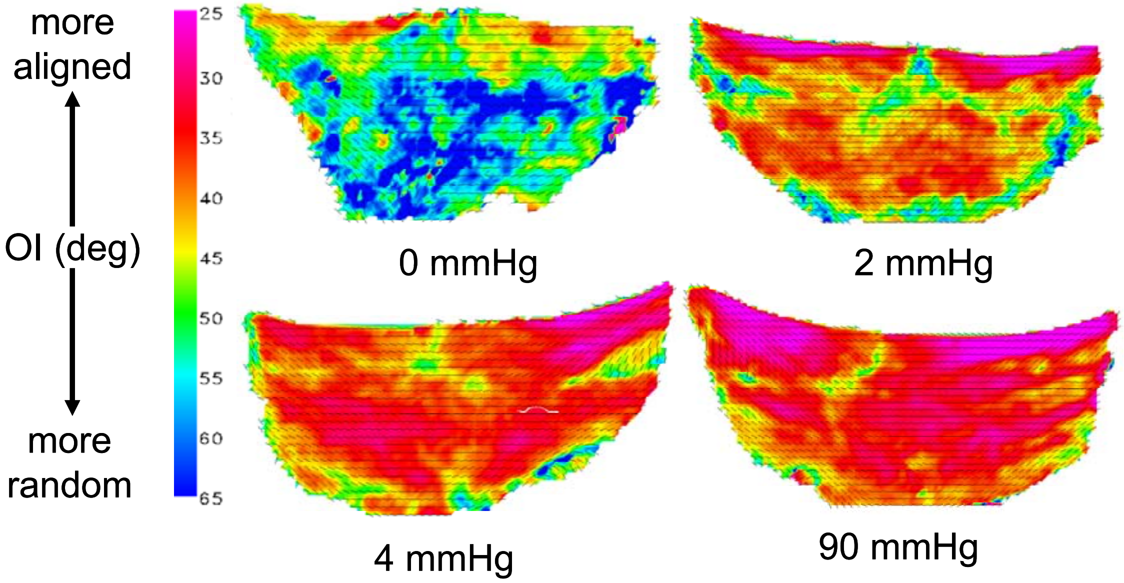

Figure 9. SALS of the native porcine AV leaflet. Leaflets were fixed at increasing transvalular pressures and analyzed for collagen orientation. OI (deg) represents the orientation index and represents 50% of the total number of fibers in that area. Essentially, pink areas have a lower OI value and are more aligned whereas blue areas have higher OI values and are less aligned.

Additionally, when the native leaflet outer layers are separated by dissecting through the spongiosa and rescanned, there is much higher degree of orientation in the fibrosa layer while the ventricularis appears to be randomly oriented. At higher pressures (>4 mmHg), differences in each layer became less pronounced and indistinguishable at 60 mmHg. These results further highlight the complexity of the leaflet structure, and demonstrate a sensitive response to low transvalvular pressures. Scaffolds and engineered leaflets may not need to exactly recapitulate this structural response, but it is believed that this should be of consideration.

1.2.8 Development of Constitutive Models for Heart Valve Leaflets

The mechanics of soft tissues are complex: they exhibit a highly non-linear stress-strain relationship, undergo large deformations, complex viscoelasticity, and complex axial coupling behaviors that defy simple experiments and material models. Much of this behavior is a direct result of changes in their internal structure with strain, which involves both straightening of highly crimped collagen fibers and rotation of these fibers toward the stretch axis. For valvular tissues, most previous work on the mechanical properties of the native and chemically treated AV has relied on uniaxial mechanical testing [41-43]. These studies demonstrate that chemical fixation of intact valves, especially under pressure, alters the mechanical properties of the leaflets. Marked decreases in the extensibility are generally attributed to "locking" the collagen fibers in the uncrimped state [44, 45]. Tests on thin tissue strips however, cannot mimic the heterogeneous multi-axial deformation fields, combined loading sequences, and native fiber kinematics found in the physiological environment. Mayne et al. [46] and Christie et al. [47] have performed equi-biaxial testing (i.e. equal levels of tension applied to each test axis) that overcomes many of the above limitations of uniaxial loading. However, derivation of a constitutive relationship solely from equi-biaxial test data is limited due to multiple co-linearities that confound the ability to obtain reliable, unique model parameter values [48].

Billiar and Sacks [19] generated the first complete biaxial mechanical data necessary for constitutive modeling of the AV leaflet. Due to the small size and heterogeneous structure of the AV leaflet, testing methods were developed and validated. Leaflet specimens were subjected to biaxial tests utilizing seven loading protocols to provide a range of loading states that encompass the physiological loading state. The leaflets demonstrated a complex, highly anisotropic mechanical behavior, including pronounced mechanical coupling between the circumferential and radial directions. Mechanical coupling between the axes produced negative strains along the circumferential direction and/or non-monotonic stress-strain behavior when subjected to equi-biaxial tension, a behavior noted by Mayne et al. [46] but was not explained. Clearly, a constitutive model is needed to truly understand the aortic leaflet behavior and its implications on the mechanics of the intact valve.

The quantified fiber architecture [20] and biaxial mechanical data [19] suggest that a structural approach is the most suitable method for the formulation of a constitutive model for the AV leaflet. Details of the model have been previously presented [30]. In this approach, the tissue’s total strain energy is assumed to be the sum of the individual fiber strain energies, linked through appropriate tensor transformation from the fiber coordinate to the global tissue coordinates. For the AV, we assume that the planar biaxial mechanical properties of the leaflet can be represented as a planar array of collagen fibers. Anatomically, these fibers most closely represent the dense, highly aligned collagen fibers in the fibrosa layer. Next, the angular fiber distribution and the density of the fibers are assumed constant throughout the tissue. Based on SALS results for the AV leaflet [20], the angular distribution of the collagen fibers, R(θ), can be represented by a Gaussian distribution,

$$R(\theta) = \frac{1}{\sigma\sqrt{2\pi}}\exp\left[\frac{-(\theta - M)^2}{2\sigma^2}\right] \tag{1}$$

where θ is the direction with respect to the x_1 or circumferential axis, σ is the standard deviation and M is the mean of the distribution. M was determined experimentally for each specimen by using the preferred fiber directions as determined by SALS [20]. The "effective" fiber stress-strain properties were represented using:

$$S_f = A\left[\exp\left(BE_f\right) - 1\right] \tag{2}$$

where S_f is the second Piola-Kirchhoff fiber stress, E_f is the fiber Green's strain. This formulation for the fiber stress-strain law avoids detailed descriptions of complex crimp distributions.

For valvular tissue, it is more convenient to work with membrane stresses due to considerations such as variable total and layer thickness, and heterogeneous layer structure [19]. Further, since the biaxial mechanical tests are run using membrane stress control using the specimen's unloaded dimensions, a Lagrangian membrane stress measure is used in the constitutive formulation. It is also assumed that inter-specimen variations in fiber volume fraction V_f and thickness h are negligible, so that the product hV_f can be conveniently absorbed into the material constant A. The resulting expressions for the Lagrangian membrane stresses T_{ij} are:

$$\begin{aligned} T_{11} &= \int_{-\pi/2}^{\pi/2} S_f^*(E_f)R(\theta)\left(\lambda_1 \cos^2\theta + \kappa_1 \sin\theta\cos\theta\right)d\theta \\ T_{22} &= \int_{-\pi/2}^{\pi/2} S_f^*(E_f)R(\theta)\left(\lambda_2 \sin^2\theta + \kappa_2 \sin\theta\cos\theta\right)d\theta \end{aligned} \quad (3)$$

where $A^*=hV_fA$ and $S_f^* = A^*\left[\exp\left(BE_f\right)-1\right]$. The parameters A^*, B, and σ were estimated by fitting Eq. 3 to the complete biaxial data set [19].

An important aspect of the structural approach is that the two distinguishing aspects of the AV leaflet biaxial behavior, namely the extreme mechanical anisotropy and the strong mechanical coupling between the axes, can be explained by the angular distribution of fibers. To more clearly demonstrate this effect, simulations were generated under equi-biaxial loading for a given set of A^* and B values by letting σ vary. These simulations indicate that the value of σ is the primary determinant of the biaxial stress-strain response. Although this assumed a simplified tissue structure in the formulation of the model, the structural approach highlighted the importance of the angular orientation of the fibers in determining the complex anisotropic mechanical behavior of the tissue.

While the above modeling approach worked well, it should be noted that the use of a membrane tension formulation ignores layer specific mechanical contributions and the implicit non-uniformity of the transmural stress distribution. To begin to address these limitations, recently conducted novel studies were performed to quantify the biaxial mechanical behavior of the two structurally distinct, load bearing AV leaflet layers: the fibrosa and ventricularis [49]. A microdissection technique was developed based on previous methods [20, 43] and modified to work with the biaxial test specimens rather than the intact leaflet. While keeping the specimen moist with PBS at all times, the ventricularis layer was gently lifted upwards with delicate forceps to expose the spongiosa layer. It was found that the spongiosa contained numerous interconnecting fibrous structures that couple the fibrosa and ventricularis. In order to separate the outer fibrous layers, it was necessary to manually sever each interconnection. This was accomplished through the use of a low power dissection microscope and ophthalmic micro-scissors. For a bilayer tissue configuration, one would normally start with the individual layers in their separated, stress free reference configuration. Sequential deformations would then arise from coupling the layers in the intact configuration (accounting for any pre-strains) and the application of external loads. These states are defined as

β_0 - the separated, unconstrained configuration,

β_1 - the intact unloaded configuration,

β_t - the current configuration of the intact tissue in response to external loads.

The equibiaxial responses of the fibrosa and ventricularis computed with respect to both β_0 and β_1. Results indicated that both layers exhibited very different non-linear, highly anisotropic mechanical behaviors. When referenced to the intact conformation (β_o) substantial differences were seen between the radial contributions of each layer. Thickness measurements enabled calculation of the corresponding first Piola-Kirchoff stresses: P^{v}_{22} = 95.74 kPa while P^{f}_{22} = 26.63 kPa at equivalent levels of stretch. These results suggest that the ventricularis layer makes profound contributions to the intact leaflet response in the radial direction. Thus, while the leaflet tissue mechanical response was dominated by the fibrosa layer, the ventricularis contributed double the amount of the fibrosa to the total radial tension, and experienced four times the stress level. Histological-based thickness measurements indicated that the fibrosa and ventricularis constitute 41% and 29% of the total layer thickness, respectively. Moreover, the extensive network of inter-layer connections and identical strains under biaxial loading in the intact state suggest that these layers are tightly bonded. In addition to advancing knowledge of the subtle but important mechanical properties of the AV leaflet, this study provided a comprehensive data base required for the development of a true 3D stress constitutive model for the native AV leaflet.

1.2.9 Native Leaflet Biomechanics and Candidate Endpoints for Engineered Leaflets

From a biomechanics point of view, the important functional properties of heart valve leaflets are compliance to adeptly open and close, and structural integrity to withstand planar tension when apposed during diastole. Therefore, the bending stiffness and biaxial response of an engineered tissue will likely need to resemble that of the native leaflet. To achieve this desired response, it is intuitive that some collagenous or otherwise organized architecture, similar to that of the native leaflet, would be required; hence, SALS is useful in evaluating this. The difficulty that faces those analyzing the engineered leaflet tissue biomechanical response is determining how to successfully couple these analyses. Flexure data do not incorporate appropriate biaxial coupling, while biaxial testing does not yield transmural tissue mechanical properties. Additionally, SALS data can only serve to demonstrate where and how the collagen fibers are arranged and oriented; this information is independent of fiber mechanical properties, which can only be determined through structural constitutive modeling. While the methods and results presented here demonstrate an ability to describe most aspects of leaflet biomechanics, they can only be utilized in as much as they are applied in concert. Furthermore, one can easily envisage a case where an engineered tissue responds as desired to one or more of these analyses, but ultimately does not function as a suitable valve replacement. Hence, it is believed that these analyses are important and directive and should compliment surgical intuition derived from hands-on *in vitro* and animal model experience.

As mentioned previously, it is believed that these analyses are important prior to pre-clinical animal studies and clinical trials; however, once in these stages, an iterative process will likely be required. While quantifying pre-implant mechanics gives an initial starting point, effects of host cell remodeling, mechanical fatigue, and biodegradation will need to be assessed in the in vivo setting. Therefore, progress must be monitored after sequential improvements or longer implant durations. From previous experience with bioprosthetic valves, it is believed that monitoring is crucial as unforeseen events can arise during both early [50] and late implant times (mechanical fatigue independent of calcification [40]). Hence, biomechanical analysis should not be relegated to *in vitro* studies before moving to *in vivo* studies; the process will likely require multiple generations of engineered valves for continual improvement of the design.

1.2.10 Future Directions for Biomechanics of Native and Engineered Valve Leaflets

The methods and results presented above are not exhaustive, in that they examine the global mechanical response of the tissue. Biomechanical analysis at smaller scales (individual fibers, cells, and molecules) would undoubtedly yield useful information; however, it is believed that initial and prolonged success of an engineered construct will ultimately be at the tissue level. The techniques presented here are well documented for AV leaflets due to their importance in understanding bioprosthetic heart valve development for adults and the resulting success and failure of these valves. However, the pediatric population would greatly benefit from an engineered heart valve due to lack of options at the present time, and the pulmonary valve will likely have better initial success due to the less demanding mechanical environment. A previous study compared native and chemically fixed aortic and pulmonary leaflets under biaxial tension and found that they are quite different with respect to their response, suggesting that the collagen content was different between the leaflets [24]. It is essential to understand this difference and if this difference is important or inconsequential. For instance, clinical explants suggest that success of the Ross procedure may be due in part to adaptive remodeling [51]; however, would the reverse be true (i.e. aortic to pulmonary switch)? If not, this would indicate that the valve is capable of adapting to greater mechanical demands but not less. Therefore, leaflets may need to be specifically designed for loads just below what they will see in vivo and adapt once implanted.

1.3 HEART VALVE DISEASE

1.3.1 Tissue Engineering, Regenerative Medicine, and Heart Valve Disease

The previous section dealt with mechanical descriptors of native heart valve leaflets and the possible endpoints for tissue engineered heart valves (TEHVs). Primarily, the target for a TEHV is the pediatric population due to the potential for the TEHV to grow and repair itself for the lifetime of the patient. On the other hand, while a TEHV could possibly benefit an older patient, there are reasonably successful alternatives (bioprosthetic or mechanical valves) available to this patient subset. Regenerative medicine or preventative measures to avoid valve disease in the aging population is the primary focus of this work. While findings here will ultimately distill down and contribute to the TEHV literature, this work aims to elucidate the mechanisms responsible for age-related valve disease and is, therefore, more in line with the field of regenerative medicine for heart valve disease.

1.3.2 Prevalence

According to Heart Disease and Stroke Statistics—2006 Update from the American Heart Association [52], valvular heart disease resulted in 19,989 deaths directly and was a contributing or underlying cause of death in 42,590 cases in 2003. Of the mortality or contributing mortality numbers, AV disease was the most prevalent with 12,471 and 26,336 cases, respectively; MV disease cases were responsible for 2,759 deaths and 6,600 contributory deaths. Right side valve cases were significantly less (PV: 11 deaths and 35 contributory deaths; TV: 16 deaths and 69 contributory deaths). It is estimated that in 2003 there were 95,000 inpatient valve procedures preformed. These numbers indicate that valvular disease is very prevalent and life threatening and additionally that the AV is the most diseased with the highest rate of morbidity.

1.3.3 Types of Valvular Disease

There exist two types of valvular heart disease: congenital and acquired [53]. Congenital valve disease is an abnormality that develops before birth and this subset of patients are who would most likely benefit most from a tissue engineered heart valve. The result of the defect may be related to improper valve size, malformed leaflets, or an irregularity in the way the leaflets are attached. This most often affects the AV or PV. A very common congenital defect is bicuspid AV disease where instead of the normal three leaflets or cusps, the bicuspid AV has only two (**Figure 10**). Without the third leaflet, the valve may be stenotic (narrowing with flow obstruction) or regurgitant (allowing backward flow). It is estimated that bicuspid AV disease affects about 2% of the population.

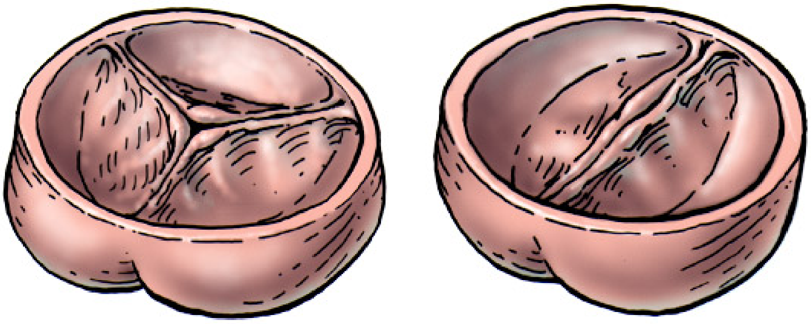

Figure 10. Drawing of tricuspid AV (left) and bicusipid AV (right). (www.surgery.ucla.edu)

Acquired valve disease pertains to problems that develop within valves that were at one time normal. This is typically referred to as age-related degenerative valve disease. In the early part of the 20th century, the primary cause of acquired valve disease stemmed from rheumatic valve disease; however, this trend has changed dramatically with a decrease in rheumatic valve disease and a concomitant increase in age-related degenerative valve disease [53].

1.3.4 Aortic Sclerosis

Modern, acquired AV disease is typically referred to as aortic sclerosis and is defined as focal thickening of an otherwise normal AV without valve obstruction. With valve obstruction, aortic sclerosis becomes known as aortic stenosis (**Figure 11**) and both of these pathologies represent the spectrum of AV disease with progressive calcification and fibrosis of the AV leaflets. Typically, aortic sclerosis is associated with age as it is most common in the elderly. In a previous clinical study [54], aortic sclerosis was found in 26% of those over 65, in 37% of those over 75, and in 48% of those over 85. By contrast, aortic stenosis was prevalent in only 2.9% of those over 75.

Figure 11. Calcified AV with significant stenosis

Aortic sclerosis can eventually lead to significant stenosis. In a large observational study [55], 2,131 patients with aortic sclerosis were followed for 7 years. Stenosis developed in 15.9% of patients. Severe stenosis was observed most often at 8 years follow-up. In a smaller study [56], 400 patients with aortic sclerosis were found to develop clinical aortic stenosis (defined as a mean gradient across the valve of 16 mmHg or velocity >2.0 m/s) within 44 ± 30 months. Both studies indicate that a significant portion of patients with aortic sclerosis eventually develop aortic stenosis within 6 to 8 years.

Aortic sclerosis is associated with increased cardiovascular morbidity and mortality [57]. Relative risk (calculated as those with sclerosis divided by those with normal valves) of death from cardiovascular causes among subjects without coronary artery disease was 1.66 for those with aortic sclerosis versus those with normal AVs. In a recent study [58], it was found that patients with aortic sclerosis have twice the number of serious cardiovascular events (death, stroke, and myocardial infarction). This is comparable to the risk associated with diabetes or prevalent cardiovascular disease. After adjusting for typical cardiovascular risk factors, aortic sclerosis independently increases the cardiovascular risk by 50%.

1.3.5 Epidemiology of Aortic Sclerosis

The risk factors for aortic sclerosis are similar to traditional clinical risk factors for atherosclerosis and coronary artery disease and include age, male gender, hypertension, diabetes, triglycerides, and smoking [54, 59, 60]. In fact, the similarities between atherosclerosis and aortic sclerosis have led to the hypothesis that acquired valve disease is primarily a manifestation of atherosclerosis [61]. The hallmark of valve pathogenesis is the formation of lesions containing cell types which are characteristic of chronic inflammation [62-64]. These include macrophages, T lymphocytes, and mast cells. Additionally, there are lipoproteins (LDL and Lp(a)) found in human AV lesions, and accumulation of these lipoproteins is mediated, in part, by ECM proteoglycans [65, 66]. Besides lipoproteins, recent evidence has shown that the renin-angiotension system, particularly, angiotensin converting enzyme (ACE) and angiotensin II (Ang II), may play a role in AV pathogenesis [67]. Ang II has a number of potential lesion forming effects, including inflammation and macrophage cholesterol accumulation. Therefore, there are multiple mechanisms for aortic sclerosis to initiate and further perpetuate in the otherwise, normally functioning valve (**Figure 12**). While there has been a marked increase in understanding of the pathogenesis of aortic sclerosis in the past 20 years, the direct effect of the aforementioned mediators on the resident cell population remains unclear. Furthermore, given the dynamic environment in which the valvular cells reside, their response both to chemical and biophysical stimuli is undoubtedly crucial.

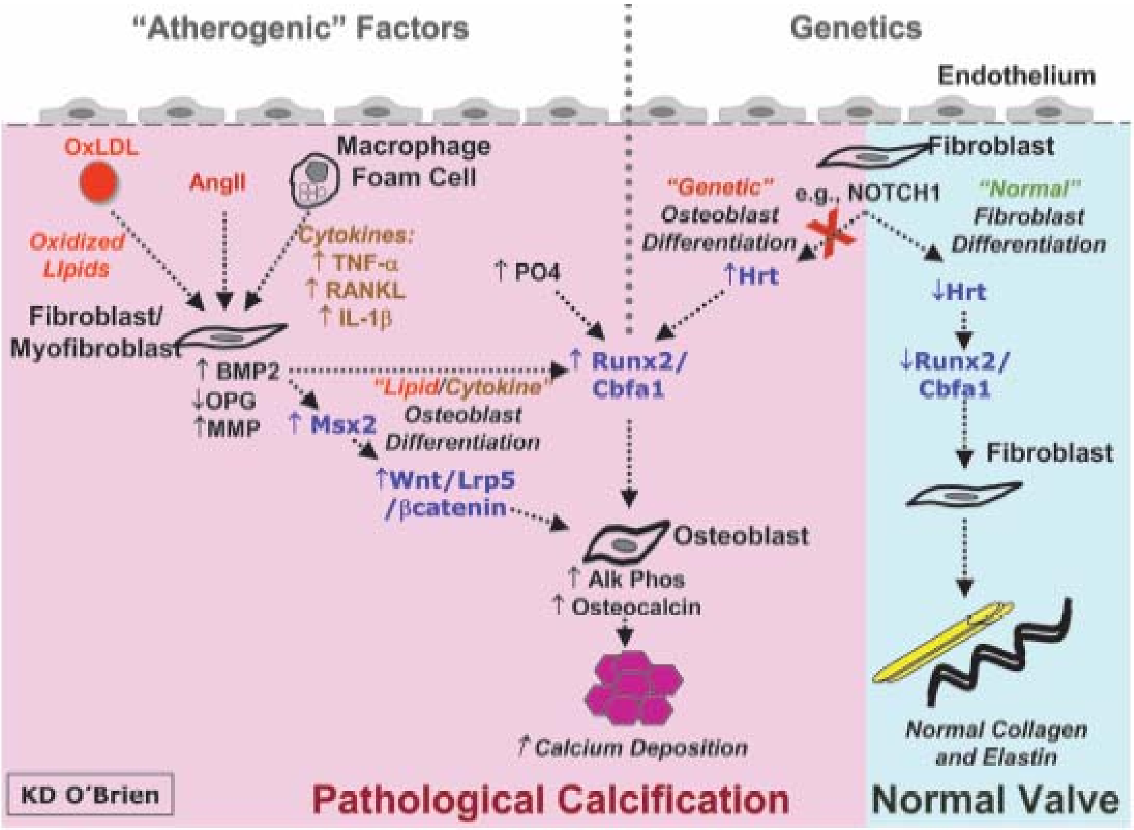

Figure 12. Potential interplay of lipids and inflammation in the pathogenesis of valve sclerosis and calcification (pink area). Light blue region deals with genetic mechanisms not discussed here. Taken from [61].

1.4 CELLS OF THE HEART VALVES

1.4.1 From Tissue to Cells

The primary focus of the Engineered Tissue Mechanics Laboratory (ETML), wherein the following research for this Disseration was conducted, has been largely on the organ and tissue level biomechanics of the heart valves (see Sec. 1.2 above). The previous section (Sec. 1.3) dealt with the pathophysiology of valve disease, which has not, to date, been an area of investigation in ETML. In this Disseration, an effort has been made to begin to probe the response to mechanical stimuli of the heart valve interstitial cells. Ultimately, their adaptive, or in some cases maladaptive, response is likely crucial in the development of certain valve pathologies.

1.4.2 Valve Endothelial Cells

The leaflets of all four HVs are sheathed by an ‘organ’ of single layer valvular endothelial cells (VECs) that have been shown to be morphologically different from aortic ECs [68, 69]. Additionally, VECs are aligned with the collagen architecture of the valve, which is circumferentially oriented [70]. The VECs are believed to regulate vascular tone, inflammation, thrombosis, and remodeling, and their dysfunction has been linked with multiple disorders [71]. Within the proximal third of the leaflets, where they are innervated, there is believed to be a feedback mechanism between the VECs and valve interstitial cells (VICs) wherein the nerves transmit information regarding released substances form the VECs [72]. Primarily, release of cytokines has been shown to cause changes in VIC structure and function [73, 74]. It has also been speculated that there exists some physical communication between the VECs and VICS. However, to date no direct junctions have been observed between the two cell populations [75].

1.4.3 Valve Interstitial Cells

Within the three layers of the leaflet tissue, there resides a heterogenic population of interstitial cells [75-78]. The heterogeneity of the interstitial cells is made up of fibroblasts, smooth muscle cells, and myofibroblasts, which have characteristics of both fibroblasts and smooth muscle cells. Studies of the interstitial cell population in both human and porcine subjects have revealed that the cell population was not localized to any one region or layer of the leaflet, but was present throughout the tissue [79]. Interest in the myofibroblast cells (typically referred to as VICs) has grown in recent years, as they are believed to be crtically important in valve pathophysiology. Primarily, VICs serve to maintain the structural integrity of the leaflet tissue by remodeling via protein synthesis and enzymatic degradation (e.g. MMPs). Their phenotype (which ranges from fibroblast-like to myo-like) is believed to be plastic and reversible, as VICs of normal, healthy valves were quiescent (predominantly fibroblasts) while in developing, diseased, and remodeling valves, the VICs were activated and contractile [80, 81]. While their dualistic nature is not fully understood, the VIC's multifunctionality may be used for cell-cell communication, tissue remodeling, wound healing, and contraction [78]. Further, it is believed that when the phenotype of the resident VIC population is myo-like, the cells are actively remodeling the ECM. This indicates that the VIC phenotypic state at any given time is likely related to the current remodeling demands of the tissue [80].

Porcine aortic VIC (AVIC) contractility has been qualitatively studied with cultured cells on silicone substrates in the presence of multiple contractile chemical agents [75, 76]. In both studies, contraction occurred for most agents within 3 minutes and reached a plateau within 10 minutes. Additionally, Messier et al. [76] found that the few cells with no initial basal tonus did not respond to the administered vasoconstriction drugs. Isoproterenol was used to elicit relaxation from active cells, from which all cells recovered their previous basal tonus within 25 minutes. While not quantitative, these findings were the first examples demonstrating an AVIC contractile response.

Strips of aortic leaflets have been exposed to elevated KCl and endothelin levels in uniaxial tension; both treatments responded similarly with cells generating modest forces in the circumferential direction, while in the radial direction the cells generated less force [82]. This measurable contraction of the cells at the tissue level is likely made possible by strong attachment to the ECM, which has been reported both in situ and in vitro [77, 78]. The concerted cell contraction is believed to be mediated by cell communication through integrins with surrounding cells and the ECM [77]; AVICs demonstrate extended connecting processes that are believed to form a cellular network for communication [75].

While each of the four valves are exposed to comparable shear stresses, flexure, and mum transvalvular pressures (TVPs; 80 and 120 mmHg, respectively) versus their right side counterparts (pulmonary, PV; tricuspid, TV; 10 and 25 mmHg, respectively) [83]. In theloading time durations, the left side valves (AV and MV) are exposed to elevated maxi AV, TVPs above ~5 mmHg predominately result in ECM compaction as the collagen fibers become uncrimped and taut [20]. From this ECM compaction, significant changes in the AV interstitial cell (AVIC) nucleus aspect ratio have been observed with increasing pressures [84] (**Figure 13**). At 60 mmHg, the AVIC nuclei aspect ratio increased from 2:1 (at 0 mmHg) to 4.8:1, demonstrating that valvular tissue stress is translated into large cell and subcellular deformations.

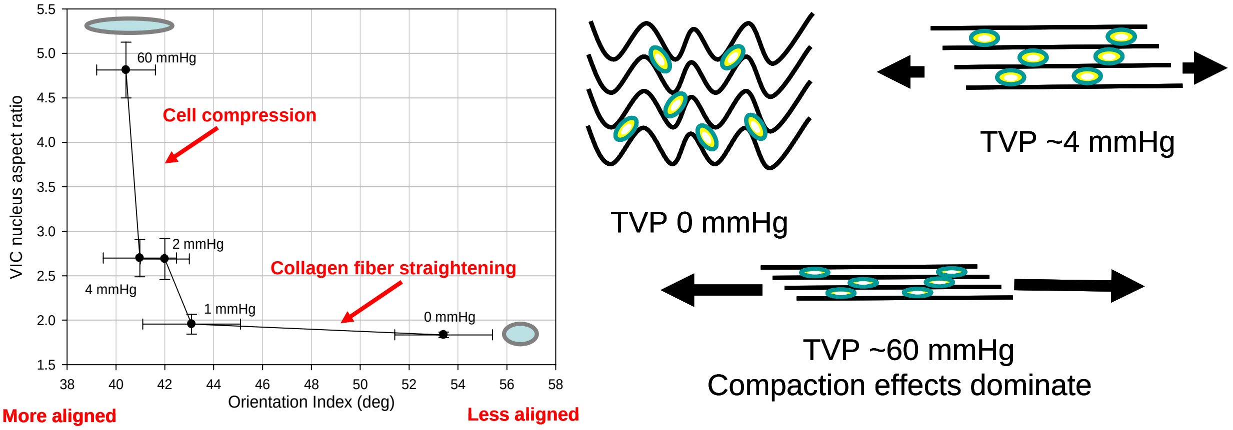

Figure 13. (Left) NAR versus OI from SALS analysis at different fixation TVP. Moving from right to left on the x-axis represents more collagen alignment and increased NAR values represent a more ellipsoidal cell. (Right) cartoon of suspected mechanism by which VIC undergo NAR changes with increasing TVP. Both adapted from [84].

1.4.4 The Myofibroblast Phenotype

The myofibroblasts phenotype has been of interest during the past 25 years as it has been found in many connective tissues and is believed to be essential for tissue remodeling during normal and pathologic wound healing. A superb review of the myofibroblast by Tomasek et al. is available for the interested reader [85]. Particular interest in the myofibroblast cell is generally relegated to tissues that are under mechanical tension. Typically, most cells found in tissue and organs are stress-shielded from excessive loads by their surround ECM. However, this stress-shielding is not necessarily evident during times of tissue growth or repair from damage. It is during these instances when one may see rise of the myofibroblasts phenotype. Originally, the notion of tissue contraction during tissue remodeling was thought to initiate from collagen shortening; however, modified fibroblasts were first observed by Gabbiani et al. in 1971, which led to the suggestion that these cells have an active role in the contraction process [86]. From this time, the overarching hypothesis of myofibroblast function has been to establish tension during tissue remodeling and, unfortunately, pathologic contracture, but this mechanism is not fully explained at this time.

Major confounding factors in elucidating the precise mechanism by which myofibroblasts modulate their phenotype are surrounding cytokines, complicated ECM connections, and various other cell signals [87]. Most work in the area of myofibroblast research has dealt with these confounding factors in an attempt to better understand how these cells alter the phenotype and biological function. Subsequently, it has been found that the myofibroblast expresses α-smooth muscle actin (SMA) [88, 89] and that SMA expression and collagen production is regulated by transforming growth factor-β1 (TGF-β1) [90]. Therefore, the morphological descriptor of myofibroblasts is the presence of a contractile apparatus comprised of actin microfilaments and non-muscle myosin, similar to stress fibers that are normally found in fibroblasts. It is these actin-myosin apparatuses that connect to the surrounding ECM at focal adhesions through transmembrane integrins. This functionally forms an active mechanotransductive system where stress is translated to the cell from the surrounding ECM, and additionally, the myofibroblast can in turn transmit contractile forces to the surrounding matrix.

Though it is clear that myofibroblasts are present during times of growth and repair, it is not entirely clear *why* they are present, as fibroblasts can sufficiently reorganize collagen matrices themselves [91, 92]. It was previously thought that if fibroblasts are aptly suited for this reorganization on their own, one would think that myofibroblasts are unnecessary. However, it was found by Hinz et al. that while fibroblasts may be able to generate sufficient forces during wound closure, it was the subsequent appearance of resistance in the surrounding ECM that induced a differentiation to the myofibroblast phenotype, and contraction shortly followed [93]. From this, it was evident that 1) some mechanistic signal in the damaged tissue, whether it be mechanical force, surrounding cytokines, etc., resulted in a phenotypic modulation of the resident fibroblasts and 2) that these newly apparent myofibroblast cells were indeed necessary for proper (but not ideal) wound repair.

1.5 MOTIVATION, RATIONAL, AND SPECIFIC AIMS

As demonstrated in the preceding sections, there is ample evidence that the heart valve leaflets are passive tissues which are exposed to large cyclical stresses from before birth to death. In particular, AV leaflets are subjected to planar strains (both extensional and shear) during diastole, as well as flexural deformations and surface shear stresses during systole. Though they serve an apparently simple physiological function, prolonged changes in leaflet stiffness can alter valve competency and severely impair valve performance, ultimately leading to valve failure. AV leaflet cells consist of a surface population of VECs and AVICs [76-78]. AVICs are primarily of a myofibroblast phenotype characterized by both fibroblast and smooth muscle cell markers (α-smooth muscle actin, SMA) and are unique from vascular interstitial cells [69, 75-77]. The AVICs are solely responsible for maintaining AV leaflet structural integrity by protein synthesis and enzymatic degradation. While there has been great interest in AV mechanical function, little attention has been given to the AVICs and their role in tissue homeostasis, adaptive remodeling, and pathologic etiologies. Since AV tissue homeostasis is believed to be dependent upon the synthetic states of the AVIC population, the local stresses transferred from the surrounding ECM to the cells and their resultant mechanotransductive effects are critical to the understanding of valve function. Because AVICs appear to be highly specialized, there is great interest in clarifying their inherent qualities that are essential in maintaining tissue homeostasis and proper valve function.

Therefore, we hypothesize that the AVIC is a unique and phenotypically dynamic cell that may alter its characteristics due to the local valvular tissue environment. The potential factors believed to alter the AVIC phenotype are both biophysical and biochemical and ultimately some of these changes to the AVIC could be catalysts for degenerative valvular disease. Hence, in this work, we examine the characteristics of the AVIC with regard to its: biomechanical properties; biomechanical contribution to AV leaflet function; tissue remodeling capabilities; synergistic response to biochemical and biophysical stimuli; and micromechanical environment under physiologic and hyper-physiologic loading. The major general foci of the heart valve research community are shown in **Figure 14**, with specific areas examined in this work in bold text. Because there have been identified many factors that alter the AVIC phenotype, we chose to focus primarily on mechanical factors and secondarily on the cytokine, TGF-β1 (**Figure 14**). Additionally, though there are many ECM proteins synthesized by the AVICs, we chose to concentrate on type I collagen as it is provides the AV leaflet with most of its structural integrity to withstand diastolic pressures. Ultimately, all factes of this study directly relate to the AVIC phenotype and resulting biosynthetic and mechanical function. The rationale progression of the following research from in vitro studies to in situ studies is shown in **Figure 15**.

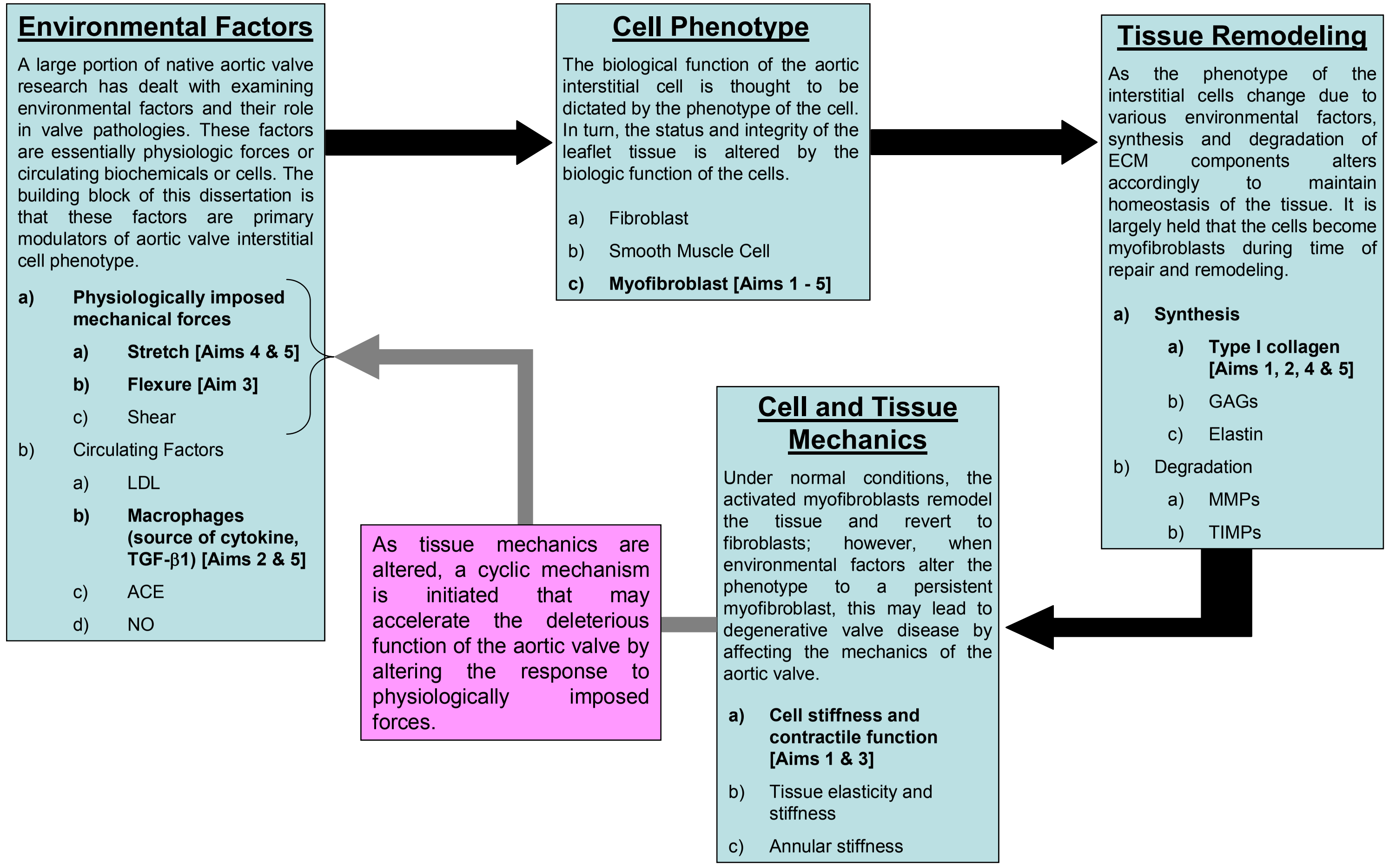

Environmental Factors

A large portion of native aortic valve research has dealt with examining environmental factors and their role in valve pathologies. These factors are essentially physiologic forces or circulating biochemicals or cells. The building block of this dissertation is that these factors are primary modulators of aortic valve interstitial cell phenotype.

- **a) Physiologically imposed mechanical forces**
  - **a) Stretch [Aims 4 & 5]**
  - **b) Flexure [Aim 3]**
  - c) Shear
- b) Circulating Factors
  - a) LDL
  - **b) Macrophages (source of cytokine, TGF-β1) [Aims 2 & 5]**
  - c) ACE
  - d) NO

Cell Phenotype

The biological function of the aortic interstitial cell is thought to be dictated by the phenotype of the cell. In turn, the status and integrity of the leaflet tissue is altered by the biologic function of the cells.

- a) Fibroblast
- b) Smooth Muscle Cell
- **c) Myofibroblast [Aims 1 - 5]**

Tissue Remodeling

As the phenotype of the interstitial cells change due to various environmental factors, synthesis and degradation of ECM components alters accordingly to maintain homeostasis of the tissue. It is largely held that the cells become myofibroblasts during time of repair and remodeling.

- **a) Synthesis**
  - **a) Type I collagen [Aims 1, 2, 4 & 5]**
  - b) GAGs
  - c) Elastin
- b) Degradation
  - a) MMPs
  - b) TIMPs

Cell and Tissue Mechanics

Under normal conditions, the activated myofibroblasts remodel the tissue and revert to fibroblasts; however, when environmental factors alter the phenotype to a persistent myofibroblast, this may lead to degenerative valve disease by affecting the mechanics of the aortic valve.

- **a) Cell stiffness and contractile function [Aims 1 & 3]**
- b) Tissue elasticity and stiffness
- c) Annular stiffness

As tissue mechanics are altered, a cyclic mechanism is initiated that may accelerate the deleterious function of the aortic valve by altering the response to physiologically imposed forces.

Figure 14. Relation between environmental factors thought to alter AVIC phenotype and the potential effects that change in phenotype has for the AVIC. Items in bold are specifically address in this work. ox-LDL=oxidized low density lipoproteins, ACE=angiotensin converting enzyme, NO=nitric oxide, GAGs=glycosaminoglycans, MMPs=matrix metalloproteinase, TIMPs=tissue inhibition of metalloproteinases.

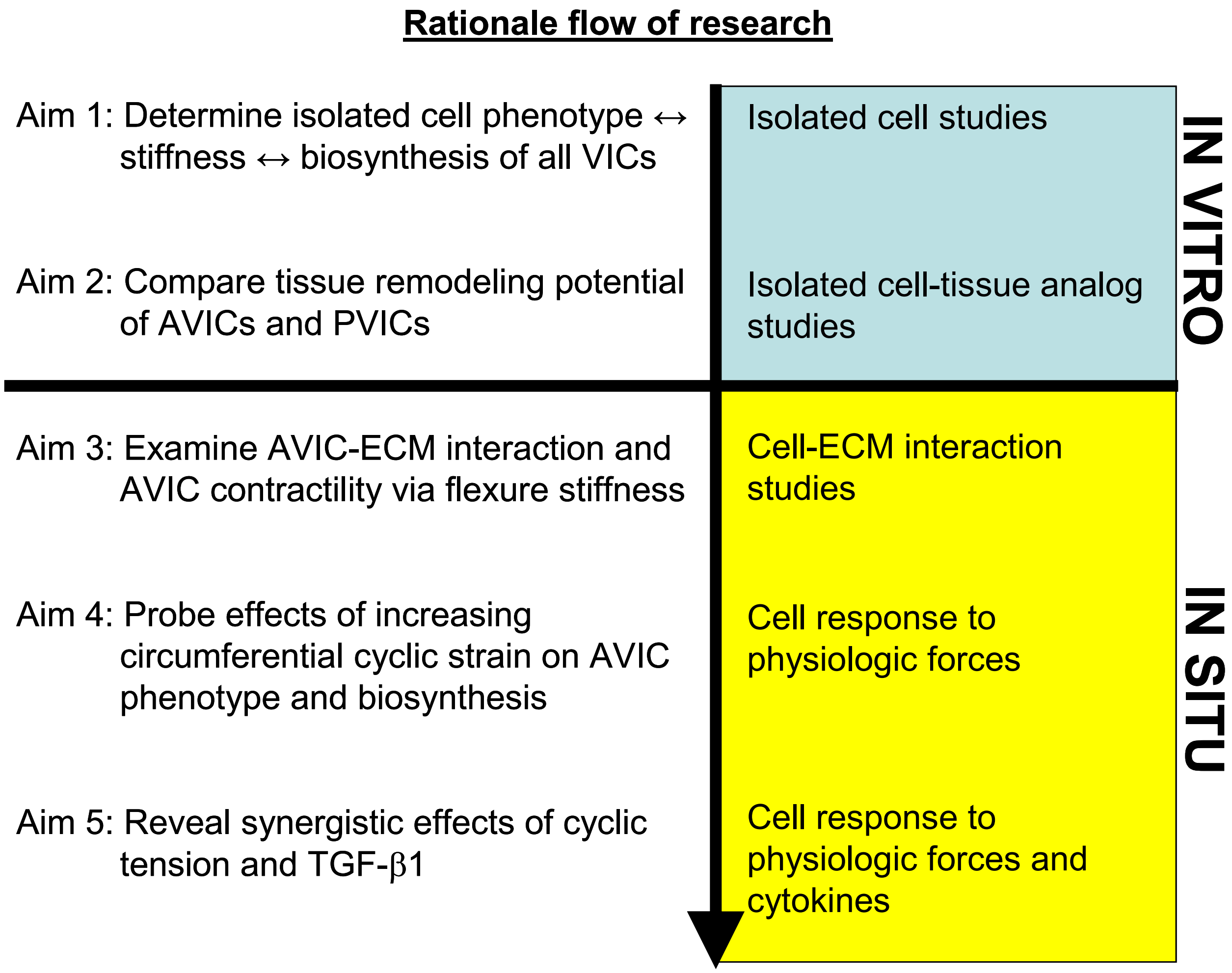

Figure 15. Rationale for the sequence of Aims and studies preformed. Aims 1 & 2 are comprised of *in vitro* experiments with isolated cells to elucidate essential physiologic differences between VICs from different valves. The *in situ* portion of the work (Aims 3-5) examines the micromechanics of the cells, their environment under different loading scenarios, and their subsequent phenotype and biosynthetic performance.

The specific aims of this study were as follows:

1. **Determine the correlation between VIC stiffness and biosynthesis in all heart valves.** We hypothesized that VICs respond to physiological tissue stresses *in vivo*, which are a direct function of transvaluvluar pressure, by altering cell stiffness via cytoskeletal composition, and that this relationship, in turn, affects collagen biosynthesis. To test this hypothesis, cell stiffness was determined by micropipette aspiration and cytoskeletal

quantity and collagen production of the VICs were quantified with surrogates SMA and heat shock protein 47 (Hsp47), respectively.

2. **Determine the tissue remodeling potential of AVICs in comparison to PVICs *in vitro*.** We hypothesized that AVICs and PVICs will reveal differential remodeling capabilities, as indicated by contraction of VIC seeded free-floating collagen gels. Further, as we have previously examined stiffness differences between the VIC populations with the micropipette aspiration technique, we sought to extend our understanding of the VIC mechanical properties by utilizing a monolayer-seeded configuration and atomic force microscopy (AFM).

3. **Determine the AVIC-ECM connectivity and biomechanical contribution of the contractile AVIC to leaflet bending stiffness *in situ*. W**e hypothesized that the AVIC population would present a significant effect on leaflet stiffness in the contracted and relaxed (basal tonus inhibited) state when tested under flexure at low strains. Evaluating valve leaflet tissue under flexure offers two advantages over uniaxial tension tests: (1) it is highly sensitive at very low strains and stresses, and (2) it allows one to probe the mechanical properties of different layers since bending in opposite directions will reveal variations in tensile and compressive layer properties.

4. **Determine the *in situ* micromechanical environment of the AVIC under varying degrees of circumferential strain and the possible effects of cellular stress overload.** We hypothesized that elevated levels of circumferential cyclic strain may affect AVIC

phenotype and subsequent collagen biosynthesis. To test this hypothesis, porcine AVLs received 3 and 6 day treatments of 0, 10, and 20% circumferential cyclic strain levels at 1Hz. To elucidate the resulting deformation of the AVICs and their nuclei at these strains, fresh tissues were fixed at the same strain levels and examined under TEM.

5. **Determine the independent and synergistic effects of cyclic tension and TGF-β1 on the AVIC *in situ*.** We hypothesized that both cyclic, circumferential tension and TGF-β1 are modulating factors for the in situ AVIC phenotype and resulting biosynthetic state; hence, each were examined independently and in concert to determine their resulting isolated and synergistic effects. This was accomplished by exposing circumferential AVL tissue strips to extended tissue cultures combinations of mechanical and/or cytokine treatments and afterwards assaying AVIC contractile and synthetic proteins, bioactive TGF-β1, and performing standard histology for ECM composition.

2.0 CORRELATION BETWEEN HEART VALVE INTERSTITIAL CELL STIFFNESS AND TRANSVALVULAR PRESSURE: IMPLICATIONS FOR COLLAGEN BIOSYNTHESIS

As mentioned in the Introduction, the transvalvular pressures (TVPs) on the left side heart valves (AV and MV) are far larger than on the right side heart valves (TV and PV). In the AV, TVPs above ~5 mmHg predominately result in ECM compaction as the collagen fibers become uncrimped and taut [20]. From this ECM compaction, significant changes in the AV interstitial cell (AVIC) nucleus aspect ratio have been observed with increasing pressures [84]. The majority of valve interstitial cells (VICs) within mammalian heart valve leaflets can be categorized as myofibroblasts, due to their dual phenotypic characteristics of both fibroblast and smooth muscle like cells [76, 78, 94, 95]. While the significance of this dualistic nature is not fully understood, the VIC's multifunctionality has been speculated to facilitate cell-cell communication, tissue remodeling, wound healing, and contraction [78]. It has been observed that VICs from healthy adult human and ovine valves were predominantly fibroblastic, whereas fetal and diseased valves contained VICs which were 'activated' and contractile [81]. Thus, it is believed that when the phenotype of the resident VIC population is myo-like, the cells are actively remodeling the ECM; hence, their contractility may be a function of their biosynthetic activity. This indicates that the VIC phenotypic state at any given time is likely related to the current remodeling demands of the tissue [80].

The primary tensile load bearing ECM component in heart valve leaflets is type I collagen [96, 97]. The rate of typical collagen biosynthesis in bovine valve leaflets has been previously studied [98] with the MV demonstrating the highest level of hydroxyproline expression, while all the leaflets demonstrated comparable collagen contents. This finding suggests that the collagen of the MV has the highest rate of turnover of all the valves. In a separate study, normal, floppy, and rheumatic MVs were labeled in an organ culture with ^{14}C-proline to determine if there was appreciable differences in collagen biosynthesis between the VIC populations [99]. Both floppy and rheumatic leaflets had a significant increase in the rate of collagen synthesis and total protein content compared to normal valves. There was no significant difference in DNA content in either abnormal state, suggesting that the VIC population was not larger but was indeed making more collagen. Hence, it appears that the VIC likely plays an important role in various valve pathologies according to their synthetic state.

Plated AVICs have been observed to deform silicone substrates in the presence of vasocontricting drugs [76]. Additionally, this population has been shown to generate small but measurable forces at the tissue level due to vasocontraction while under uniaxial tension [100]. Cultured human AVICs have demonstrated increased proliferation and collagen synthesis in the presence of vasoconstrictors [101]. This finding has lead us to speculate that the contractile state of VICs is related to the corresponding biosynthetic levels, and ultimately valve ECM homeostasis. However, it has not been shown that these two are indeed correlated. Moreover, the distinct TVPs experienced by the right and left side heart valves suggest different leaflet tissue stress levels, resulting in varying local VIC stress fields. Thus, examination of the VICs from each leaflet provides an excellent scenario for determining the relationship between tissue stress, VIC stiffness, and related biosynthetic activity.

We thus hypothesize that VICs respond to physiological tissue stresses *in vivo*, which are a direct function of TVP, by altering cell stiffness via cytoskeletal (CSK) composition, and that this relationship, in turn, affects collagen biosynthesis. This stiffness-synthesis relationship presumably exists since higher tissue stresses in the left side valves require greater amounts of collagen to be synthesized for proper valve leaflet tissue homeostasis. In the present study, cell stiffness was determined by micropipette aspiration and CSK quantity and collagen production of the VICs were quantified with surrogates SMA and heat shock protein 47 (Hsp47), respectively. Our goal in the present work was to conduct an initial study to investigate VIC functionality by examining isolated cells from healthy hearts.

2.1 PROTOCOLS

2.1.1 VIC Isolation and Cell Culture

Ovine hearts (N=5) from young sheep (~10 months, ~150 lbs, Animal Technologies, Inc., Tyler, TX) were shipped in PBS containing antibiotics at 4°C and dissected within 24 hours of euthanasia. Hearts were grossly dissected in a laminar flow biologic safety cabinet using sterile materials. From each valve, all leaflets were excised and each was individually placed in a 35mm tissue culture dish; mitral leaflets were halved as they are significantly larger than the other leaflets. Standard tissue culture medium was used (DMEM, 10% FBS, L-glutamine supplement, all from Mediatech, Inc., Herndon, VA), and antibiotic concentrations were doubled while the leaflets remained in the culture wells to prevent infection (200μg/mL penicillin-streptomycin and 2μg/mL amphotericin B, Mediatech, Inc., Herndon, VA). The dishes were housed in an incubator at 37°C, 5% CO_2, and the media was changed every 2 days. When VICs appeared, the leaflets were removed from the dishes and cells from the same valve were combined and replated in culture media with normal antibiotic levels (day 5). Endothelial cells were believed to be abolished after this culture time since the media used was not optimal for endothelial cell survival [102, 103]. VICs were carried to approximately 80% confluence, and after 12 days, the cells were trypsinized and cryopreserved at -80°C in DMEM with 10% DMSO. Cells from each valve were divided into two groups for mechanical testing and protein quantification. The cells were thawed and plated simultaneously so that the plating time for both mechanical testing and protein assay populations were the same (5 days).

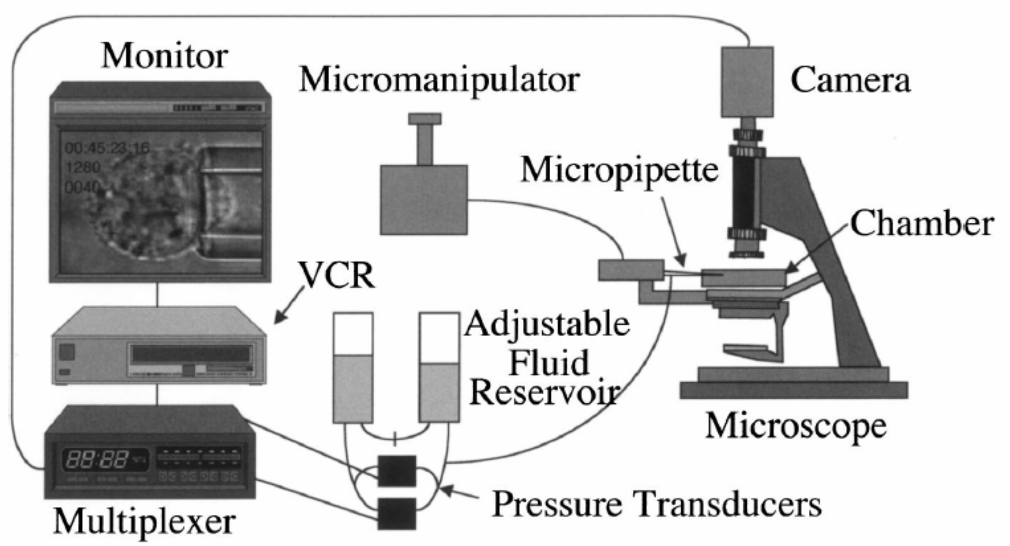

Figure 16. Micropipette aspiration system schematic. Taken from [104].

2.1.2 Micropipette Aspiration of VICs

Micropipette aspiration has been used to determine the mechanical response of multiple cell types [104-109], and the experimental setup (**Figure 16**) used here has been described previously [110]. Briefly, cells were trypsinized, pelleted (1500 rpm, 5 min), and resuspended in media prior to testing. For each population, 80μL of cell suspended media was aspirated and placed in a chamber that allows entry of a pipette from the side [108]. Capillary tubes (A-M

Systems, Inc,. Carlborg, WA) were fabricated into micropipettes with a pipette puller (David Kopf Instruments, Tujunga, CA) and then fractured with a microforge to achieve an inner diameter of 6-9μm. The micropipettes were then coated with Sigmacote (Sigma, St. Louis, MO) to prevent cell adhesion.

Pressures were applied to the surface of a VIC through the micropipette via a custom-built water reservoir with an in-line pressure transducer having a resolution of 1 Pa (Model no. DP15-28, Validyne Engineering Corp., Northridge, CA). While pressure was applied, digital images of the cell aspiration were recorded to a DVD-R with a CCD camera (COHU, San Diego, CA) through a bright-field microscope (Diaphot 300, Nikon Inc., Melville, NY), using either a 40x or 60x oil immersion objective and a 10x wide field eyepiece (Edmund Scientific Co., Barrington, NJ). Applied pressure and time were both displayed on a video monitor using a digital multiplexer (Vista Electronics, Ramona, CA). Pipette inner diameter, cell diameter, and aspiration length was determined with single frame digital images analyzed after testing (SigmaScan, Systat Software Inc., Point Richmond, CA).

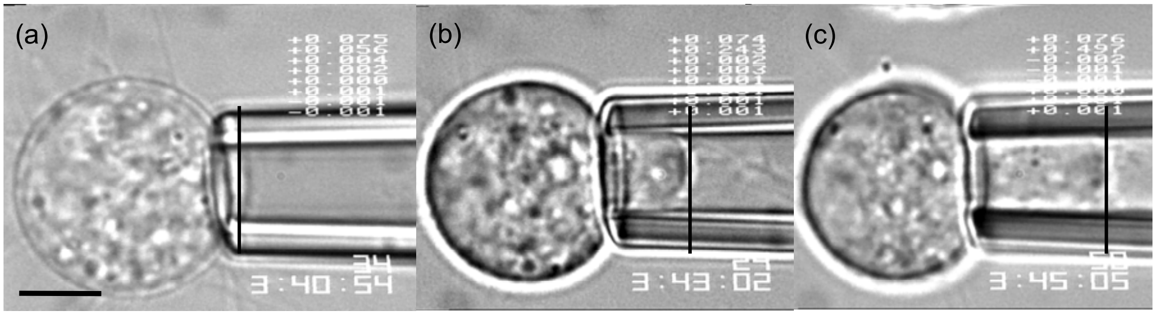

Figure 17. TVIC under micropipette aspiration at (a) Initial tare pressure (56 Pa), (b) 1st pressure step increase (243 Pa), and (c) 2nd pressure step increase (497 Pa). Drawn vertical bars show aspiration length. Horizontal reference bar equals 5μm.

Aspiration of VICs was achieved in a three step process: 1) initial tare pressure (~50 Pa, 60 s, **Figure 17a**) to assure that a seal was formed between the micropipette and the cell, 2) first instantaneous pressure step increase to ~250 Pa for 120 s (**Figure 17b**), and 3) second instantaneous pressure step increase to ~500 Pa for 120 s (**Figure 17c**). At the end of each step, the applied pressure and aspirated length of the cell was recorded.

2.1.3 Derivation of the Theret Model for Cell Stiffness with Micropipette Aspiration

Analysis of cell deformation with micropipette dates back to the mid-1970s with Evans and Hochmuth's seminal studies on erythrocyte membrane viscoelasticity [109, 111-115]. As red blood cells are suspended in blood, examining their properties with micropipette aspiration was very advantageous as it very closely mimicked the physiologic *in situ* state. Their methods were soon adapted for analysis of endothelial cell viscoelasticity by Nerem and others [106, 116-118]. From their work, a homogeneous half-space model for analysis of endothelial cells was proposed [119]. This model was needed in order to form a comparative framework of analysis for endothelial cells that had been exposed to various flow states and therefore had altered geometrical configurations (elongation). As evidenced by the title of the paper, the work was focused on the development of a homogenous model which utilized a half-space, as opposed to a plate model which was deemed as tractable but much more complicated.

The Theret model, as it will be referred to here, uses idealized loading of a tensile stress applied over a circular region, which is equilibrated by the stress distribution in the contact zone of the cell and micropipette. Additionally, two variations of the Theret model have been considered: the force model and the punch model. We will deal with the punch model here as it has a more physically realistic boundary condition of no slip in the contact zone versus the boundary condition of constant force over the contact zone of the force model. The characteristics of the micropipette, for the use of this model, are contingent upon the inner and outer radii being much less than the dimensions of the cell and the radius of curvature of the cell in the vicinity of the contact zone. This boundary condition imposes that the cell surface displacement (U_z) is equal to zero within the contact zone (**Figure 18**). The simplified explanation which follows can be seen in its entirety in [119].

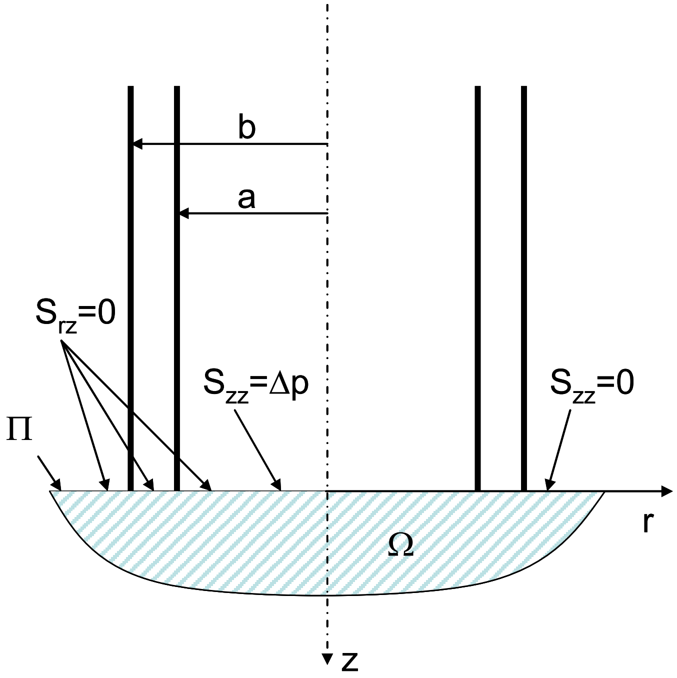

Figure 18. Schematic of the Theret punch model and boundary conditions. Ω represents the half-space of the cell and Π denotes the boundary of Ω. S_{zz} and S_{rz} represent stresses (in cylindrical coordinates). a and b are inner and outer radii of the micropipette, respectively.

The governing equations for an isotropic, incompressible elastic medium in the absence of body forces is written as

$$\begin{aligned} &\operatorname{div} S = 0 \\ &e = \frac{1}{2}[\operatorname{grad} U + (\operatorname{grad} U)^T] \\ &\operatorname{div} U = 0 \\ &S = -p1+2\mu e \end{aligned} \qquad \text{(Eq.1).}$$

Here, S denotes the stress tenor, U the displacement vector, and e the infinitesimal strain tensor. The first of the four equations is the equilibrium equation, the second relates the infinitesimal strain to the symmetric portion of the displacement gradient, and the third stipulates incompressibility. The fourth is the form of the stress-strain relation appropriate for an incompressible medium. –p represents the mean stress, which is indeterminate. Modulus of rigidity (μ) is related to the Young's modulus through

$$\mu = \frac{E}{3} \qquad \text{(Eq. 2).}$$

As the model is axisymmetric, it is beneficial to use polar coordinates (**Figure 18**) where displacements are U_r and U_z; strains are e_{rr}, e_{zz}, and e_{rz}; and stresses are S_{rr}, S_{rz}, and S_{zz}. Therefore, the boundary conditions are as follows:

$$\begin{aligned} &S_{zz}\,(r,0) = \Delta p \text{ for } 0 \le r < a, \quad S_{zz}\,(r,0) = 0 \text{ for } r > b \\ &U_z\,(r,0) = 0 \text{ for } a < r < b \qquad \text{(Eq. 3).} \\ &S_{rz}\,(r,0) = 0 \text{ for } 0 \le r < b \end{aligned}$$

The overall complexity can be reduced to a boundary-value problem with a single scalar field which is identified as a constant multiple of one of two displacement potentials in for half-space problems where only normal surface loads are present [120]. This is represented by

$$U = \frac{1}{2\mu}(z \text{ grad } \Psi - \Psi e_z) \text{ on } \Omega \qquad \text{(Eq. 4)}$$

where e_z denotes a unit vector in the z-direction, and $\Psi = \Psi\,(r,z)$ satisfies

$$\nabla^2\, \Psi = 0 \text{ on } \Omega \qquad \text{(Eq. 5)}$$

and set

$$p = \frac{\partial \Psi}{\partial z} \qquad \text{(Eq. 6).}$$

It follows that div U = 0 on Ω. Therefore, if the following is set

$$\begin{aligned} &e = \frac{1}{2}\,[\text{grad } U + (\text{grad } U)^T] \\ &S = -p1 + 2\mu e \end{aligned} \qquad \text{(Eq. 7)}$$

it follows that the governing (Eq. 1) equations are satisfied.

The follow gives the displacements in cylindrical components and in terms of Ψ,

$$U_r = \frac{1}{2\mu} z \frac{\partial \Psi}{\partial r},\; U_z = \frac{1}{2\mu}(z\frac{\partial \Psi}{\partial z} - \Psi) \qquad \text{(Eq. 8)}$$

and the components of stress are represented by

$$S_{rr} = -\frac{\partial \Psi}{\partial z} + z\frac{\partial^2 \Psi}{\partial r^2},\ S_{zz} = -\frac{\partial \Psi}{\partial z} + z\frac{\partial^2 \Psi}{\partial z^2},\ S_{rz} = z\frac{\partial^2 \Psi}{\partial r \partial z} \qquad \text{(Eq. 9).}$$

To move forward in the solution of this problem, it is necessary to introduce the potential

$$\chi = \frac{1}{\Delta p}\Psi \qquad \text{(Eq. 10).}$$

With equations c, e, and i, χ is found to be the solution to the mixed boundary-value problem

$$\begin{aligned} &\nabla^2 \chi = 0 \text{ on } \Omega \\ &\frac{\partial \chi}{\partial z} = 1 \text{ for } z = 0 \text{ and } 0 \leq r < a \\ &\frac{\partial \chi}{\partial z} = 0 \text{ for } z = 0 \text{ and } r > b \\ &\chi = 0 \text{ for } z = 0 \text{ and } a < r < b \end{aligned} \qquad \text{(Eq. 11).}$$

To reduce the system of mixed problems above to a linear integral equation, the following adapted scheme was devised in the 1960's by Collins [121]

$$g(t) + \frac{1}{\pi^2}\int_0^a \frac{g(S)}{t^2\text{-}S2}\left[2 \sin\left(\frac{b\text{-}t}{b+t}\right)\text{-}2t\ln\left(\frac{b\text{-}S}{b+S}\right)\right] dS = -\frac{2}{\pi}t,\ 0 \leq t \leq a \qquad \text{(Eq. 12).}$$

In terms of g, the potential χ appears as

$$\begin{aligned} \chi(r,z) = {} & \frac{1}{2i}\int_0^a g(t)\left[\frac{1}{\left(r^2+(z\text{-}it)^2\right)^{1/2}} - \frac{1}{\left(r^2\text{-}(z+it)^2\right)^{1/2}}\right] dt \\ & + \frac{1}{2}\int_b^\infty j(t)\left[\frac{1}{\left(r2+(z\text{-}it)^2\right)^{1/2}} - \frac{1}{\left(r2+(z+it)^2\right)^{1/2}}\right] dt \end{aligned} \qquad \text{(Eq. 13).}$$

where

$$
\begin{aligned}
&\mathrm{j(t)} = \frac{2}{\pi}\int_0^a \frac{\mathrm{Sg(S)}}{\mathrm{t2\text{-}S2}}\,\mathrm{dS} = \frac{1}{\pi}\ \frac{\mathrm{g(S)}}{\mathrm{t\text{-}S}}\ \mathrm{dS},\ \mathrm{t} > \mathrm{b}\\
&\left(\mathrm{r}^2+(\mathrm{z}+\mathrm{it})^2\right)^{1/2} = \xi \mathrm{e}^{1/2\mathrm{i}\eta}\\
&\left(\mathrm{r}^2+(\mathrm{z}-\mathrm{it})^2\right)^{1/2} = \xi \mathrm{e}^{-1/2\mathrm{i}\eta} \qquad \text{(Eq. 14)}\\
&\xi \geq 0,\ 0 < \eta \leq \pi\\
&\xi^2\cos\eta = \mathrm{r}^2+\mathrm{z}^2-\mathrm{t}^2\\
&\xi^2\sin\eta = 2\mathrm{zt}
\end{aligned}
$$

The surface profile is described by

$$
\begin{aligned}
\mathrm{U_z(r,0)} &= -\frac{3\Delta \mathrm{p}}{2\mathrm{E}}\int_r^a \frac{\mathrm{g(t)}}{\sqrt{\mathrm{t}^2-\mathrm{r}^2}}\,\mathrm{dt} \text{ for } 0 \leq \mathrm{r} < \mathrm{a}\\
&= 0 \text{ for } \mathrm{a} \leq \mathrm{r} \leq \mathrm{b} \qquad \text{(Eq. 15)}\\
&= \frac{3\Delta \mathrm{p}}{2\mathrm{E}}\int_b^r \frac{\mathrm{j(t)}}{\sqrt{\mathrm{r}^2-\mathrm{t}^2}}\,\mathrm{dt} \text{ for } \mathrm{r} > \mathrm{a}
\end{aligned}
$$

and the contact pressure between the micropipette and the cell is given by

$$
\mathrm{S_{zz}(r,0)} = -\frac{\Delta \mathrm{p}}{\mathrm{r}}\frac{\mathrm{d}}{\mathrm{dr}}\left[\int_0^a \frac{\mathrm{tg(t)}}{\sqrt{\mathrm{r}^2-\mathrm{t}^2}}\,\mathrm{dt} - \int_b^\infty \frac{\mathrm{tj(t)}}{\sqrt{\mathrm{t}^2-\mathrm{r}^2}}\,\mathrm{dt}\right],\ \mathrm{a} < \mathrm{r} < \mathrm{b} \qquad \text{(Eq. 16).}
$$

The length is described as

$$
\mathrm{L} = -\mathrm{U_z(0,0)} = -\frac{3\Delta \mathrm{p}}{2\mathrm{E}}\int_0^a \frac{\mathrm{g(t)}}{\mathrm{t}}\,\mathrm{dt} \qquad \text{(Eq. 17).}
$$

To simplify the analysis and make apparent the role of the wall parameter in the model it is useful to introduce the following relation

$$
\mathrm{y(x)} = \frac{\pi}{\mathrm{a}}\mathrm{g(ax)},\ 0 \leq \mathrm{x} \leq 1 \qquad \text{(Eq. 18).}
$$

Using the integral equation for g (Eq. 11) and the relation above, the integral equation for y is

$$
\mathrm{y(x)}+\frac{2}{\pi^2}\int_0^1\left[\xi \ln\left(\frac{1+\eta\text{-x}}{1+\eta+\mathrm{x}}\right) - \mathrm{x}\ln\left(\frac{1+\eta\text{-}\xi}{1+\eta+\xi}\right)\right]\frac{\mathrm{y}(\xi)}{\mathrm{x}^2\text{-}\xi^2}\,\mathrm{d}\xi = -2\mathrm{x},\ 0 \leq \mathrm{x} \leq 1 \qquad \text{(Eq. 19).}
$$

From here, it is evident that y depends on a and b only through the wall parameter, η, and this is emphasized with the notation of $y(\xi;\eta)$ Therefore, form Eqs. 17 and 18 the following relationship is achieved

$$\frac{L}{a} = \frac{3\Delta p}{2\pi E}\Phi(\eta),\ \Phi(\eta) = -\int_0^1 \frac{y(\xi;\eta)}{\xi}d\xi \qquad \text{(Eq. 20).}$$

and through numerical integrations using Eqs. 17, 14, and 13 it can be found that value of $\Phi(\eta)$ is essentially ~2.1 for values of η from 0.1 to 1.

2.1.4 Determining Cell Stiffness with Micropipette Aspiration

From the previous section, the effective stiffness, E, of the cell was determined with a half-space model, to demonstrate the intrinsic stiffness of cell populations and was not intended to fully characterize the mechanical behavior of the cells. With this model, E of the cell is given by

$$E = \frac{3a}{2\pi}\frac{\Delta p}{L}\Phi(\eta) \qquad \text{(Eq. 21)}$$

where $\Phi(\eta)$ is defined as the wall function, and is set equal to 2.1 (dimensionless parameter calculated from the ratio of the pipette inner radius to the wall thickness); a is the micropipette inner radius and $\Delta P/L$ is determined from the slope of the applied pressure versus aspirated length of the cell.

2.1.5 Quantification of VIC Protein Levels

SMA and Hsp47, which interacts with procollagen in the endoplasmic reticulum (ER), were quantified by ELISA for CSK and synthesized collagen protein levels, respectively. Hsp47 is believed to bind to procollagen after it enters the ER and dissociates prior to secretion [122], and it has been shown that type I collagen synthesis is dependent upon Hsp47 levels [123]. In Rocnik et al., they demonstrated that selectively transfecting smooth muscle cells with a retrovirus containing Hsp47 cDNA resulted in increases of both intra- and extracellular steady state type I collagen production. Furthermore, Northern blots of total RNA from their cells showed a tandem increase in both Hsp47 and procollagen. Hence, Hsp47 was deemed a suitable surrogate for type I collagen in this study.

A 96 well plate was prepared by coating the entire surface of each well with 100μL of primary antibody. The primary antibodies were prepared as 2 ng/mL of monoclonal mouse anti-Hsp47 (Clone M16.10A1) or monoclonal mouse anti-SMA (all from AbCam, Cambridge, MA). The plate was wrapped in parafilm and incubated for 24 h at 20°C. Prior to use, each well was washed 4x with 400 μL of wash buffer (0.01% PBS-T). 400 μL of blocking buffer (1% BSA, 5% sucrose in 0.01% PBS-T) was added to each well and incubated for 1 h at 20°C. Wells were washed again 4x with wash buffer, allowed to air dry, and sealed in parafilm until used.

VIC populations were lysed with RIPA buffer (100mM Tris-HCl, 150mM NaCl, 1% DOC, 1% Triton X-100, 1 gm/mL SDS/dH_2O), scrapped, and placed on ice for 10 min. The solution was pelleted for 10 min at 14,000 rpm at 4°C. Following, the DNA was carefully removed with a P200 tip, and the supernatant was removed and stored at -20°C. Total protein was determined for each population with BCA kit (Pierce, Rockford, IL). 100μg/mL of VIC lysate protein was added to the wells along with 100 μL of antibody diluent (1% BSA, 0.1% PBS-T) and allowed to incubate at 20°C for 2 h; each sample was assayed in triplicate. Wells were washed 4x with wash buffer. 100 μL of detection antibody (polyclonal rabbit Hsp47 or polyclonal rabbit SMA, AbCam, Cambridge, MA) was added at 1:1000 with antibody diluent. Wells were washed 4x with wash buffer. 100 μL of tag antibody (goat anti-rabbit HRP, AbCam, Cambridge, MA) was added at 1:1000 with antibody diluent and 0.1% Tween. Wells were washed 4x with wash buffer. 100μL of TMB "Sure Blue" Peroxidase Substrate 1 (KPL, Gaithersburg, MD) was added for 20 min while covered. 50 μL of stop solution (1N HCl) was then added. CD31 was determined with a commercial ELISA kit (#850.710.192, Cell Science Inc., Canton, MA). Plates were read with a Versumax plate reader (Molecular Devices, Sunnyvale, CA) using a 4-PL curve with standards and samples at 450 and 570 nm (450 and 620 nm for CD31).

In order to demonstrate the actual *in situ* biosynthetic and cytoskeletal state of VICs, single leaflets from two additional ovine heart valves were assayed for SMA and Hsp47. Leaflets were acquired and assayed as above, with the exception that these were sonicated and homogenized. This was a key validation step that was intended to simultaneously show the difference between *in vitro* and *in situ* cell states, while also demonstrating that any changes resulting from *in vitro* isolation occurred proportionally among all the valves.

2.1.6 Statistics

Cell stiffness, dimensional measurements, and ELISA absorbance values are expressed as mean ± one standard error. Statistical differences were determined by one-way ANOVA test and group comparisons were determined with the Tukey *post-hoc* test; $p<0.05$ was deemed as statistically significant. Data correlations were determined from mean values using a Pearson-product moment correlation and are reported with the correlation coefficient, r, and the associated p value. (SigmaStat, Systat Software Inc., Point Richmond, CA). Variable pairs with positive correlation coefficients and p values below 0.05 tend to increase together.

2.2 RESULTS

2.2.1 VIC Stiffness

VICs from the four valves of two hearts (H1 and H2) were successfully tested, along with additional AVICs and TVICs from a third heart (H3). Stiffness results of VICs were pooled together to make up the total cell populations (TVIC, n=21; PVIC, n=17; MVIC, n=18; AVIC, n=25); pooling was deemed appropriate after no difference was found between VICs from the same valve source between hearts (i.e. AVICs were not different between H1 and H2). Average $\Delta P/L$ values for the VIC populations demonstrated two distinct mechanical responses (**Figure 19a**). The E values for AVIC ($E=0.449 \pm 0.024$ kPa) and MVIC (0.479 ± 0.025 kPa) populations were significantly stiffer ($p<0.001$, **Figure 19b**) than those of the PVIC (0.276 ± 0.023 kPa) and TVIC (0.285 ± 0.030 kPa) populations. No differences were found between the AVIC and MVIC stiffness, nor the PVIC and TVIC stiffness. Additionally, there were no differences between cell or micropipette diameters (**Figure 20a**) or the ratio of these two (**Figure 20b**). This indicates that there was not an influence from of the testing geometries on the results affecting the results.

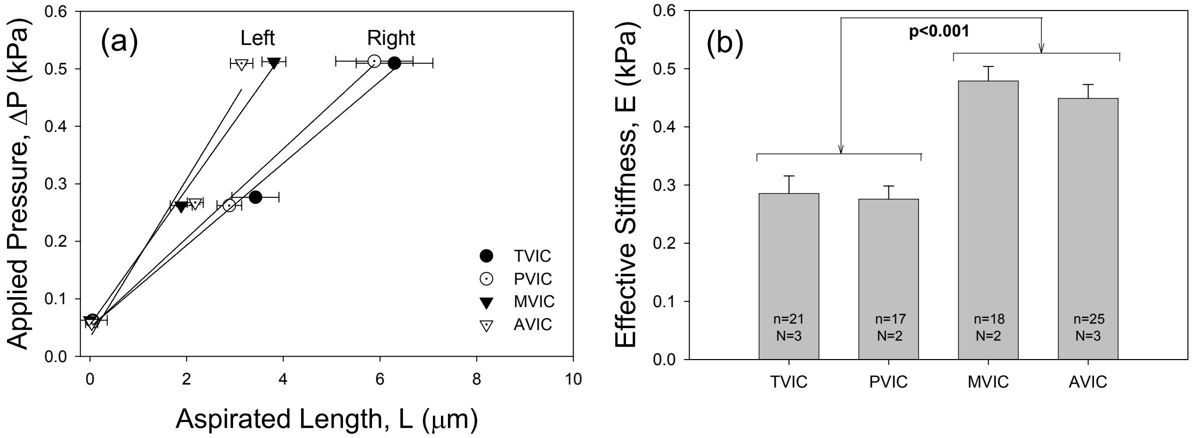

Figure 19. (a) Applied pressure versus VIC aspirated length. Note the distinct response between the left and right side VICs. (b) Effective stiffness, E, of VICs. There exist highly significant differences ($p<0.001$) in mechanical properties between the AVIC and MVIC populations and the PVIC and TVIC populations. N=hearts used and n=cells tested for each valve type.

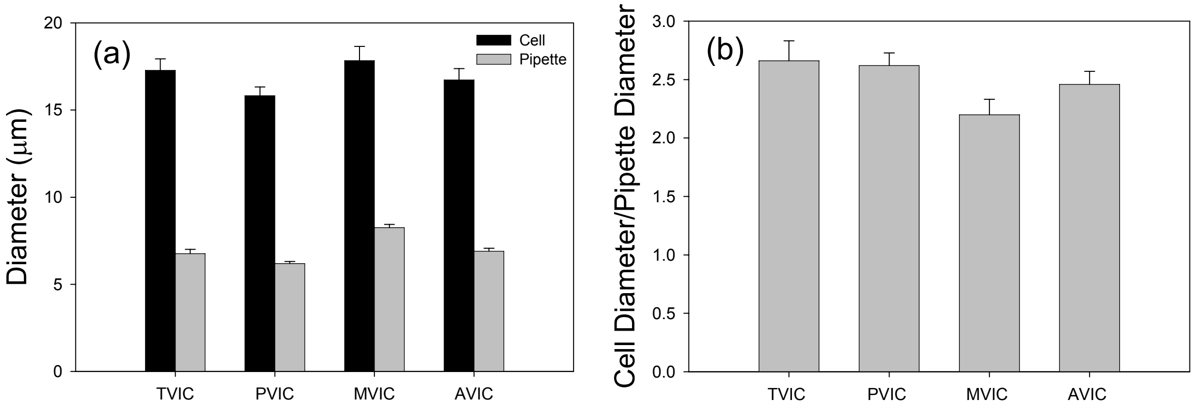

Figure 20. (a) Cell and pipette mean diameters. (b) Ratio of cell/pipette diameter. No significant difference was found between these ratios, emphasizing that changes in E (Eq. 1) were not biased by cell or pipette geometry.

2.2.2 VIC Protein Quantification

VICs from H1 and H2 were assayed for SMA and Hsp47 protein levels. ELISA absorbance results (in pg/mL) for each showed that, consistent with the stiffness results, the AVIC (SMA 616.77 ± 2.26, Hsp47 411.57 ± 2.35) and MVIC (SMA 612.68 ± 2.66, Hsp47 395.62 ± 2.21) protein levels were significantly greater ($p<0.001$) than the PVIC (SMA 495.63 ±

2.37, Hsp47 317.63 ± 4.86) and TVIC (SMA 367.18 ± 4.91, Hsp47 244.52 ± 3.58) proteins (**Figure 21a**). No differences were found between the AVIC and MVIC protein levels, nor the PVIC and TVIC protein levels. Additionally, the protein levels of *in situ* VICs (H4 and H5) revealed similar differences, with the left side valve proteins significantly greater ($p<0.05$) than the right side valve proteins (**Figure 21b**). There were also clear similar trends with increasing protein levels from the tricuspid to the AV in both the *in vitro* and *in situ* VICs (**Figures 21a and 21b**). However, the *in situ* VICs had a 3-fold greater level of both Hsp47 and SMA compared to the *in vitro* VICs. Note that PVL and MVL Hsp47 values were not statistically different (* denotes $p=0.786$, **Figure 21b**). Results from the CD31 ELISA (TVIC, 63.33 ± 12.29; PVIC, 95 ± 16.28; MVIC, 68.33 ± 23.30; AVIC, 76.50 ± 16.80) revealed that there were very few contaminating endothelial cells in any of the cultured VIC populations compared to the manufacturer's positive control (9608 ± 154), hence the tested cells were almost certainly fibroblasts or myofibroblasts.

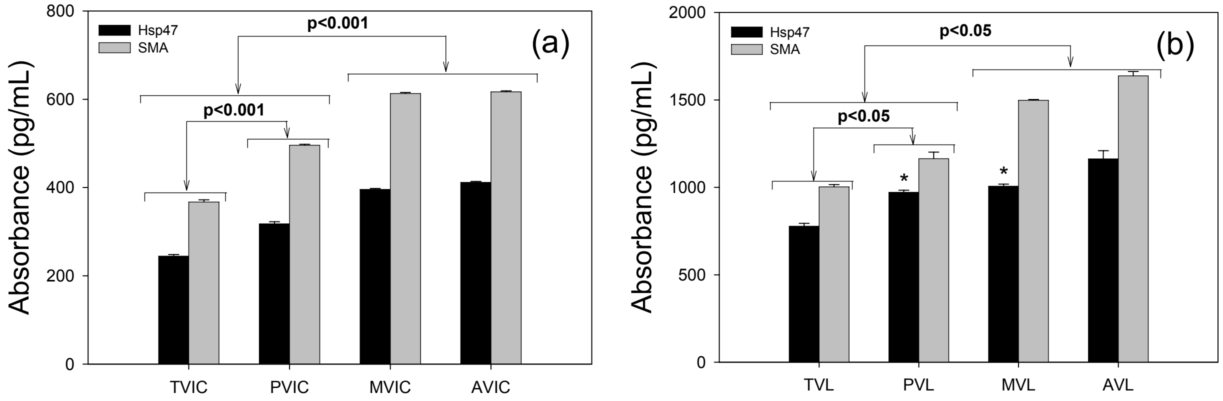

Figure 21. ELISA results for SMA and Hsp47. (a) SMA and Hsp47 absorbance from the in vitro VIC populations. Significant difference was found between the AVIC and MVIC populations compared to the PVIC and TVIC populations ($p<0.001$). Additionally, the PVIC protein levels were significantly greater than the TVIC levels. (b) SMA and Hsp47 absorbance from in situ VICs of explanted heart valve leaflets (TVL, PVL, MVL, AVL). Note the difference in the data range (y-axis) for the in situ VIC samples compared with the in vitro VICs. As with the in vitro VICs, the left side valve protein levels were significantly greater ($p<0.05$) than the right side valve levels, and the PVL levels were greater than the TVL. Hsp47 was not statistically different between the MVL and PVL groups (* denotes $p=0.786$).

2.3 DISCUSSION

2.3.1 Measured Differences between Right and Left Side VICs

This is the first known study to report VIC mechanical properties, as well as the possible implications of these measurements on valvular collagen biosynthesis. The findings of this study revealed that AVICs and MVICs are significantly greater than PVICs and TVICs with respect to cell stiffness, CSK protein content, and collagen production as determined by SMA and Hsp47 surrogates, respectively. These results represent an initial attempt to elucidate the differences in VIC function between the four heart valves. Though these *in vitro* measurements on isolated VICs provide an indirect examination of VIC functionality, they do serve to support the hypothesis that local stress does affect VIC mechanical and biosynthetic properties *in vivo*.

2.3.2 VIC Phenotypic Plasticity

The VIC phenotype has been observed to be both plastic and reversible depending on the remodeling state of the tissue due to development, disease, and adaptation [81]. In that study, it was found that 2.5% of the VIC population in normal adult human and ovine valves was SMA+, whereas the "developing/activated/diseased" states were significantly higher (19%-62% SMA+). Additionally, the phenotypic characteristics of AVICs have been shown as distinct from aortic smooth muscle cells in that they have increased ability to synthesize matrix components in collagen gels [69]. While it has long been known that the VIC phenotype is dualistic in nature [76, 78, 94], it has remained unclear what implications this has on valve function and biosynthesis.

It has been speculated that the contractility of the VIC population may serve in some biomechanical capacity with respect to valve function [100]. However, the contractile forces generated by the cells are many orders of magnitude below the forces imposed on the leaflets during normal valve function [100]. In addition, the delivery of endothelin-1 or KCl levels needed to elicit a measurable contraction within the leaflets is unrealistic *in vivo*. While VIC contractile forces are too small to affect valve function, it has been demonstrated that the vasoactive agent 5-hydroxytryptamine induces mitosis and collagen synthesis in cultured VICs [101]. Taken together, these studies reveal the VIC population as:

1) Phenotypically dynamic
2) Contractile when remodeling is necessitated
3) Mitogenic and secretory when contractility is induced by vasoconstrictors.

2.3.3 VIC Functional Correlations

The local stress-strain fields in the vicinity of a cell are highly dependent on a number of factors, including cell shape, orientation, and the relative properties of the cell and ECM [124]. Thus, it is not clear how the pressures imposed on different sides of the heart translate into local stress on the VICs. To answer this question a multi-scale mechanical analysis is necessary, which is a function of many factors including leaflet dynamic geometry [125], leaflet mechanical properties [19], tissue layer thickness and composition [97], and VIC-ECM connectivity. Clearly, proceeding from the organ to the cell and subcellular levels is a complex progression (**Figure 22**). Hence, predictions of the effects of TVP on cellular level stress are still largely speculative at this time, and sophisticated computational models and experimental validation data are needed to further describe this relationship.

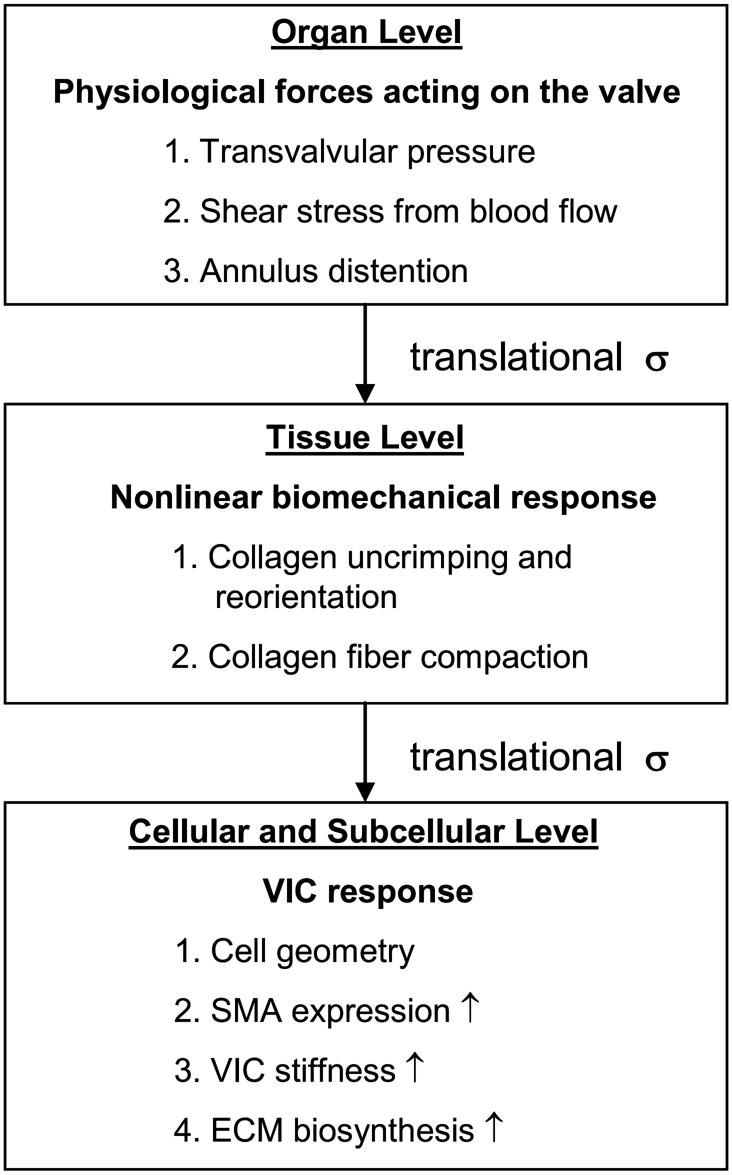

Figure 22. Hypothesized mechanism by which transvalvular pressure translates into local tissue stress on the VIC and the resulting response.

While we do not know the precise local VIC stress state, we believe that the higher left side pressures do translate into *some* increase in local stress on the VICs. For instance, when the VIC stiffness measured in this study is plotted versus the maximum TVP [83] experienced by the respective valves (**Figure 23a**), there appears to be a strong dependence on the stress level imposed on the cells (*r*=0.974 with p=0.026). Moreover, the normal AV leaflet is ~700 μm thick while the PV is ~400 μm thick. This 2-fold difference in thickness between the PV and the AV is small compared to the 8-fold difference in their resting TVPs, further suggesting that left side VICs are subjected to elevated stresses.

Relations between the CSK protein (SMA) and the collagen biosynthetic protein (Hsp47), were also strong (**Figure 23b**). The correlation coefficient for the SMA vs. Hsp47 relationship was *r*=0.996 with p=0.004. This relationship implies that VICs are responsive to their mechanical environment in order to maintain proper tissue homeostasis. The increased SMA in left side VIC populations suggests that the cells are adapted for the stresses imposed on them, while the increased Hsp47 is necessarily expressed to synthesize larger amounts of collagen, the primary structural component of heart valves. Furthermore, SMA and Hsp47 quantified from VICs *in situ* reveal a similar correlation, though not as strong (*r*=0.923, p=0.077, **Figure 23c**). More importantly is the fact that though the *in situ* VICs contain higher levels of both proteins, their relative levels remained consistent after the cells were isolated from the tissue. This result validates that the VICs tested *in vitro* retained the majority of their *in situ* characteristics.

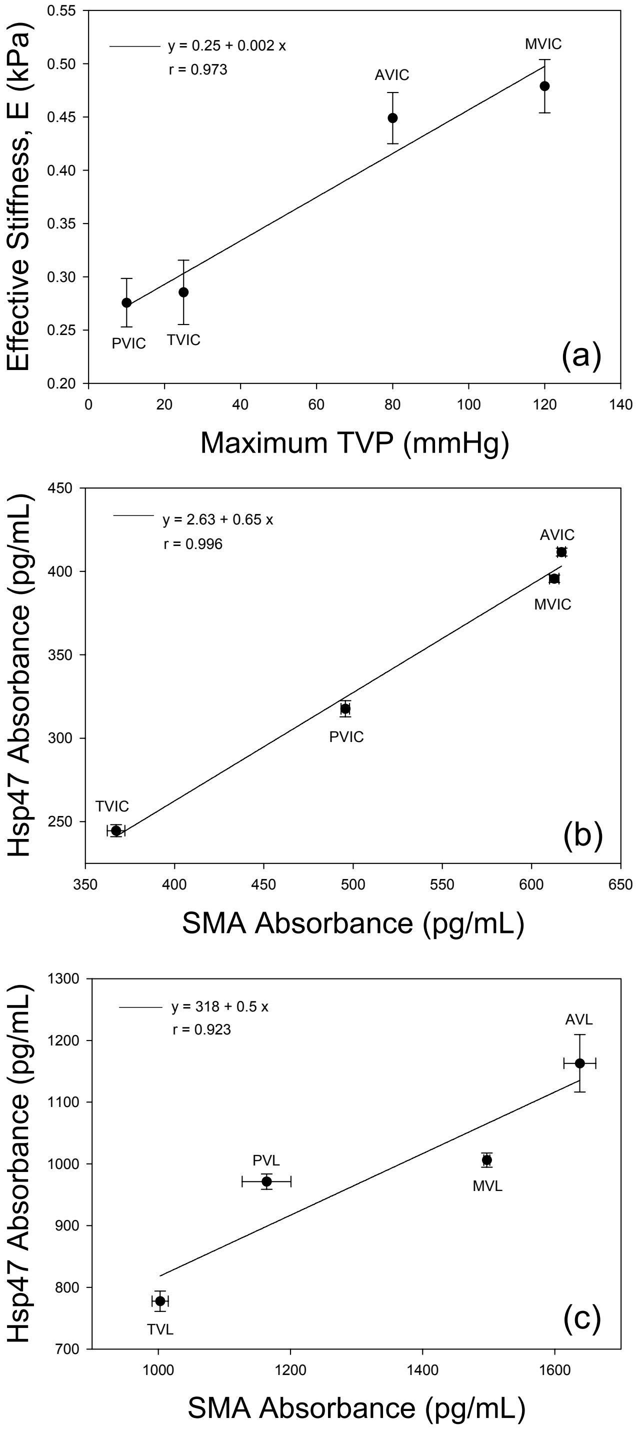

Figure 23. Functional correlations of E vs. TVP and Hsp47 vs. SMA. (a) Stiffness of VICs plotted versus maximum TVP (at rest) experienced by their respective valves. The correlation coefficient (r) for this relationship was 0.973. (b) Hsp47 absorbance versus SMA absorbance from in vitro VICs. Note the strong correlation between the two proteins (r = 0.996) as the one progresses from the right to the left side of the heart. (c) Hsp47 absorbance versus SMA absorbance from in situ VICs from heart valve leaflets (TVL, PVL, MVL, AVL). Though the protein levels were much higher (~3x) in the in situ VICs, note the similar slope of the linear regression when compared with (b). The correlation coefficient was less for the in situ VICs, however it was still good (r = 0.923)..

While our data show a strong correlation between SMA and Hsp47 of VICs, the mechanism underlying this relationship is not clear. It can be speculated that SMA (or Hsp47) expression is the byproduct of Hsp47 (or SMA) expression, or the two may be up-regulated simultaneously. The correlation coefficient found for this relationship simply indicates that the two are correlated, but does not assign one as the dependent variable.

A full explanation of the mechanisms behind these correlated protein expressions is beyond the scope of the current study; however, other groups have reported findings that shed light on this collagen-CSK relationship. Previously, it was found that in human wound closure, myofibroblasts were associated with thicker collagen fibers exclusively, and wound contraction, presumably facilitated by the SMA+ cells, contributed to 88% of closure [126]. In another study, human dermal fibroblasts expressed SMA upon confluence when plated in monolayer culture at low density; however, this expression was reduced by 50% when the cells were covered with a collagen lattice for 24 hours [127]. This finding was believed to be due to inhibition of cell-cell communication via cadherins, which was speculated to interrupt the communicative tension from cell to cell needed to maintain a contractile phenotype. Collagen fibril formation in vascular smooth muscle cells has been observed as dependent upon both integrins and actin filaments [128]. Forming fibrils were found parallel to actin microfilament bundles. Additionally, incubating the cells with cytochalasin D resulted in noinhibited collagen fibril assembly, while cells transduced with dominant-negative RhoA developed minimal collagen fibril assemblies. These findings using different myofibroblast cells support our results of VIC collagen synthetic activity as functionally linked to SMA content.

2.3.4 Limitations of Study

VICs in the present study may have different functional and biosynthetic properties than VICs *in situ* due to the platting technique used to isolate the cells. It has been previously found that VIC populations isolated in a similar fashion had increasing SMA+ cells with longer culture times [129]. To quantify the biosynthetic changes that were incurred due to the isolation of the cells, we compared the *in vitro* and *in situ* VIC protein levels. Our results demonstrate that with respect to SMA and Hsp47, the VICs were performing at a relatively normal, though diminished capacity *in vitro* (**Figures 23b and 23c**), and it should be noted that changes were proportional among all valves. Finally, the indirect methodology of quantifying collagen biosynthesis via the Hsp47 surrogate was utilized to avoid using radioisotopes, which are costly and potentially harmful. While previous works have shown a dependence of collagen biosynthesis on Hsp47 quantities at the RNA level [122, 123], the exact constitutive dependence of the relationship has not yet been determined to the authors' knowledge.

Cell stiffness may also be altered as the CSK filaments are relieved of stress at their focal adhesions when the cells are removed from the tissue. Additionally, the monolayer culture time used to expand the VICs (22 days) likely had an effect on the properties measured here. However, all VICs were obtained and cultured under identical conditions, which allowed for comparison between properties of the cells, and significant differences were apparent. While we hypothesized that these properties were different between the valves, we do not believe that the *in vivo* VIC can be fully described by these results. Ultimately, it would be most appropriate to measure cellular stiffness *in situ*; however, mechanical testing of intact cells is much more complex, as boundary conditions are difficult to define. Therefore, while we feel confident that our current results demonstrate actual differences in VIC mechanical behavior, one must be cautious to use these values for a comprehensive model of valve mechanics or remodeling capabilities.

2.3.5 Role in Valvular Physiology, Pathology, and Tissue Engineering

On the most fundamental level, our results suggest the physiological differences of VICs isolated from healthy ovine hearts. It is feasible that the stiffness-synthesis relationship that persists for VICs may be applicable to cells of other tissues exposed to cyclic loads (blood vessels, tendons, ligaments, myocardium, etc.). With regard to valve physiology and pathology, this normal VIC functional relationship is likely not conserved in degeneratively diseased or genetically malformed valves (*e.g.* bicuspid aortic leaflets) as they typically present with fibrosis and altered collagen architectures, respectively. In fact, over-expression of Hsp47 has been found in multiple fibrotic diseases and is associated with fibrosis following myocardial infarction [130]. This finding has led to the suggestion that Hsp47 is a potential biomarker for a number of diseases, and we speculate that heart valves may appropriately be added to this repertoire of aforementioned tissues that are prone to fibrotic disease.

Defining the functional endpoints of engineered tissues from native tissue states based on the properties and function of native tissues has been understudied to date. The relations shown here may serve as a useful index of VIC functionality for tissue engineered heart valves (TEHVs). Currently, most TEHVs are constituted from non-valvular cell sources and monitoring their adaptation during development is critical. As this study involved young healthy sheep, the *in vitro* development of a TEHV could be compared to this relationship to determine if TEHV cells are experiencing proper local tissue stress. For instance, a tissue engineered PV would not require the same developmental endpoint before implantation that a tissue engineered AV would.

Hence, this SMA-Hsp47 relationship could prove beneficial for assigning homeostatic cellular endpoints and tracking VIC destiny under different loading regimes.

2.3.6 Summary

This work is the first to report VIC stiffness and the correlation with TVP, and the subsequent implications on biosynthesis of collagen proteins. These results suggest a conserved homeostatic VIC state from the right to the left side heart valves which are exposed to largely different TVPs. Additionally, demonstrated differences were observed between the *in vitro* and *in situ* VIC biosynthetic function, which reveals the effect of isolation and extended culture on VICs. Future work will aim at understanding the *in vivo* local stress environment of the VIC, with special attention given to the tensile loading strain rate, which is germane to valves only [131], and the cell-ECM junctions via integrins.

3.0 VISCOELASTIC PROPERTIES OF THE AORTIC VALVE INTERSTITIAL CELL

While the primary biomechanical function of the AV is at the organ level, the long term durability of the constituent tissues is maintained by the population of interstitial cells (AVICs). Due to the dynamic biomechanical environment in which AVICs reside, recent work has examined the mechanical stimuli-dependent biosynthetic and contractile response of these cells [132-134]. In these studies, many idealized assumptions have been made regarding the mechanical properties of the AVIC and their relation to the underlying cytoskeleton (CSK) [132, 133], cell-ECM connectivity [29, 100], and the in-vivo deformations during the cardiac cycle [84]. Ultimately, while all these assumptions are appropriate for initial studies, they have universally assumed that AVICs are elastic, homogenous materials.

The primary mechanical modes of loading of the AV leaflet are flexure during opening and closing, shear stress while open, and planar tension when closed. During diastole (closed valve) the AV is exposed to ~80 mmHg transvalvular pressure, which translates to ~250-400 kPa average tissue stress. We recently observed that valve interstitial cells from the aortic and mitral valves were significantly stiffer ($p<0.001$) than those from the pulmonary and tricuspid valves [132]. Moreover, AVICs undergo very large deformations during valve closure [84] which occur at very high rates, with AV opening and closure occurring in ~0.05 s [131].

In our previous study of AVIC mechanical properties [132], viscoelastic effects were ignored and only the equilibrium stiffness E_∞ was reported after signs of viscoelastic creep had apparently dissipated (>100 s). Hence, in the present study we sought to quantify AVIC viscoelastic properties using micropipette aspiration. We then performed simulations of loading during valve closure and subsequent creep and stress relaxation during diastole to estimate if viscoelastic effects play a significant role in AVIC deformation, and therefore mechanobiology.

3.1 PROTOCOLS

3.1.1 AVIC Isolation

Ovine AV leaflets were harvested from a young lamb upon sacrifice. The leaflets were dissected, surfaces scrapped with a razor blade to remove all endothelial cells, minced into 1x1 mm^2 pieces, and digested with collagenase A (Sigma, St. Louis, MO) for 30 min with gentle rotation (10 rev/min). Following digestion, the cell-tissue solution was strained with a 0.5 μm cell strainer. The population was plated in complete media (DMEM, 10% FBS, 1% pen/strept, and 0.5% fungizone, all from Gibco) for 10 days.

3.1.2 Viscoelastic Micropipette Aspiration of AVICs

The micropipette aspiration system and setup used here has been described previously [104, 132]. Briefly, AVICs were trypsinized, pelleted (1500 rpm, 5 min), and resuspended in media prior to testing. 80μL of cell suspended media was aspirated and placed in a chamber that allows entry of a micropipette from the side [108]. Capillary tubes (A-M Systems, Inc,. Carlborg, WA) were fabricated into micropipettes with a pipette puller (David Kopf Instruments, Tujunga, CA) and then fractured with a microforge to achieve an inner diameter of 7-9μm. Pressures were applied to the surface of an AVIC through the micropipette via a custom-built water reservoir with an in-line pressure transducer having a resolution of 1 Pa (Model no. DP15-28, Validyne Engineering Corp., Northridge, CA). While pressure was applied, digital images of the cell aspiration were recorded to a DVD-R with a CCD camera (COHU, San Diego, CA) through a bright-field microscope (Diaphot 300, Nikon Inc., Melville, NY), using a 40x oil immersion objective and a 10x wide field eyepiece (Edmund Scientific Co., Barrington, NJ). 11 AVICs were tested by applying a tare pressure of ~50 Pa for 60 s, then a single step pressure was applied for a final pressure of ~500 Pa. Aspiration length was recorded until the cell had reached equilibrium and no more displacement was detectable (~100 s).

3.1.3 Viscoelastic Models of AVIC Deformation

In much of the micropipette aspiration literature a standard linear solid (SLS) model is typically utilized under the assumption of instantaneously applied aspiration pressure [104]. However, the loading time for micropipette aspiration is finite, with the pressure ramped from zero to maximum over several seconds. We thus utilized Boltzmann superposition [135] to account for aspiration length creep during loading in the SLS model

$$L(t)=\int_0^t \frac{\phi a}{\pi k_1}\left[1-\frac{k_2}{k_1+k_2}e^{\frac{-t}{\tau_\varepsilon}}\right]\frac{dP}{d\tau}d\tau, \qquad \tau_\varepsilon=\frac{\mu(k_1+k_2)}{k_1k_2} \qquad \text{(Eq. 22)},$$

where ϕ is defined as the wall function (a dimensionless parameter calculated from the ratio of the pipette inner radius to the wall thickness) and is set to 2.1, a is the micropipette inner radius, dP is instantaneous differential step pressure, L(t) is the measured aspiration length at time t, and

k_1, k_2, and μ are the SLS model parameters. We refer to this model as the Boltzmann SLS (BSLS) throughout for clarity. The traditionally used SLS model simply employs a ΔP term and assumes application of a Heaviside step function such that the applied pressure is achieved at $t>0$. Parameter values were determined by fitting each t-L(t) experimental response with the BSLS and SLS models using the Marquardt Levenberg algorithm [136] (MathCad, MathSoft). From the parameters, the instantaneous stiffness $E_0=3/2(k_1+k_2)$ and equilibrium stiffness ($E_\infty=3/2\,k_1$) were determined.

3.1.4 Simulations of AVIC deformation under physiologic loading rates

With parameters determined for the BSLS and SLS, the following simulations were performed based on the micropipette aspiration test. Using a loading time for full AV closure of ~0.05 s [137], we estimated the AVIC deformation response at physiologic loading rates using a linear pressure ramp which applied a 500 Pa pressure in 0.05 s. Next, we explored the potential effects of AVIC viscoelasticity by simulating creep and relaxation over a typical diastolic time period (when the AV is closed and the AV tissue fully loaded) of 0.3 s. For creep, simulations proceeded from using the same loading history as described above, with the 500 Pa aspiration pressure held for an additional 0.3 s. Similarly, stress relaxation was quantified by applying a linear aspiration length ramp to the level achieved for that particular AVIC while loading in the micropipette aspiration experiments mentioned above in 0.05 s, then held for an additional 0.3 s. All results and parameter values are reported as mean ± standard error (SEM).

3.2 RESULTS

3.2.1 AVIC Time-Dependent Response to Micropipette Aspiration

The average applied pressure to the AVICs during the micropipette aspiration tests was 519 ± 36 Pa, and the average ramp time to apply the pressure was 2.48 ± 0.31 s. This applied pressure history resulted in an AVIC response similar to other cells, with a large initial change in aspiration length which began to plateau at ~60 s (**Figure 24**). Both model parameter values (**Table 1**) were typical of cells measured previously [104].

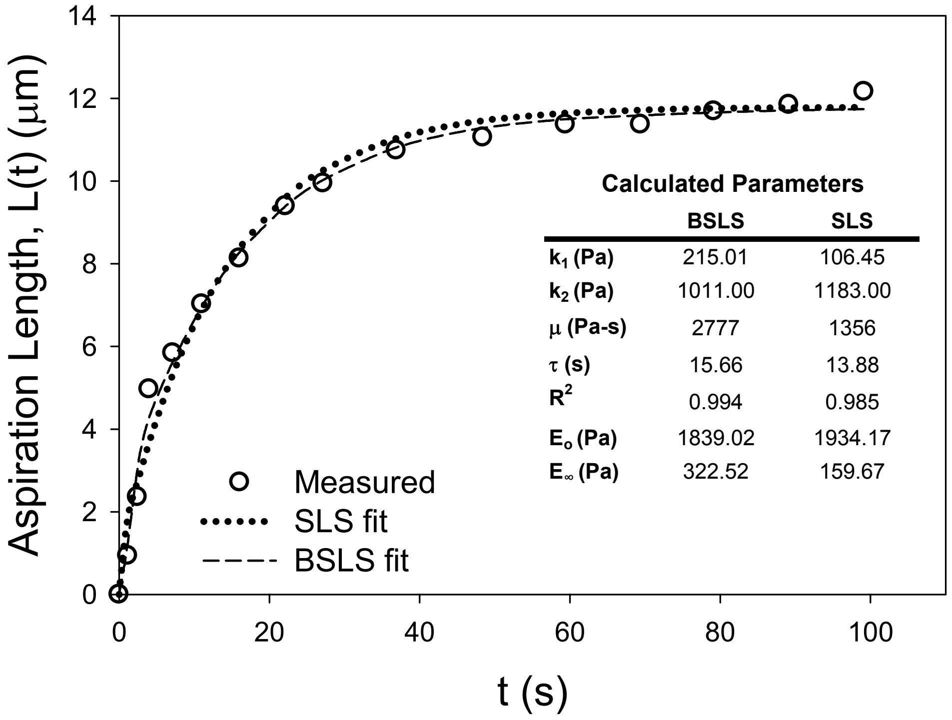

	BSLS	SLS
k_1 (Pa)	215.01	106.45
k_2 (Pa)	1011.00	1183.00
μ (Pa-s)	2777	1356
τ (s)	15.66	13.88
R^2	0.994	0.985
E_o (Pa)	1839.02	1934.17
E_∞ (Pa)	322.52	159.67

Figure 24. Representative response of an AVIC under micropipette aspiration (circles) with both the SLS and mSLS model fits. Inset stable shows determined parameters from both models.

Table 1. Calculated parameters from SLS and mSLS

n=11 AVICs	BSLS model		SLS model	
	AVG	± SEM	AVG	± SEM
k_1 (Pa)	188.32	49.36	119.83	20.16
k_2 (Pa)	613.88	130.52	650.65	92.68
μ (Pa-s)	3479.09	563.24	2591.18	368.13
τ (s)	37.04	7.02	31.08	5.31
R^2	0.980	0.003	0.967	0.004
E_o (Pa)	1203.29	262.11	1155.73	149.08
E_∞ (Pa)	282.48	74.05	179.75	30.25

3.2.2 AVIC Loading Simulations

To explore the rate dependent influence of viscous effects during AV closure, we simulated aspiration length-time responses for 0.05, 0.5, 2.5, and 5.0 s loading times using parameters determined for the AVIC and the BSLS model. For near physiological loading rates we observed little viscous effects (**Figure 25a**). At 0.5 s, there were negligible viscous effects (0.74 ± 0.21% increase) versus 0.05 s loading. However, at 2.5 and 5.0 s the viscous effects were very pronounced (36.59 ± 9.35% and 66.84 ± 15.20% increases, respectively) compared to the 0.05 s loading case (**Figure 25b**).

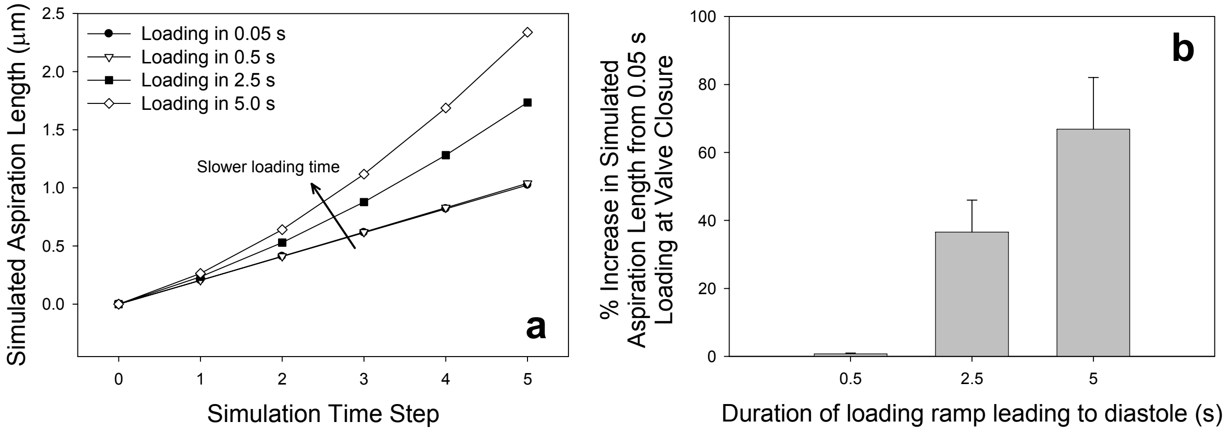

Figure 25. (a) Viscous effects due to varying simulation loading times for an AVIC at 0.05, 0.5, 2.5 and 5.0 s. (b) % increase in simulated aspiration length at the end of the applied pressure ramp versus 0.05 s. As loading time increases, viscous effects are more pronounced. While below 0.5 s viscous effects appear to be negligible, it is interesting to note that at 2.5 s, the time needed to apply pressure during the micropipette aspiration experiment, viscous effects are very pronounced.

3.2.3 Creep and Stress Relaxation Simulations

Using the BSLS and SLS models, the representative creep and stress relaxation simulations, respectively, are shown for the same cell (**Figures 26 and 27**). For the BSLS model, average creep during diastole was 4.65 ± 1.34%, and similarly, the average stress relaxation during diastole was 4.39 ± 1.12% (**Table 2**). These basic simulations suggest that during diastolic loading timescales viscous-dependent deformations can occur in AVICs. For the SLS model, average creep during diastole was 7.92 ± 1.88%, and similarly, the average stress relaxation during diastole was 7.35 ± 1.51% (**Table 2**).

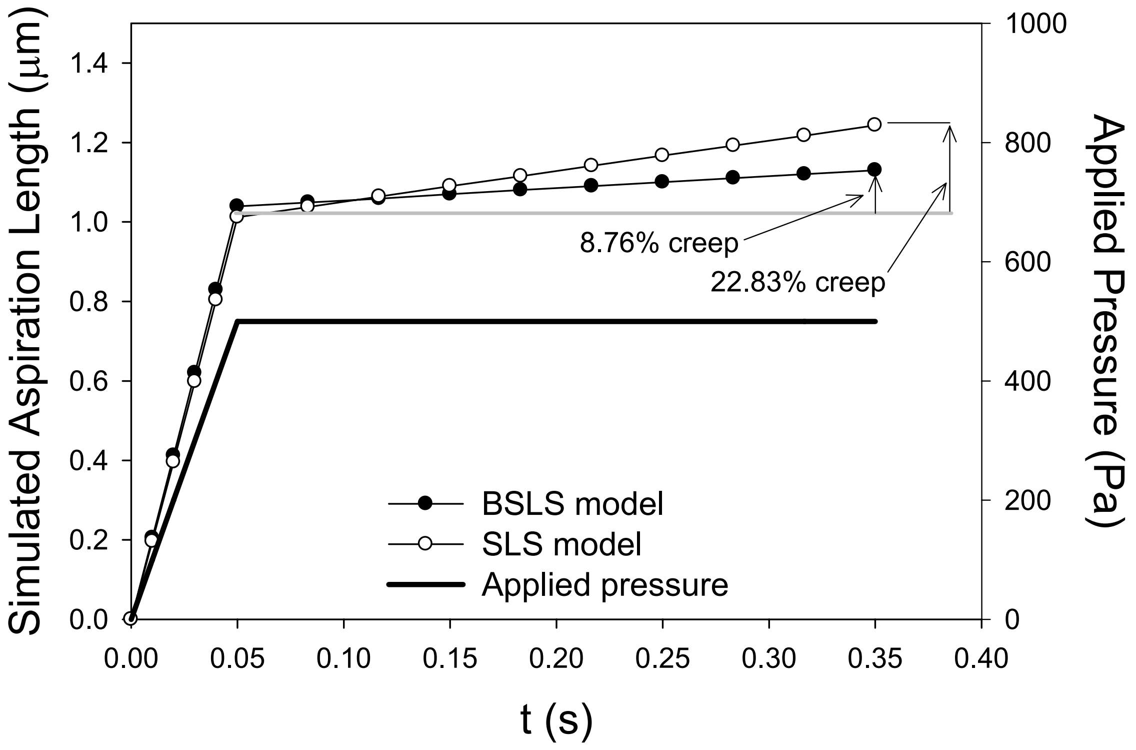

Figure 26. Representative creep simulation response for an AVIC loaded to 500 Pa in 0.05 s and held for 0.3 s using both the BSLS and SLS models.

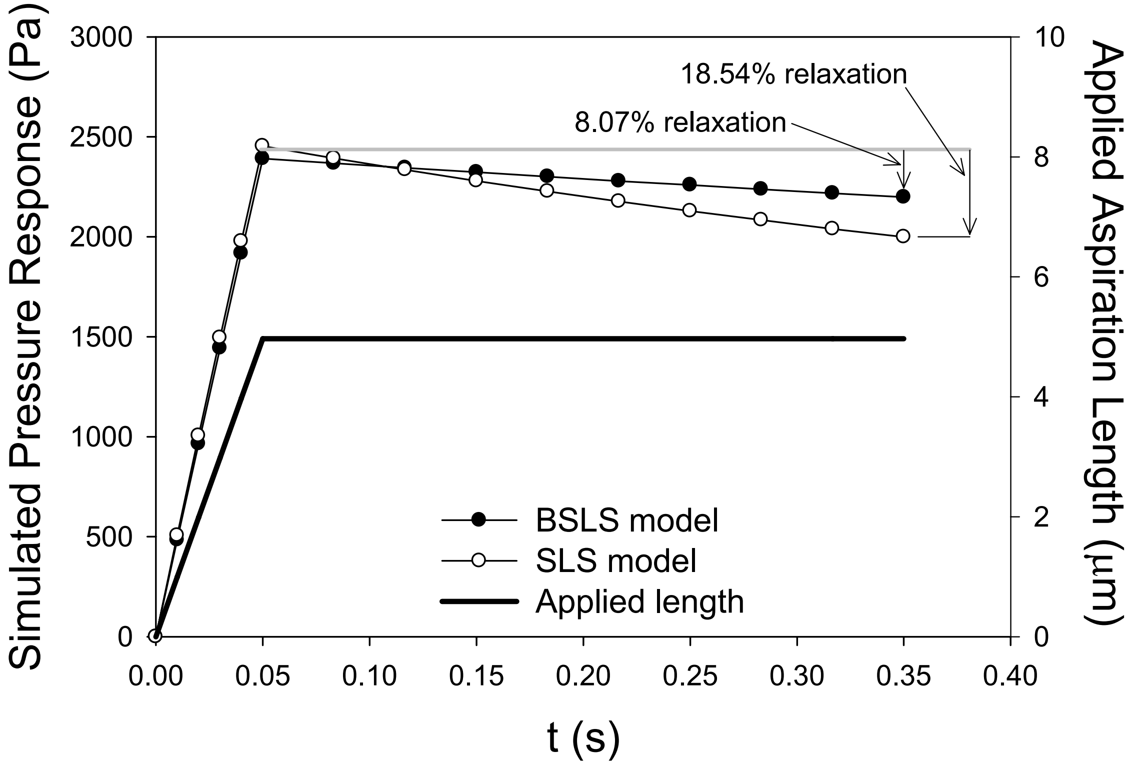

Figure 27. Representative stress relaxation simulation response for an AVIC aspirated to 2.3 μm in 0.05 s and held for an additional 0.3 s using both the BSLS and SLS models. Note that 4.96 μm was the actual aspiration length occurring for that AVIC during the micropipette aspiration experiments.

Table 2. Micropipette aspiration simulations of stress relaxation and creep using the parameters from Table 1. For both simulations, a loading time of 0.5 s was used, followed by a 0.3 s period where either L or P were held constant for stress relaxation and creep simulations, respectively.

Creep Simulations

n=11	BSLS Simulation			SLS Simulation		
	$L_{0.05s}$ (μm)	$L_{0.35s}$ (μm)	% creep	$L_{0.05s}$ (μm)	$L_{0.35s}$ (μm)	% creep
AVG	2.68	2.77	4.65	2.07	2.21	7.92
±SEM	0.58	0.59	1.34	0.31	0.31	1.88

Stress Relaxation Simulations

n=11	BSLS Simulation			SLS Simulation		
	$P_{0.05s}$ (Pa)	$P_{0.35s}$ (Pa)	% relaxation	$P_{0.05s}$ (Pa)	$P_{0.35s}$ (Pa)	% relaxation
AVG	1112.91	1035.18	4.39	1085.45	985.45	7.35
±SEM	273.82	233.96	1.12	154.01	117.92	1.51

3.3 DISCUSSION

3.3.1 Physiologic Relevance of AVIC Viscoelasticity

In the present study, AVIC viscoelastic behavior over physiological timescales was simulated using micropipette aspiration, a well established technique for the study of cell biomechanics. Our goal was to examine the potential for viscoelastic contributions to in-vivo deformation during AV loading, as well as changes during diastole when the AV is closed. A model incorporating Boltzmann superposition (BSLS) was used, as the rapid loading times (0.05 s) that occur in the valve could not be attained with the micropipette aspiration testing system. As the AVIC *in vivo* deformations have only begun to be explored [138], we used micropipette aspiration tests to emulate this response. Physiologic loading, creep, and stress relaxation simulations were performed as bounds on possible in-vivo AVIC behavior.

Interestingly, we observed that under physiologic loading time scales there were negligible effects of viscoelasticity on AVIC deformation (**Figure 25**). Not surprisingly, this result suggests that the 0.05 s loading times are sufficiently fast enough that no cellular strain rate effects occur. Interpretation of these results suggests an elastic response of the AVIC during physiologic loading times. Yet, under a diastolic time frame of 0.3 s, model simulations for creep and stress relaxation suggest that some degree of time-dependent deformation can occur (**Figures 26 and 27**). Thus, our simulation results suggest that, while not large, AVIC time-dependent deformations may occur when the AV is closed.

3.3.2 Use of Boltzmann Superposition for Micropipette Aspiration Analysis

While the use of Boltzmann superposition is routine in viscoelastic modeling [135] and utilized in most biomechanical testing modalities, it is surprisingly absent in most micropipette aspiration studies. The commonly used SLS model [104] ignores any creep that occurs during application of the pressure (~2.5 s in this study), which we believed to be important for study of the AVICs. The use of the SLS model in this case resulted in decreased parameter values for k_1 and μ and increased parameter value for k_2 versus the BSLS (**Table 1**). These changes in model parameters produced substantial differences in predicted creep and relaxation responses (**Figures 26 and 27**). While not large for valvular timescales, these results suggest that for AVIC mechanical studies one needs to be cognizant of time-dependent effects that occur during the experiment. Clearly, implementation of the correct model could prove beneficial for highly viscoelastic cellular studies.

3.3.3 Limitation of Study

Previously, the stiffness of ovine AVICs measured by micropipette aspiration [132] and porcine AVICs measured with atomic force microscopy (AFM) [133] has been reported. In the current study, micropipette aspiration was used to examine the viscoelastic properties of the ovine AVIC, which are primarily influenced by the cell membrane and unanchored cytoskeleton. From a biomechanics perspective, it can be argued that AFM gives a more accurate representation of the mechanical properties of the cell than micropipette aspiration as the cells are generally attached to an underlying substrate such that the CSK is extended and rigid as it is anchored at focal adhesions. This configuration is in contrast to testing with micropipette aspiration where the CSK is largely free and not in a physiologic state as the cells float in a solution. However, the AFM testing modality does not lend itself well to high speed testing and examination of viscoelastic properties.

Regardless of the specific testing modality, the biomechanical environment of the AVIC remains ill defined. Current evidence suggests that AVICs are tightly attached to the surrounding ECM [29, 139] and are subjected to substantial compression [138]. While the micropipette simulations utilized in this study clearly do not emulate the AVIC in-vivo environment, they do provide useful insight into the potential for time-dependent effects.

3.3.4 Summary

The viscoelastic properties of AVICs were measured for the first time using micropipette aspiration. Simulations using the micropipette aspiration loading configuration suggest the loading time for the AVIC is sufficiently fast that viscous effects are negligible. However, during diastole when the AV tissue is subjected to its largest planar stresses, viscoelastic effects may contribute to AVIC deformations. These results are believed to be important for mechanobiological studies of the AVIC, wherein the AV mechanical environment is being emulated.

4.0 DIFFERENCES IN TISSUE REMODELING POTENTIAL OF AORTIC AND PULMONARY HEART VALVE INTERSTITIAL CELLS

Heart valve interstitial cells (VICs) are important for their roles in valve physiology [77, 132, 140] and pathology [81, 141-144], and have come under increasing scrutiny in recent years as a design endpoint in the development of tissue engineered heart valves (TEHVs) [69, 80, 145, 146]. They are believed to be primarily responsible for the maintenance of the valvular tissue matrix through biosynthesis and enzymatic degradation. The biosynthetic demands in the different valves have been shown to be different and unique to each valve, thus depending on the local stress/strain environment of the VICs [132]. As is the case for most biosynthetic cells in a mechanically demanding environment, their mechanobiological response is related to the cell's cytoskeleton (CSK) structure and function. Hence, there is a need to examine the structural and functional properties of the aortic and pulmonary VIC (AVIC and PVIC, respectively) CSK for further understanding of valvular tissue remodeling.

Phenotypically, the VIC is usually referred to as a myofibroblast due to its dualistic expression of both fibroblast and smooth muscle cell markers (particularly, α-smooth muscle actin, (SMA)) [76, 78, 94, 147]. Yet, when observed histologically the population is typically heterogeneous with fibroblasts, smooth muscle cells, and the aforementioned myofibroblasts present. It is not clear if the population contains one or two distinct phenotypes [78], but recently it has been proposed that the VIC phenotype is both dynamic and reversible, depending on the synthetic requirements of the tissue in times of development, remodeling, or disease [81]. In healthy adult valves, the percentage of smooth muscle cells and myofibroblasts is low (~2.5%) compared to cells from valves that are in developing, diseased, or remodeling states (19-62%) [81]. This finding suggests that the phenotype of the VIC population is not only an indicator for the state of the valvular tissue, but also could be involved in the actual etiology for some types of pathology.

The physiologic importance of phenotypically dynamic and reversible VICs is not entirely clear, althougth it is generally believed that this plasticity is likely essential to effectively maintain valvular tissues under varying physiological states. Furthermore, while autologous VICs are not believed to be an ideal cell source for TEHV due of donor site morbidity, the chosen cell source's function will likely be paramount since it will form the de novo ECM and be responsible for subsequent repair and regeneration over time. Thus, understanding the mechanism by which VICs become contractile and remain in this state is undoubtedly a crucial functional endpoint in our continued progress towards a TEHV. Given the reported biosynthetic and mechanical differences between the VICs of the different heart valves [132], there is a need to understand the different remodeling capabilities between the semilunar VIC's.

Based on the above, in the present study we hypothesized that AVICs and PVICs will reveal differential remodeling capabilities, as indicated by contraction of VIC seeded free-floating collagen gels. Further, we have previously shown stiffness differences between the VIC populations [132] with the micropipette aspiration technique. To extend our understanding of the VIC mechanical properties, we utilized a monolayer-seeded configuration and atomic force microscopy (AFM). Taken together, it is believed that this information will be useful in understanding the remodeling potential of VICs in normal and pathologic valvular tissue remodeling and during the early stages of TEHV development.

4.1 PROTOCOLS

4.1.1 VIC Isolation

Porcine AVICs and PVICs were isolated from the same animal (~10 months old, ~200 lbs.). Upon sacrifice at a USDA approved abattoir (Thoma Meat Market, Saxonburg, PA), the aortic and pulmonary valves were submerged separately in Hypothermosol FRS (BioLife Solutions, Binghamton, NY) at 4ºC to ensure interstitial cell survival during transport. Within three hours of sacrifice, the leaflets were dissected, surfaces scrapped to remove all endothelial cells, minced into 1x1 mm^2 pieces, and digested with collagenase A (Sigma, St. Louis, MO) for 30 min with gentle rotation (10 rev/min). Following digestion, the cell-tissue solution was strained with a 0.5 μm cell strainer. Both populations were plated separately in 250 ml culture flasks in complete media (DMEM, 10% FBS, 1% pen/strept, and 0.5% fungizone, all from Gibco). Media was changed every three days and the cells were passaged at 7 days. After 14 days, the flasks were combined and each population was cryopreserved in DMEM with 10% DMSO at a density $1x10^6$ cells/ml in a volume of 2 ml.

4.1.2 VIC Stiffness with AFM

To perform AFM measurements of cellular stiffness, a monolayer of seeded VICs were prepared for each cell type. VICs were thawed and plated for 72 hours before AFM experiments were performed. Cover slips were prepared for collagen coating the day before seeding cells with poly-d-lysine (5 mg/50 ml, Sigma) treatment for 5 minutes. Collagen (14 μl of 5.90 mg/ml rat tail, type I collagen (BD Biosciences) + 2 ml of 0.02 N acetic acid) was then placed on the cover slip surface and left overnight before being rinsed with PBS. VICs were trypsinized, plated on the cover slips, and allowed to attach for 3 hours.

AFM VIC stiffness measurements were made per cell using the so-called tapping mode. The cantilever probes used were calibrated by thermal vibrations using software from the AFM manufacturer (MFP-3D Inverted Optical Model, Asylum Research, Santa Barbara, CA), with cantilever spring constants having values between 65.23 and 72.93 pN/nm. For each VIC, approximately 70 indentions were made over the surface of each cell using a rectilinear grid sampling pattern (**Figure 28a**). These measurements were carried out on a total of 7 cells from each cell type (AVIC and PVIC), for a total of 14 cells measured.

The apparent stiffness of the cell, E, was calculated based on the Hertzian model [148] of the AFM probe modeled as a conical tip with a probe opening angle of 35º using

$$E = \frac{F(1-\upsilon^2)}{\pi \cdot \phi(\delta)} \qquad \text{(Eq. 23)},$$

where $\phi(\delta)$ is a function of the conical tip probe [149]. $\phi(\delta)$ is defined as

$$\phi(\delta) = \delta^2 \left[\frac{2 \cdot \tan(\alpha)}{\pi^2} \right] \qquad \text{(Eq. 24)},$$

where α represents the probe opening angle (35º) and δ describing the indentation depth of the probe. The terms υ and F in Eq. 23 represent the Poisson's ratio (set to 0.5, which assumes an incompressible material) and the force applied to the cell by the AFM tip, respectively. With these assumptions, E was determined as

$$E = \frac{F}{0.594 \cdot \delta^2} \qquad \text{(Eq. 25)}.$$

The resulting relation between the indentation depth and applied force (Eq. 25) was then fit with a Levenberg-Marquardt variation of the Gauss-Newton method for fitting parameters to a nonlinear equation (MathCAD, Mathsoft Inc.).

In analyzing the data, measurement locations with fits that had r^2 values above 0.9 were included for analysis (**Figure 28b**). A ceiling value of 150 kPa was also used to remove measurements that were believed to be predominantly influenced by underlying cover glass and not the VIC. This ceiling value was chosen as smooth muscle cells tested with AFM previously had a stiffness of ~100 kPa [148]. A target indentation depth of ~800 nm, previously used for the fibroblast cell line Cos-7 to determine changes in cell stiffness after disruption of the CSK network [150], was used here in order to fully assess the mechanical consequence of the underlying CSK. Since the VICs were ~6 μm in height when seeded, this indentation depth was deemed acceptable.

4.1.3 VIC Gel Contraction

As with AFM measurements, VICs were thawed and plated for 72 hours before the gel contraction assay was begun. As a comparison to myofibroblast cells, human adult dermal fibroblasts (DFs, from a 66 year-old male, provided by Dr. Patricia Hebda, Dept. of Otolaryngology, Children's Hospital of Pittsburgh) were seeded on another set of gels at the same concentration. The free floating collagen gel assay used in these studies is a modification of the standard fibroblast populated collagen lattice [151]. Collagen gels with a volume of 200 μl were cast in ½" Teflon rings (Seastrom Manufacturing Company, Twin Falls, ID) in 60×15 mm Petri dishes (Cardinal Health, Warrendale, PA). The collagen source, Vitrogen (Angiotech Biomaterials, Palo Alto, CA), was prepared using the manufacturer's protocol of a 8:1:1 ratio of

Vitrogen, 10X PBS, and 0.1 M NaOH while adjusting the final pH with a small amount of 0.1 M HCl (all from Sigma, St. Louis, MO), to a final concentration of 2.4 mg/ml. The Petri dishes were placed in a 37°C water bath for one hour to allow for collagen gelation.

Cells were placed on top of the collagen gels inside the rings in a volume of 200 μl containing ~3.0×10^4 cells in complete medium. The dishes were incubated for 30 minutes to ensure cell adhesion to the collagen gels. Then, 7 ml of medium was added to the dish, the Teflon rings were removed, and the collagen gels were loosened from the surface with a pipette tip. The dishes were incubated for another 30 minutes to allow for equilibration of the medium. To examine the effects of TGF-β1 on the VICs, additional groups of PVIC (PVICs+TGF) and AVIC (AVICs+TGF) gels were fabricated as above; however, in the 7 ml added after cell adhesion, a single dose of TGF-β1 (0.5 ng/ml, T5050 from Sigma) [152] was added.

Collagen gels were imaged at 0, 2, 4, 24, 48, and 72 hours following the final incubation with a digital camera (Diagnostic Instruments, Sterling Heights, MI) connected to a dissecting microscope (Olympus, Melville, NY). Changes in collagen gel area were measured using Metamorph software (Universal Imaging, Downingtown, PA). Percent contraction was calculated as the change in area from the initial area at time 0. Dishes were imaged with a 1x1 cm^2 visible grid underneath to ensure uniform scaling during image analysis. Cellular viability was assessed at each time point with a 10x light microscope to ensure that the VICs were spread and healthy.

4.1.4 VIC Migration and Morphology

To qualitatively assess the location and migration of the VICs at each time point, one gel for each VIC type and time point was imaged via fluorescence microscopy. As there was no evidence of differences between gel specimens for each VIC population at each time point (i.e. all contracted similarly), one gel was deemed sufficient. Gels were fixed in 2% Para formaldehyde and imaged by fluorescence microscopy. Gels were treated with 0.1% Triton X-100 for 20 minutes to allow for infiltration of the stains. After washing 3x with 1xPBS, gels were stained with Rhodamine Phallodin for 1 hour to label the total actin of the cells. Cell nuclei were then stained with DAPI (4'6-diamidino-2-phenylindole). Gels were put in a chambered Borosilicate coverglass (Lab-Tek) with the cell-seeded surface facing the cover glass. The chambered cover glass was then mounted on an inverted Laser Scanning Confocal Microscope (Olympus Fluoview 1000). DAPI (excitation: 405 nm) and Cy3 (excitation: 543 nm) filter combinations were set to sequentially image the cell nuclei and actin. For each gel, three 10x images were taken encompassing an area from the center to the edge of the gel. These images were concatenated to form a single image.

4.1.5 Statistics

Cell stiffness and % area contraction from time 0 are reported as mean ± SE. Stiffness values were compared with an unpaired student t-test (SigmaStat) and % area contraction differences were first compared with a two-way ANOVA and where significant differences were found, *post-hoc* testing was done with the Tukey pair wise test (at each time point). For each gel contraction group, a total of six gels were analyzed. Note that gels used for fluorescence imaging were not taken from the n=6 group but were made in addition.

4.2 RESULTS

4.2.1 VIC Stiffness

Analysis of the AFM indentation tests data resulted in a at least 60 acceptable AFM measurements per cell. As the location of the organelles varied between cells in relation to the AFM measurement location grid (**Figure 28a**), the stiffness values for each cell were sorted by magnitude then averaged with the other cells from the same group. This allowed us to more easily visualize the VIC AFM stiffness distribution (**Figure 28c**). In addition, the 60 stiffness values were averaged together to obtain an estimated single value of E for the VIC being tested. Resulting distributions indicated that the averaged apparent stiffness (**Figure 28d**) of the AVICs (55.06 ± 4.17 kPa, n=7) was approximately twice ($p<0.001$) the averaged apparent stiffness of the PVICs (24.11 ± 3.02 kPa, n=7). Since these values are averaged from multiple indentations over the surface of both VIC populations (mean population values are shown as horizontal lines on **Figure 28c**), it indicates that there exists a significant overall stiffness difference between valve cells.

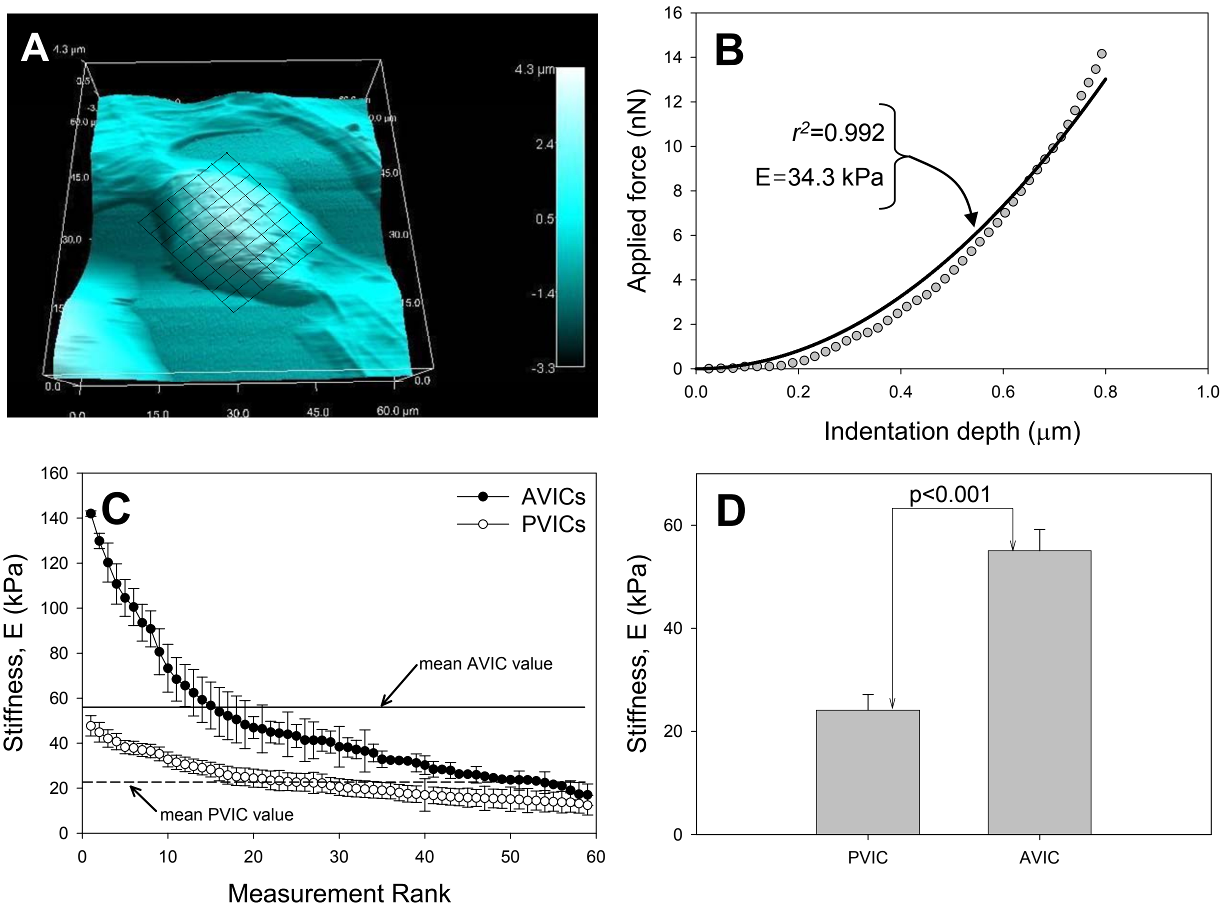

Figure 28. A: Atomic force microscopy (AFM) surface topography map of a PVIC, showing the corresponding tapping mode grid where ~70 indentations were applied to the cell surface to estimate local surface stiffness. B: Applied force vs. indentation depth data (circles) from a single indentation of a PVIC with AFM. Data points fit (black line, r2=0.992) with the Levenberg-Marquardt variation of the Gauss-Newton method to give the resulting apparent stiffness, E (34.3 kPa), of the PVIC at that indentation site. C: Average sorted stiffness values (greatest to least) from all indentations of both VIC populations. Average stiffness values shown as drawn horizontal lines. D: Averaged E of both VIC populations showing that aortic valve interstitial cells (AVICs) more than twice as stiff as the PVICs ($p<0.001$).

4.2.2 VIC Gel Contraction

Both VIC populations appeared to be viable and well attached during the duration of the contraction experiment (**Figure 29**). All gels were circular at 0 hours and underwent uniform contraction over the 72 hour duration of the experiment (**Figure 30**). With two-way ANOVA, both factors of time and cell type were significant ($p<0.001$) for the gel contraction experiment;

all further statistical comparisons are with the Tukey pair wise test. Gel contraction by the VIC populations at 2 hours was negligible (AVICs, 0.22 ± 0.52%; PVICs 0.78 ± 0.42%); however, the DFs had significantly contracted the gels (23.21 ± 1.79%, $p<0.001$, **Figure 31**). Similarly, both VIC populations contracted the gels insignificantly (AVICs, 0.51 ± 0.86%; PVICs, 0.64 ± 0.57%) after 4 hours; DF gels were significantly contracted (47.54 ± 2.67%, $p<0.001$) compared to both VIC gels.

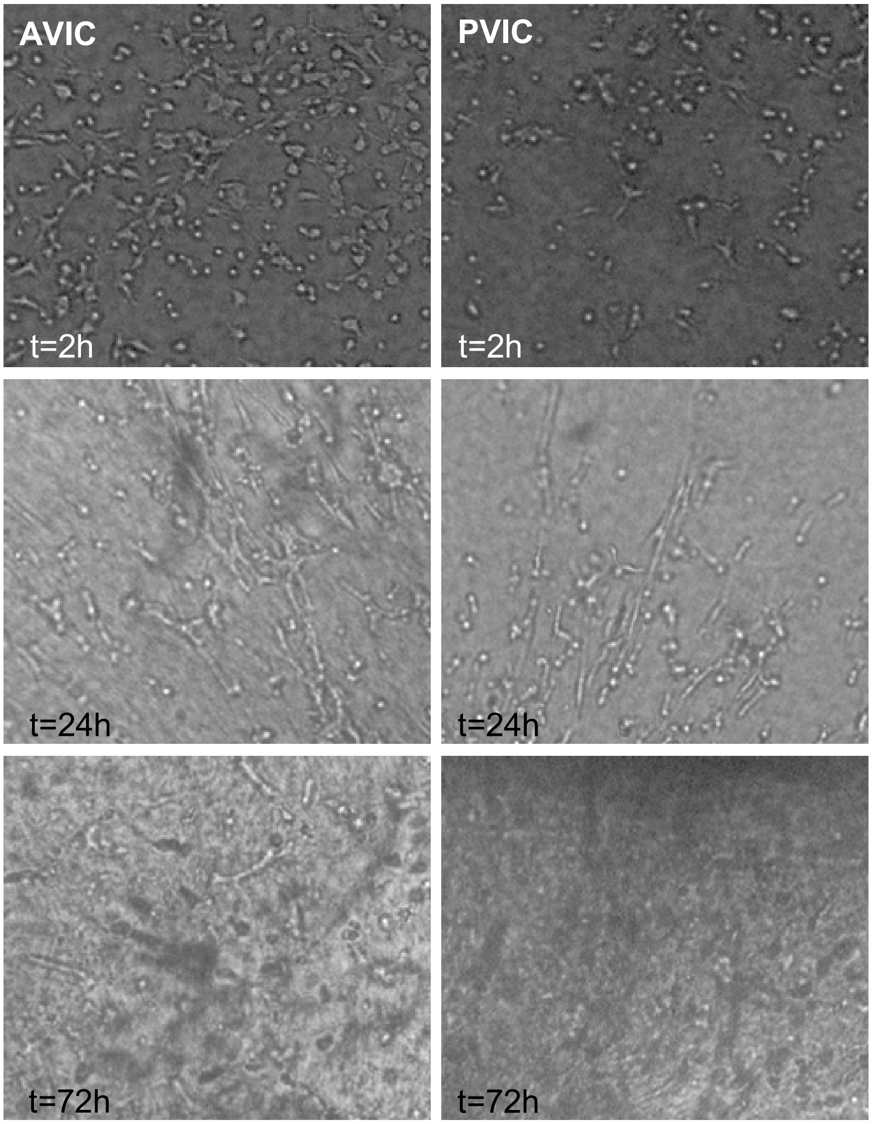

Figure 29. 10x light microscopy images of AVICs (left panel) and PVICs (right panel) seeded on the free floating collagen gels at 2, 24, and 72 hours. Note the spread and attached nature of the AVICs and PVICs at each time point.

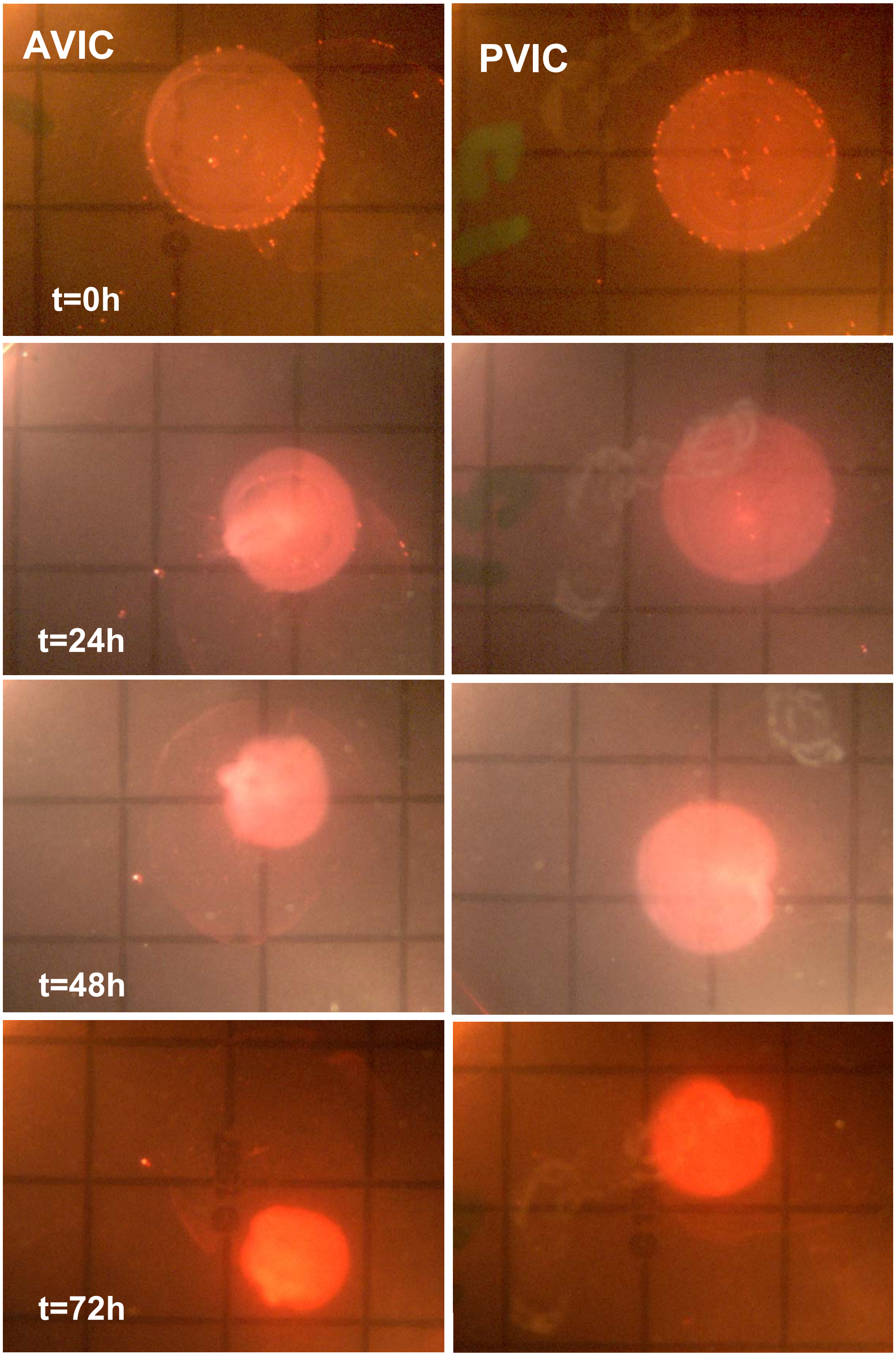

Figure 30. Time course contraction of VIC seeded collagen gels (AVICs, left panel; PVICs, right panel) imaged at 1x; underlying grid is 1x1 cm2 and is necessary for uniform scaling during analysis.

At 24 hours, the AVIC population (31.99 ± 3.44%) contracted the gels significantly more ($p<0.001$, **Figure 31**) than the PVIC population (7.57 ± 1.81%). DF gels were highly contracted at 24 hours (79.46 ± 0.96%, $p<0.001$) and no subsequent contraction was observed. Similarly at 48 hours, the AVIC (50.68 ± 2.39%) gels were significantly more contracted ($p=0.009$, **Figure 31**) than the PVIC gels (34.70 ± 4.34%). Gel contraction differences were insignificant at 72 hours (AVICs, 58.96 ± 1.03%; PVICs, 53.96 ± 2.29%). From the shape of the contraction curves, it was deemed best to fit all data sets with a four-parameter sigmoid function, thereby making it possible to calculate the greatest rate of contraction (dA/dt_{max}) for each group. For AVIC gels, dA/dt_{max} occurred at 15.18 hours and for PVIC gels at 43.59 hours (**Figure 31**). DF gel contraction was nearly linear up to 4 hours; however, dA/dt_{max} occurred at 2.25 hours.

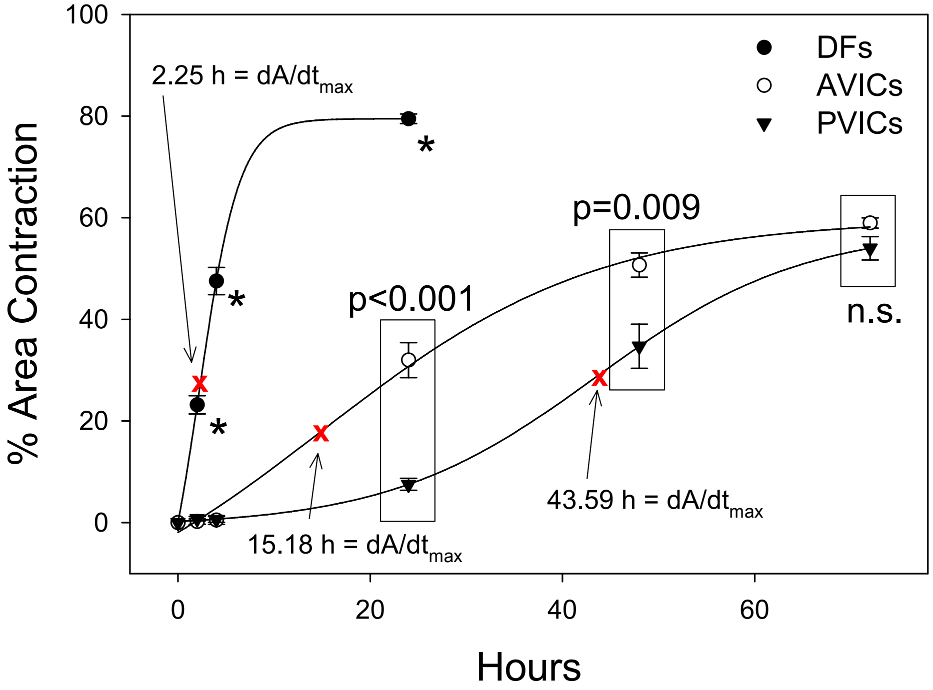

Figure 31. Percent area contraction by both VIC populations and dermal fibroblasts (DFs). DFs contraction was significantly greater (*, $p<0.001$) than both VIC populations at each time point. AVICs and PVICs were not different at 2 or 4 hours; however, AVIC gels were statistically more contracted at 24 hours ($p<0.001$) and 48 hours ($p=0.009$) than PVIC gels. All data points are fit with a four-parameter sigmoid function. x's indicate the greatest rate of contraction (dA/dtmax); both VIC time points occur after VIC clustering shown in Fig. 33. No difference was observed at 72 hours as both populations had reached a steady state and contraction was ceased.

VIC induced gel contraction in the presence of TGF-β1 was more rapid and substantial than VIC gels without cytokine treatment. At 2, 4, and 24 hours, the AVICs+TGF and PVICs+TGF gels were significantly more contracted ($p<0.001$, **Figure 32**) than the normal AVIC and PVIC gels. However, there was no difference between the cytokine treated gels at 2 or 4 hours. At 24 hours, the AVIC+TGF gels (81.6 ± 1.28%) were significantly more contracted ($p<0.001$) than the PVIC+TGF gels (70.11 ± 1.2%). Contraction of the TGF treated gels could not be observed past 24 hours as they became spherical with no apparent seeded surface.

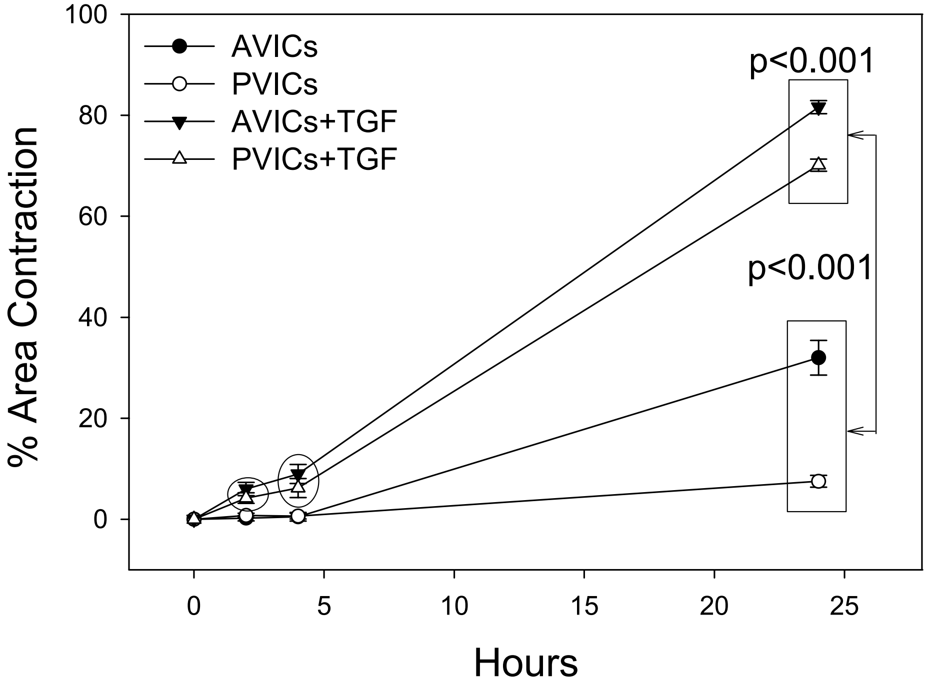

Figure 32. Comparison of VIC contraction results shown in Fig. 31 up to 24 hours with VICs treated with TGF-β1 (AVICs+TGF and PVICs+TGF). Both TGF treated groups (circled) were statistically more contracted ($p<0.001$) at 2 and 4 hours versus the AVIC and PVIC groups. Additionally, at 24 hours both TGF treated groups were significantly more contracted ($p<0.001$) than untreated VIC groups, and the AVICs+TGF group was statistically more contracted ($p<0.001$) than the PVICs+TGF group.

All cell populations were spatially distributed at 0 hours (one hour after seeding, **Figure 33**). In the AVIC gels, the cells appeared to cluster and organize around 4 hours, whereas the PVICs lagged behind and clustered closer to 24 hours (**Figure 33**). Following central clustering, both populations generated their largest rate of contraction (shown as x's in **Figure 32**). This was then followed, in the next time point, with the VICs radiating out from the center of the gel (**Figure 33**, 24h for AVICs and 48h for PVICs) and a decreased rate of contraction at subsequent observations.

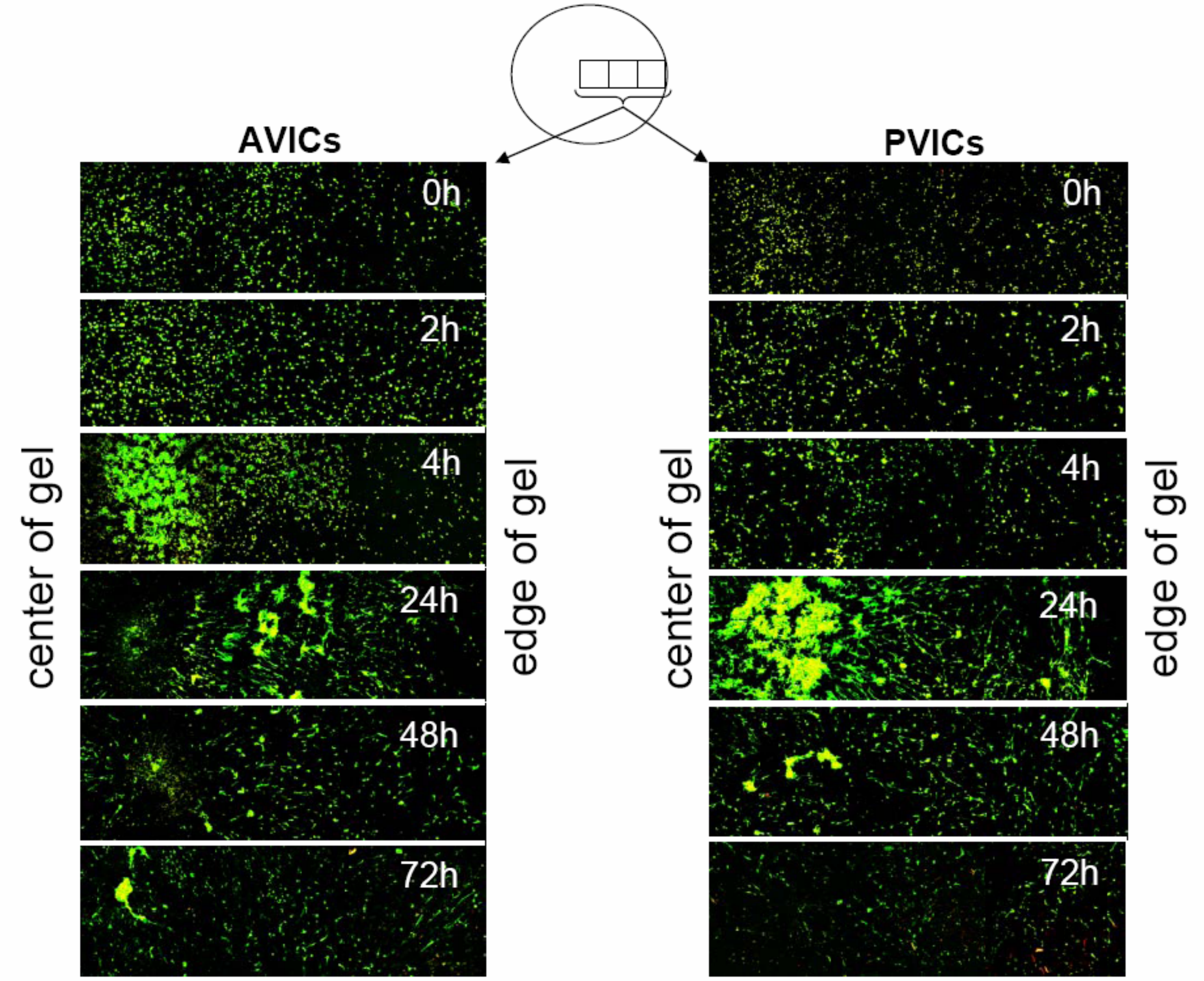

Figure 33. Concatenated fluorescence images (10x, total actin (green) and VIC nuclei (yellow)) of time course migration of VIC populations seeded on free floating collagen gels (AVICs on left and PVICs on right) at each point of gel contraction measurement shown in Fig. 31. Three images were made from the center (left) to the edge (right) of gel; central diagram shows geometry of image capture. Note the AVIC clustering near 4 hours and PVIC clustering near 24 hours. Following this clustering, both populations contracted the gels at their greatest rate (shown as x's in Fig. 31). After clustering, the cells appear to radiate outward from the center of the gel and though contraction continued, it was less pronounced.

4.3 DISCUSSION

4.3.1 Observed Differences in VIC Stiffness

An important aspect of this study was the observation that, as seen previously with ovine VICs measured by micropipette aspiration [132] the stiffness of the AVICs was ~2-fold greater than the PVICs. However, it is important to note that the AFM values were also ~100x greater than the micropipette values, as anticipated based on studies with other cell types [104, 106, 148, 153]. The best explanation offered to reconcile these differences concerns the assumptions used to model the force-deformation relation and the actual loading technique used. With AFM, a localized force is applied to a focal point on the cell membrane, which is supported by the nearby structural components (microfilaments, nucleus, etc.). The resulting response is modeled from this small, highly localized deformation state. Micropipette aspiration, on the other hand, examines the macro-mechanics of the cell and is primarily influenced by the cell membrane and unanchored cytoskeleton. Our previous VIC results with micropipette aspiration were modeled by assuming the cell to be an isotropic, elastic, and incompressible material that was homogenous (discontinuities, such as nuclei and organelles, were ignored).

Overall, it can be argued that VIC stiffness as measured with AFM allows for a more accurate representation of the cellular properties and architecture of the cell than micropipette aspiration. This is a result of the fact that the cells are seeded and attached to an underlying collagen substrate so that the CSK is extended and rigid as it is anchored at focal adhesions. This configuration is in contrast to testing with micropipette aspiration where the CSK is freed and not in a physiologic state as the cells float in a solution. Ultimately, interpretation and meaning of all cellular mechanical analysis techniques (nonlinear viscoelastic, heterogeneous materials) are tenuous and direct conclusions about cell function and biology are difficult to draw. Therefore, while these testing techniques do not result in similar stiffness values, they do allow for direct comparisons between PVICs and AVICs.

When considering the differences in CSK composition [132], the measured differences in stiffness reveals that the underlying CSK of the AVICs is a strong contributor to overall cell stiffness. The necessity of greater CSK content in the AVIC is believed to be required in order to effectively synthesize or expel synthesized proteins into the ECM [132]. This has been observed previously for other types of myofibroblasts, where human wound closure was facilitated by these dermal myofibroblasts as they produced thicker collagen fibers than fibroblasts and contributed to 88% of closure [126]. Therefore, the mechanical properties of the AVIC imply a greater ability to remodel the surrounding ECM compared to the PVIC.

4.3.2 VIC Contraction of Collagen Gels

The primary finding from this study is the greater ability of AVICs to contract free floating collagen gels compared to PVICs under identical experimental conditions. Though the substrate of a free floating collagen gel does not fully represent all the characteristics of the in vivo ECM of valvular tissue, it does support cell survival, attachment, and contraction. Therefore, comparing the contractility of both VIC populations indicates their CSK activity and resulting potential for tissue remodeling.

Human adult DFs, used for comparison in the present study, caused rapid contraction of the gels which were ~80% contracted at 24 hours; further contraction could not be detected as the gels became spherical. Not only did the DFs contract the gels much faster, but the time course of their contraction was unlike the VIC populations (**Figure 31**). DFs did not migrate and form a central cluster at any time point (images not shown), but essentially attached to the collagen gel and exerted local contraction without appreciable migration. Conversely, both VIC populations attached to the gel and did not exert any measurable contraction at 2 or 4 hours, but appeared to migrate to form an organized cluster in the center of the gel. Though there was an apparent lag by the PVICs (dA/dt_{max} for PVIC gels was ~28 hours later than for AVIC gels), once they did form the central cluster, they reached the level of AVIC contraction at 72 hours. After clustering by both VIC populations, they appeared to disperse and form radiating lines of cellular organization, which we speculate is similar to a response that would be seen with smooth muscle cells.

Walker et al. [144] has reported AVIC gel contraction in the presence of the TGF-β1 and cytochalasin D. This study examined AVICs only and the dose dependence of TGF-β1 on free floating and attached collagen gels. Our results support their findings in that the AVICs+TGF group did contract the gels significantly more at 24 hours than the AVIC group; however, our results are much more pronounced than theirs for the AVICs+TGF-β1 group (~80% versus ~20%). It is unclear why such a large difference was observed, but we speculate that it may be due to different size collagen gels, number of seeded cells, or culture conditions. This is supported by results from untreated AVIC gels, as their contraction was nearly 20% less than our observed values. Moreover, Fu et al [154] investigated ascorbic acid and growth factors (including bFGF and TGF) on human pediatric AVICs for their effect on tissue development when seeded on PGA coated with P4HB. Results indicated that after 7 and 28 days of culture the bFGF and TGF groups showed significantly higher DNA content compared to the control. They also found denser, more organized tissue development with pronounced matrix protein formation in the tissue engineered structures in the TGF group after 28 days, while the addition of bFGF led to a markedly higher collagen synthesis after 28 days. Our results corroborate and further support these studies and further indicated that TGF-β1 does serve to significantly activate the remodeling activity both semi-lunar valve cell types.

4.3.3 Role of CSK Contraction in Valve Physiology and Pathology

As the VICs are the resident population of cells responsible for maintaining valvular tissue homeostasis, their mechanobiological function is clearly important. Previously, the level of SMA found in each VIC population correlated well with the molecular chaperone HSP47 [132], which was used as a surrogate for collagen synthesis [122, 123, 130]. Therefore, the difference observed in gel contraction between the AVIC and PVIC populations has two implications. First, it implies that the pulmonary valvular tissues remodel more slowly and have less biosynthetic demand than aortic valvular tissues, which was suspected from the outset.

The second and unexpected implication from the groups treated with TGF-β1 involves valvular pathology. Our results indicate that PVICs respond similarly as AVICs to TGF-β1 which is known to be a byproduct of infiltrating macrophages [155], and is thought to initiate AV calcification [156]. From this fact alone, one would suspect that pulmonary valves may be as susceptible to pathologic conditions as AVs, but this is not supported clinically or epidemiologically. Therefore, one explanation for not seeing pathologic similarities between these two valves is either a lack of TGF-β1 near the PVICs or TGF-β1 may not be as effective on PVICs. Current work is aimed at understanding the roll of mechanical stimulation in the presence of TGF-β1 on the AVIC to better understand the etiologies of AV fibrosis and calcification [134].

4.3.4 Role of CSK Contraction in TEHV Development

The desired endpoint of any engineered tissue is functional equivalence of the replaced tissue or organ. Similarly the goal of a TEHV is accomplished largely at the tissue level where the tissue biomechanical behavior is paramount [146]. Much activity has been focused on identification and biosynthetic activity of candidate TEHV cell sources during in-vitro tissue formation prior to implantation [157-160]. The long-term ability of the chosen cell source to continually remodel the ECM will be crucial for success of a TEHV. With this in mind and due to the phenotypic plasticity of the native VIC population [80, 81], a requirement of biosynthetic sensitivity to various cytokines may be necessary in choosing a suitable cell source that can be activated early during the in vitro portion of TEHV development and later quiescent under steady state, in vivo conditions. Regardless of the cell source chosen for a TEHV, be it for the aortic or pulmonary position, remodeling potential should be considered in light of results shown here.

4.3.5 Summary

This work is the first to demonstrate a potential difference in tissue remodeling ability between the AVIC and PVIC. Moreover, seeded cell stiffness values measured with AFM revealed a 2-fold difference between AVICs and PVICs, confirming our earlier result using micropipette aspiration [132]. These results suggest a marked difference between the two VIC populations with respect to free floating gel contraction which is believed to be an indication of tissue remodeling potential. Overall, the PVIC appears to be a similar, but less robust version of the AVIC in that it acts slower and in a less pronounced fashion. Future work will be needed to elucidate the effects of both local tissue stress and surrounding cytokines on the VIC phenotype and biosynthetic function. Additionally, the question of native VIC phenotypic plasticity and resulting biosynthetic function will have to be addressed for development of a successful TEHV with whatever cell source is ultimately chose

5.0 THE EFFECTS OF CELLULAR CONTRACTION ON AORTIC VALVE LEAFLET FLEXURAL STIFFNESS

Efficiently and elegantly designed, the native AV leaflet is optimized for dynamic motion while maintaining the ability to withstand transvalvular pressures greater than 80 mmHg during diastole. Studies of native and bioprosthetic AV microstructure, both compositionally and mechanically, have been predominantly focused on the extra-cellular matrix (ECM) components, including collagen [27, 96, 161] and elastin [97, 162]. Additionally, examination of normal, pathological, and substitute valves has demonstrated that: 1) valvular ECM is the principal determinant of valve durability, and 2) the quantity and quality of valvular ECM depends on viability and function of aortic valvular interstitial cells (AVIC). As the most numerous AV cell type, the AVIC population constitutes ~30% volumetric density in mice leaflets [75] and ~78% cellular population in human leaflets detected by smooth muscle α-actin [77].

AVIC are a dynamic population of resident cells of multiple phenotypes that synthesize the several types of valvular ECM molecules and express matrix degrading enzymes such as matrix metalloproteinases (MMPs), and their inhibitors (TIMPs), that mediate ongoing ECM remodeling and repair. AVIC phenotypes range from fibroblast-like to myofibroblasts [77, 140, 147]. AVIC proteins include α and β myosin heavy chain and troponin isoforms [103] and valve leaflet contraction has been demonstrated in response to vasoactive agents [82], some investigators have suggested that contractile AVIC may have a function in generating a cyclical force that enhances valvular function or adaptation to altered hemodynamic forces. In further support of this concept, vasoactive agents have been shown to induce AVIC growth and collagen synthesis [101]. However, the mechanical role of AVIC contraction in native leaflet function is not well understood.

Studies of the AVIC population in both human and porcine subjects have revealed that the cell population was not localized to any one region or layer of the leaflet, but was present throughout the tissue [79]. Porcine AV myofibroblast contractility has been qualitatively studied with cultured cells on silicone substrates in the presence of multiple contractile chemical agents [75, 76]. In both studies, contraction occurred for most agents within 3 minutes and reached a plateau within 10 minutes. Additionally, Messier et al. [76] found that the few cells with no initial basal tonus did not respond to the administered vasoconstriction drugs. Isoproterenol was used to elicit relaxation from active cells, from which all cells recovered their previous basal tonus within 25 minutes. While not quantitative, these findings were the first examples of AVIC contractility.

Recently, strips of aortic leaflets were exposed to high KCl (90 mM) and endothelin levels in uniaxial tension; both treatments responded similarly with cells generating modest forces in the circumferential direction (0.31 mN - 0.66 mN), while in the radial direction the cells generated less force (0.11 mN -0.23 mN) [82]. From these results, it was proposed that the AVIC may help to sustain the hemodynamic forces exerted during systole by managing the stresses experienced on the hinge or basal attachment of the leaflet during motion.

This measurable contraction of the cells at the tissue level is likely made possible by strong attachment to the ECM, which has been reported both *in situ* and *in vitro* [77, 78]. The concerted cell contraction is believed to be mediated by cell communication through integrins with surrounding cells and the ECM [77]. AVIC demonstrate extended connecting processes that are believed to form a cellular network for communication, while no junctions have been found between the AVIC and valvular endothelial cells [75]. Additionally, these cells may use their contractile elements to mechanically communicate with the local environment since the presence of vasoactive agents has been shown to increase in collagen synthesis *in vitro* [101]. While the very low magnitude of the generated force levels make it unlikely that AVIC contraction directly affect valvular function, they are a dynamic cell source whose mechanical capabilities may serve a role in maintaining valve leaflet tissue homeostasis.

Bending is a major mode of cusp deformation *in vivo* (during opening and closing of the valve) [163]. Evaluating valve leaflet tissue under flexure offers two advantages over uniaxial tension tests: (1) it is highly sensitive at very low strains and stresses, and (2) it allows one to probe the mechanical properties of different layers since bending in opposite directions will reveal variations in tensile and compressive layer properties. Because of these two advantages, flexure testing is highly suited for measuring slight changes in leaflet stiffness due to mechanical alterations of the AVIC population. In the present study, we hypothesized that the AVIC population would show a significant effect on leaflet stiffness in the contracted state when tested under flexure at low strains.

5.1 PROTOCOL

5.1.1 Tissue Preparation

Porcine hearts from young hogs (~10 months old, ~250 lbs) were grossly dissected at a local USDA approved abattoir immediately after sacrifice and the intact AV was removed. The entire valve-root complex was submerged in a preservation media, (HypoThermosol HTS-FRS, BioLife Solutions, Binghamton, NY) and placed in an ice bath to ensure optimal cell survival during transportation. Valves remained in the preservation media at 4°C until the leaflets were excised in the lab. Circumferential strips were removed by cutting just below the nodulus of Arantus with razor blades of a constant width, w (**Figure 34**). Following dissection, the leaflet strips were rinsed to remove the preservation media and placed in Dulbecco's Modified Eagle Medium (DMEM) with high glucose.

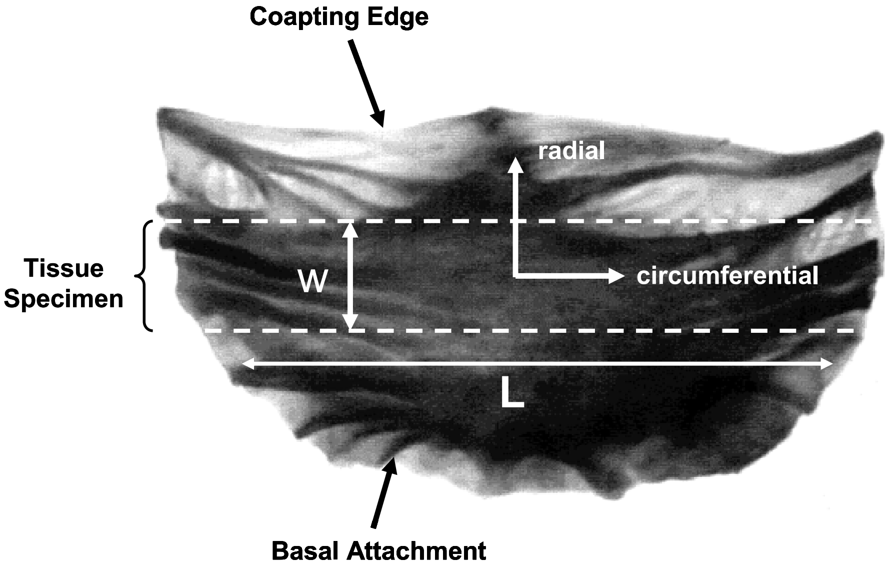

Figure 34. AV leaflet showing orientation of circumferentially oriented specimen in relation to intact leaflet.

A total of 36 strips were chosen at random from the valve leaflets (i.e. no regard to which leaflet they were dissected from) and divided into four testing groups: (1) leaflets bent against (AC) the natural curvature of the leaflet (**Figure 35**), (2) leaflets bent with (WC) the natural curvature, (3) leaflets treated overnight with 10μM thapsigargin (a calcium ATPase inhibitor) in physiological saline to prohibit any smooth muscle contraction and then bent in the AC direction (AC_{thap}), and (4) leaflets treated overnight in thapsigargin and bent in the WC direction (WC_{thap}). From each group, n=9 specimens were tested, however the WC_{thap} group had one leaflet which would not bend properly (n=8). In the present study, we defined improper bending when a hinge-like bending shape was observed versus a smooth, parabolic bending shape.

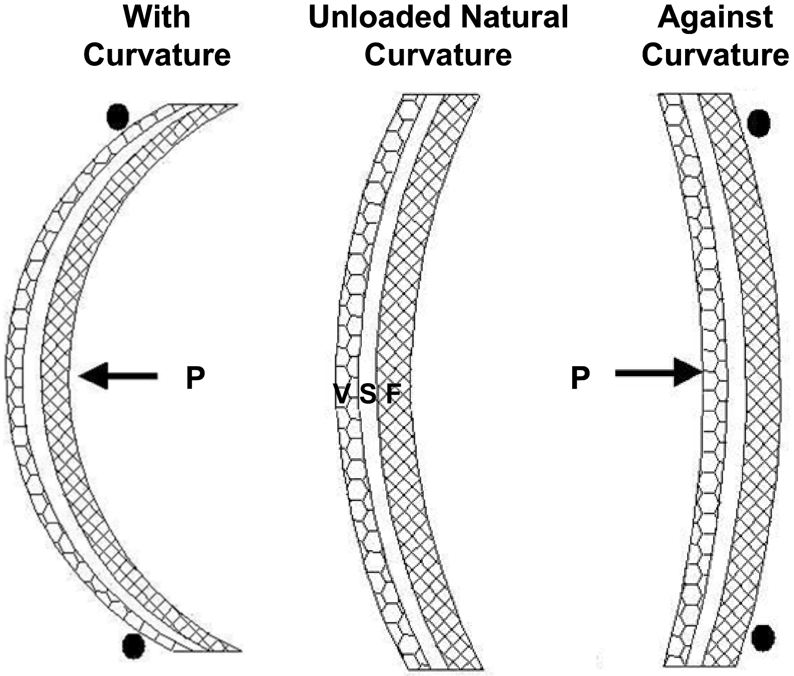

Figure 35. Directions of bending for the AV with respective layers (V=ventricularis, S=sponsgiosa, and F=fibrosa). Note that respective layers are alternating tension and compression resulting from flexural directions.

5.1.2 Flexure Testing

The flexural mechanical testing method has been previously presented [33]. Briefly, the mean strip thickness, t, was calculated from averaged measurements over the strip's entire length with the use of high precision calipers (0.0254 mm resolution); recordings were made upon initial contact to minimize viscoelastic effects from the soft tissue. Next, between 8 and 12 graphite markers were attached with minimal amounts of cyanoacrylate to the cut surface nearest the coapting edge. The specimen was held upright with two sleeves, which were supported by stationary posts while the bending bar was applied to the center of the tissue. In order to determine the deflection of the bending bar during testing, a reference rod was attached to the stage that was displaced equivalently with the bending bar base. Therefore, with all the aforementioned components, it is possible to record while testing, the stationary posts, bending bar, reference rod, and specimen markers (**Figure 36**). As the specimen was deflected, the image was recorded on a VHS tape which was used for analysis afterwards.

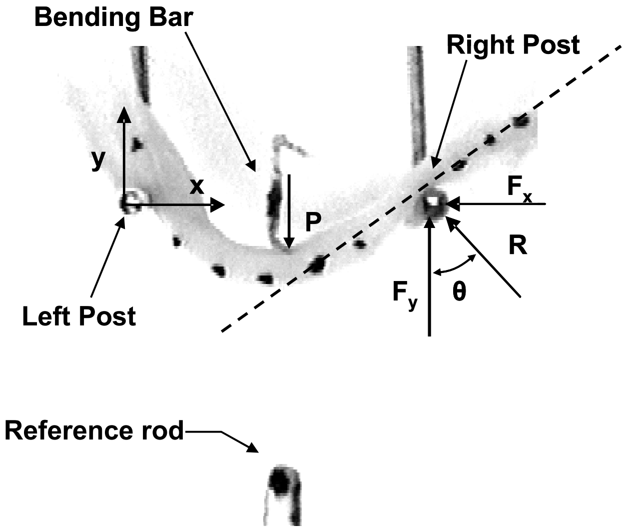

Figure 36. An example of a leaflet specimen in the flexure testing configuration, with the graphite markers attached to the top of the specimen nearest to the coapting edge. The reaction forces Fx and Fy are generated about the post acting as a pin due to applied load P during testing.

The marker, post, and bending bar positions were entered into a custom Matlab program that calculated the resulting moment, M (mN*mm), about the right post from the centrally applied load, P, and the change-in-curvature, $\Delta\kappa$ (mm^{-1}) , of the tissue at small time increments during the loading. Note that the local radius of curvature was determined from the parabolic curve fit to the markers. The applied moment M versus the change in curvature $\Delta\kappa$ is related by the Bernoulli-Euler moment-curvature equation

$$M=E_{eff}\,I\,\Delta\kappa \qquad \text{(Eq. 26)}$$

where $E_{eff}\,I$, termed flexural rigidity, corresponds to the slope of M-$\Delta\kappa$ curve, where I is the second moment of inertia calculated as

$$I={}^{1}/_{12}t^{3}w \qquad \text{(Eq. 27)}$$

The terms t and w are the thickness and width of the sample, respectively. The physical meaning of E_{eff} is the instantaneous effective modulus for a given $\Delta\kappa$. As it was not possible to know the level of $\Delta\kappa$ during the test, each specimen was bent by moving the reference rod to a predetermined position marked on the video monitor. This method allowed similar bending for all samples; however, because of the initial geometry of the tissue, the AC samples were bent to a greater $\Delta\kappa$ (**Table 3**).

All AC and WC samples were tested in Dulbecco's Modified Eagle Medium (DMEM) with high glucose (containing 5 mM KCl), and the AC_{thap} and WC_{thap} samples were tested in Hank's Balanced Salt Solution (HBSS) without $CaCl_2$, to prevent cells from becoming contractively active. Each tissue specimen was loaded and unloaded five times while the process was optically recorded. The control media with 5 mM KCl was removed from the testing bath and media with an additional 90 mM KCl was added. The specimen was left in the hyper-KCl solution for 3 minutes. Following the initial 3 minutes, the specimen was tested again using the same protocol. E_{eff} from each M vs. $\Delta\kappa$ plot was determined from a linear regression of the data up the maximum $\Delta\kappa$ value (**Table 3**).

Table 3. Summary of specimen dimensions and maximum curvature and applied moment.

Sample #	t (mm)	I (mm^4)	5mM KCl Max M (mN-mm)	5mM KCl Max $\Delta\kappa$ (mm^{-1})	90mM KCl Max M (mN-mm)	90mM KCl Max $\Delta\kappa$ (mm^{-1})
1	0.53	2.53E-02	1.489	0.216	1.975	0.207
2	0.38	9.22E-03	2.494	0.430	2.080	0.186
3	0.32	5.33E-03	2.523	0.295	2.949	0.289
4	0.34	6.72E-03	1.571	0.266	1.673	0.243
5	0.28	3.63E-03	1.353	0.278	2.111	0.261
6	0.34	6.72E-03	1.485	0.309	1.631	0.299
7	0.37	8.32E-03	1.126	0.238	1.493	0.216
8	0.44	1.46E-02	0.850	0.181	0.903	0.155
9	0.39	1.02E-02	0.876	0.195	0.856	0.17
Mean± SEM	**0.38± 0.03**	**1.0E-02± 2.18E-03**	**1.529± 0.204**	**0.268± 0.025**	**1.741± 0.215**	**0.225± 0.017**

Sample #	t (mm)	I (mm^4)	5mM KCl Max M (mN-mm)	5mM KCl Max $\Delta\kappa$ (mm^{-1})	90mM KCl Max M (mN-mm)	90mM KCl Max $\Delta\kappa$ (mm^{-1})
1	0.56	5.82E-02	3.017	0.288	2.588	0.320
2	0.51	4.37E-02	3.837	0.337	4.471	0.366
3	0.44	2.93E-02	1.413	0.197	1.188	0.167
4	0.44	2.93E-02	1.763	0.297	2.407	0.446
5	0.42	2.45E-02	0.320	0.301	0.829	0.407
6	0.52	4.71E-02	1.299	0.303	1.115	0.303
7	0.56	5.82E-02	1.649	0.169	1.808	0.356
8	0.44	2.93E-02	0.303	0.153	0.746	0.154
9	0.62	7.79E-02	1.357	0.152	1.463	0.280
Mean± SEM	**0.50± 0.02**	**4.41E-02± 6.0E-03**	**1.662± 0.382**	**0.244± 0.025**	**1.846± 0.393**	**0.311± 0.033**

Sample #	t (mm)	I (mm^4)	5mM KCl Max M (mN-mm)	5mM KCl Max $\Delta\kappa$ (mm^{-1})	90mM KCl Max M (mN-mm)	90mM KCl Max $\Delta\kappa$ (mm^{-1})
1	0.43	2.68E-02	1.591	0.092	1.164	0.194
2	0.39	2.03E-02	1.144	0.214	1.192	0.197
3	0.51	4.37E-02	1.054	0.113	1.081	0.128
4	0.37	1.67E-02	2.862	0.089	3.914	0.124
5	0.44	2.93E-02	1.693	0.148	1.201	0.157
6	0.38	1.84E-02	1.076	0.121	1.585	0.107
7	0.42	2.45E-02	1.995	0.214	1.889	0.224
8	0.52	4.71E-02	2.328	0.234	2.341	0.217
9	0.39	2.03E-02	1.570	0.148	1.499	0.151
Mean± SEM	**0.43± 0.02**	**2.75E-02± 3.65E-03**	**1.701± 0.203**	**0.153± 0.018**	**1.763± 0.301**	**0.166± 0.014**

Sample #	t (mm)	I (mm^4)	5mM KCl Max M (mN-mm)	5mM KCl Max $\Delta\kappa$ (mm^{-1})	90mM KCl Max M (mN-mm)	90mM KCl Max $\Delta\kappa$ (mm^{-1})
1	0.37	1.67E-02	3.297	0.044	2.732	0.060
2	0.77	1.55E-01	2.140	0.171	2.016	0.203
3	0.44	2.93E-02	1.516	0.257	1.451	0.247
4	0.34	1.34E-02	1.439	0.178	1.585	0.188
5	0.74	1.33E-01	0.674	0.149	0.944	0.155
6	0.57	6.22E-02	1.344	0.200	1.569	0.197
7	0.51	4.37E-02	1.388	0.209	1.295	0.200
8	0.52	4.71E-02	1.018	0.198	1.218	0.284
Mean± SEM	**0.54± 0.05**	**6.25E-02± 1.66E-02**	**1.602± 0.284**	**0.176± 0.022**	**1.601± 0.196**	**0.192± 0.023**

5.1.3 Determining AVIC Density through Leaflet Thickness

To demonstrate the effects of transmural cellular density, previous histological slides used for a study of transvalvular effects on AV collagen orientation [20] were examined to determine layer thickness and cell counts in the individual layers. All slides used were from the control group (two valves for a total of six leaflets) of the previous study, which were fixed at 0mmHg and stained with either Masson's Trichrome or Hematoxylin and Eosin. From each leaflet, four transmural cross-sections were taken, and five digital images from each section were made at 400x magnification. Due to the limited view-range of the microscope, five over-lapping photomicrographs were concatenated to view all three layers of the leaflet simultaneously. These panoramic images were analyzed to determine both cell density and thickness of layer. Cell nuclei counts were performed by counting upon gross inspection, and leaflet thickness was determined by layer segmentation upon gross inspection (**Figure 37**). Thickness measurements and cell counts from each layer were normalized as a percentage of the total thickness and total cellular population.

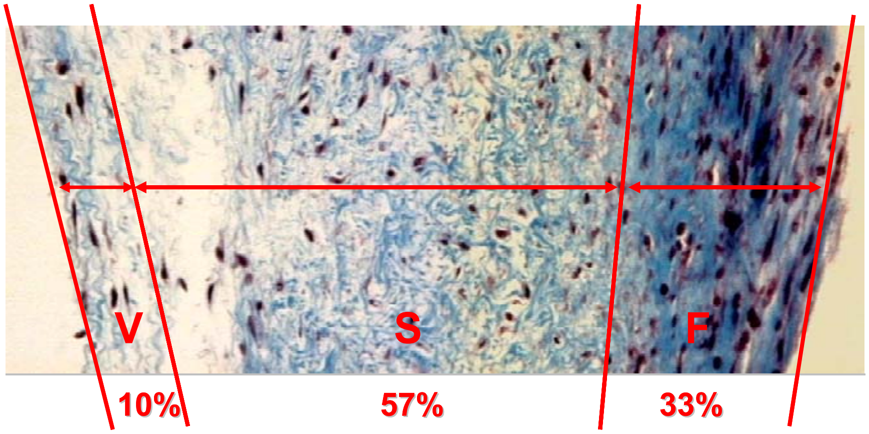

Figure 37. Masson's Trichrome stained porcine AV fixed at 0 mmHg pressure. Black circular regions represent cell nuclei, but are not specific to any one cell type. Lines represent approximate layer locations (V=ventricularis, S=spongiosa, and F=fibrosa) segmentation of the leaflet. 10% for V, 57% for S, and 33% for F represent the respective average layer thickness observed.

5.1.4 Statistics

All data are expressed as mean ± one standard error (SEM). Significance was determined by paired, two-tailed student t-tests between control (5 mM KCl) and treatment groups (90 mM KCl) with values of $p<0.05$ significant. When the data were not normally distributed (Normality test $p<0.05$), as in the case of the AC samples, the Wilcoxon signed-rank test was used. Comparison between different testing groups (i.e. AC vs. AC_{thap}) was determined with unpaired, two-tailed student t-test. When the data were not normally distributed, the Mann-Whitney rank sum test was used.

5.2 RESULTS

5.2.1 Flexural Stiffness of Aortic Valve Leaflets

The parabolic curve fit to the markers to determine $\Delta\kappa$ fit the data well, with an average r^2 value for all tests of 0.943±0.007 at the maximum deflection, indicating that the deformed leaflet shape was nearly parabolic. Note that in this study all leaflets were chosen at random and their corresponding numbers imply no particular leaflet (i.e. right, left, or non coronary, **Table 4**). Linear regression of the M vs. $\Delta\kappa$ relations in both bending directions revealed a bi-directional linearity, with an average r^2 value of 0.913±0.013 (**Figure 38**, **Table 4**). With the addition of 90 mM KCl, there was a 48% increase in E_{eff} for the AC specimens due to vasoconstriction of the AVIC ($p=0.004$); however, there was only a 5% increase for the WC specimens (**Figures 38a and 39**). Significance was also observed between the hypertonic cases of AC and WC (p=0.027) whereas AC and WC controls were not different.

Table 4. E_{eff} and r^2 values at the maximum deflection point for each specimen.

	Sample #	E_{eff} (kPa)	r^2	E_{eff} w/ KCl (kPa)	r^2
AC	1	252.65	0.9669	380.91	0.8867
	2	529.07	0.9492	856.77	0.8815
	3	1417.55	0.9809	2290.07	0.9032
	4	962.24	0.7832	1156.82	0.8277
	5	1187.12	0.9954	2056.97	0.9896
	6	605.86	0.9747	785.42	0.9931
	7	564.71	0.9598	826.53	0.9873
	8	323.14	0.9986	413.39	0.9819
	9	485.15	0.9796	599.09	0.93
	Mean± SEM	**703.05± 132.58**	**0.9543± 0.0220**	**1040.66± 229.01**	**0.9312± 0.02**

	Sample #	E_{eff} (kPa)	r^2	E_{eff} w/ KCl (kPa)	r^2
AC_{thap}	1	191.70	0.9743	152.50	0.9831
	2	267.99	0.9216	234.86	0.9866
	3	353.85	0.6864	308.81	0.3531
	4	177.74	0.876	151.02	0.894
	5	47.64	0.9753	84.63	0.6497
	6	94.93	0.8725	95.82	0.8597
	7	190.24	0.9526	95.41	0.9817
	8	81.07	0.6558	196.87	0.7804
	9	112.38	0.934	56.22	0.9805
	Mean± SEM	**168.62± 32.52**	**0.8721± 0.0133**	**152.90± 27.27**	**0.8299± 0.0236**

	Sample #	E_{eff} (kPa)	r^2	E_{eff} w/ KCl (kPa)	r^2
WC	1	463.29	0.7106	289.38	0.8479
	2	335.51	0.8444	366.32	0.8059
	3	188.34	0.9259	142.04	0.9527
	4	1538.43	0.9508	1637.70	0.9591
	5	330.34	0.8213	246.19	0.9138
	6	469.30	0.9941	916.71	0.9828
	7	396.31	0.9618	373.55	0.9883
	8	233.77	0.9783	212.41	0.9949
	9	469.96	0.9553	464.21	0.9747
	Mean± SEM	**491.69± 135.17**	**0.9047± 0.0312**	**516.50± 159.00**	**0.9356± 0.0223**

	Sample #	E_{eff} (kPa)	r^2	E_{eff} w/ KCl (kPa)	r^2
WC_{thap}	1	654.55	0.9584	448.65	0.8972
	2	37.42	0.9938	38.31	0.9932
	3	284.92	0.9908	291.23	0.9963
	4	300.85	0.9172	352.59	0.8882
	5	46.76	0.9528	66.66	0.9929
	6	111.84	0.9952	100.65	0.908
	7	254.24	0.9251	405.14	0.6817
	8	103.90	0.9729	92.92	0.9749
	Mean± SEM	**224.31± 71.85**	**0.9633± 0.0108**	**224.52± 59.16**	**0.9166± 0.0373**

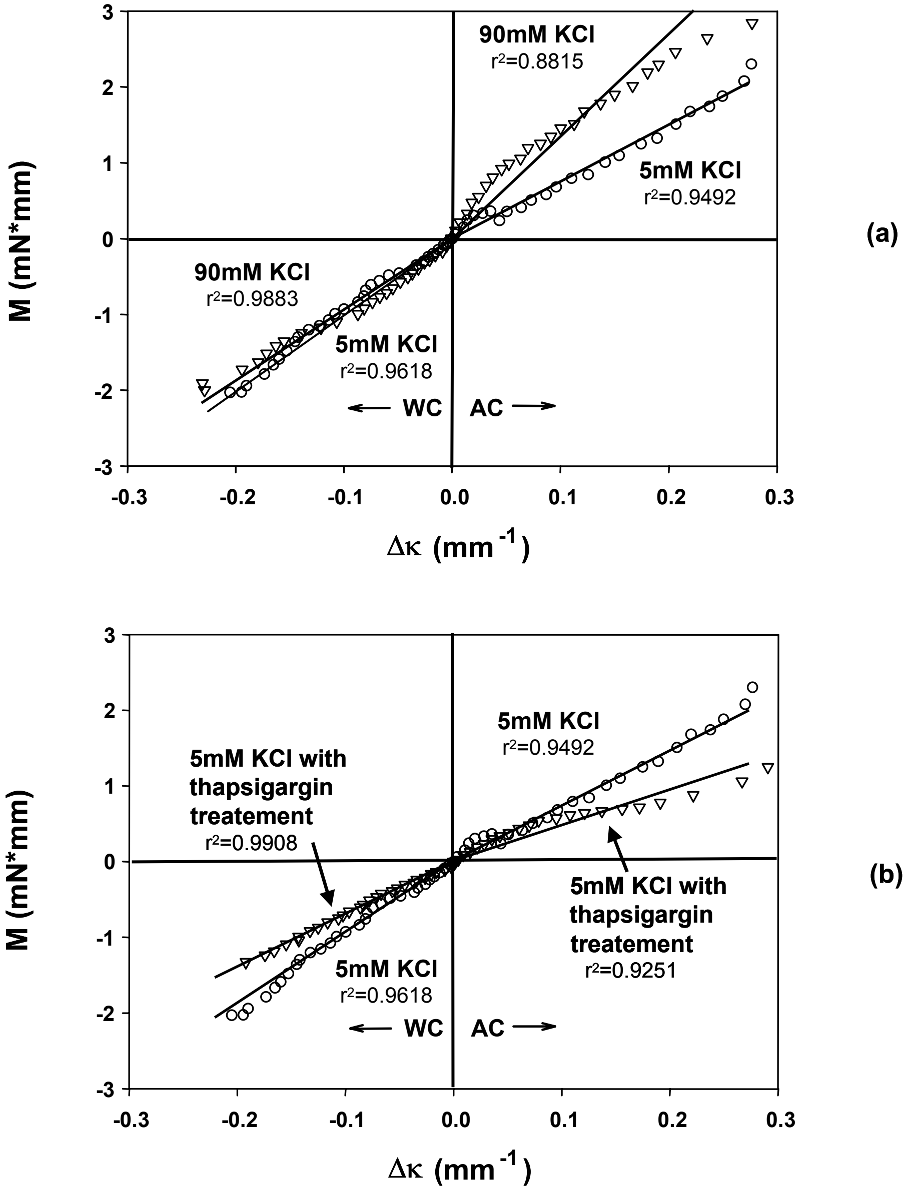

Figure 38. M vs. Δκ relations in both the AC and WC directions for (a) specimens tested in 5 mM and 90 mM KCl, and (b) specimens flexed in 5 mM KCl and samples treated in 10 μM thapsigargin overnight and then flexed in 5 mM KCl.

Thapsigargin treated specimens revealed a decreased bending stiffness (**Figure 38b**). E_{eff} in the 5 mM KCl AC_{thap} specimens was 76% less than the 5 mM KCl AC specimens (p=0.001). Similarly, E_{eff} for the WC_{thap} 5 mM KCl groups was 54% less than the WC specimens with physiological KCl levels (p=0.036). There was no change in leaflet stiffness in the thapsigargin treated leaflets after administration of 90 mM KCl, demonstrating the desired effect of inhibiting the smooth muscle aspect of the AVIC population (**Figure 39**).

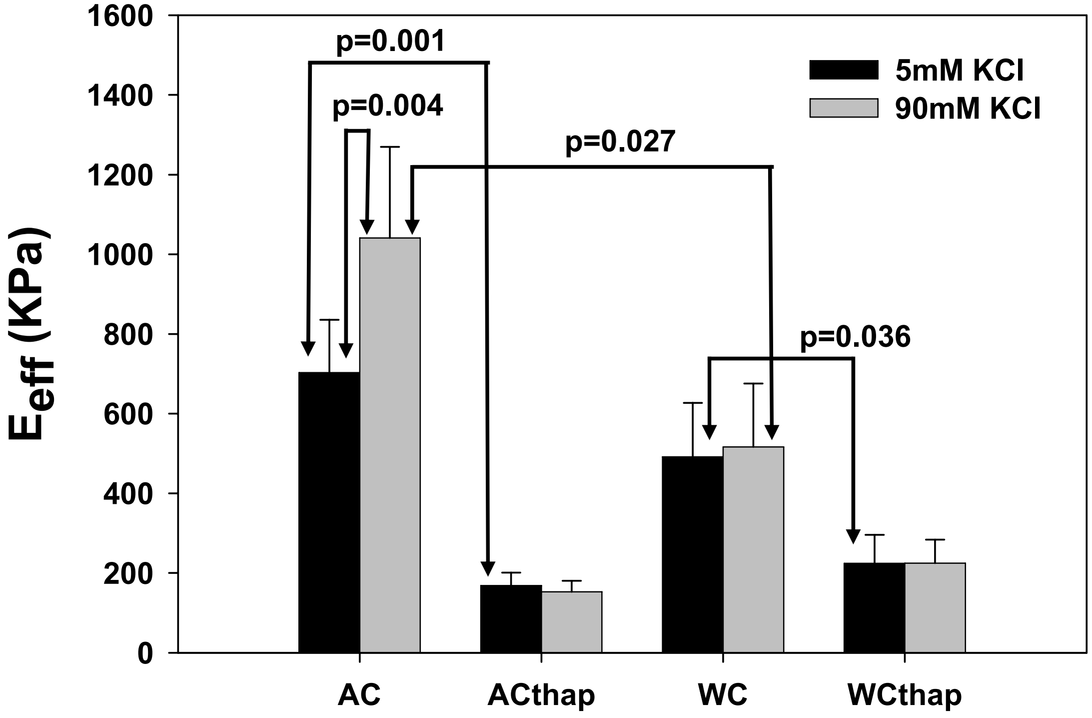

Figure 39. Effective stiffness E_{eff} determined from the slope of the M vs. $\Delta\kappa$ relations for the AC, WC, AC_{thap}, and WC_{thap} specimens before and after KCl addition. On average, increasing the KCl concentration of the bathing solution to 90 mM only affected the normal leaflet in the AC bending direction. Moreover, both bending directions experienced a loss of stiffness with the addition of thapsigargin to the bathing medium.

5.2.2 Cellular Distribution through Leaflet Thickness

The histological sections from the AV leaflets revealed that both the normalized thickness and cellular population (represented by cell nuclei) was consistent between leaflet layers with approximate values of 10% ventricularis, 57% spongiosa, and 33% fibrosa (**Figure 40**). This result demonstrated that there is not dominance in the spatial distribution or density of cells in any layer of the leaflet.

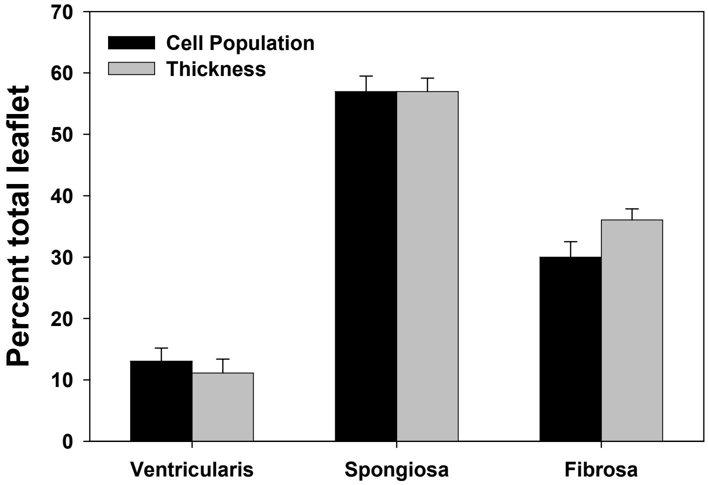

Figure 40. Normalized leaflet thickness and cell population over the total leaflet transmural axis, indicating that cellular density is relatively uniform within the leaflet layers.

5.3 DISCUSSION

5.3.1 Choice of Testing Method

As flexure is one of the natural modes of deformation in the AV, we sought to determine the change in flexural rigidity of circumferential porcine leaflet strips with altered AVIC states. Previous uniaxial results of leaflet tissue strips revealed low stresses generated (~0.5 mN) due to AVIC contraction [82]. Because of these previous findings, a low stress/strain technique was needed. The method of soft biological flexure testing offers higher accuracy at low strains than uniaxial tension, which is where forces generated by the cells are influential. Moreover, flexure testing allows bending in both directions to reveal any layer stiffness differences; therefore, it was deemed ideal for this study.

5.3.2 Effects of Cellular Contraction

After 3 minutes of exposure to 90mM KCl, there was a significant increase in the AC E_{eff} (48%, p=0.004, **Figure 39**). We speculated that the large increase found solely in the AC direction can be explained by the unique structure of the ECM in the respective leaflet layers. When bending in the WC direction, the ventricularis is in tension and the fibrosa is under compression (**Figure 35**). The layer in compression would presumably not show effects of cellular contraction because the cells are already being compressed. Thus, the ventricularis is the primary contributing layer in the active contractile state when the leaflet specimens are flexed in the WC direction. Since the ventricularis is composed of both collagen and elastin, we speculated that the cells are in fact contracting in this layer, but the compliant elastin is accommodating the contraction. This hypothesis is supported by the bending results in the AC direction (**Figure 39**); wherein the fibrosa (which predominantly contains collagen fibers) is in tension, cellular contraction is apparent because the more rigid collagen fibers are being stressed (**Figure 41**).

Though the collagen fibers are highly undulated in the unloaded leaflet [20], we have demonstrated that during bending of heart valve leaflet biomaterials the maximum surface strain is ~7% for $\Delta\kappa$ = 0.15-0.25 mm^{-1} [164]. At 7% strain, the collagen fibers of the native aortic leaflet would presumably be past the initial toe-region of the stress-strain curve observed in the circumferential direction during equibiaxial testing [19, 30]. Thus, some of the undulated collagen fibers would become uncrimped and allow for some level of force transmission from the cell to the ECM. Uncrimping would be greatest at the upper surface of the fibrosa layer, where it would also induce the greatest effect on bending stiffness due to the distance from the neutral axis. Additionally, there may be a preferential cell connection to collagen fibers in the fibrosa that is not prevalent in the elastin rich ventricularis layer.

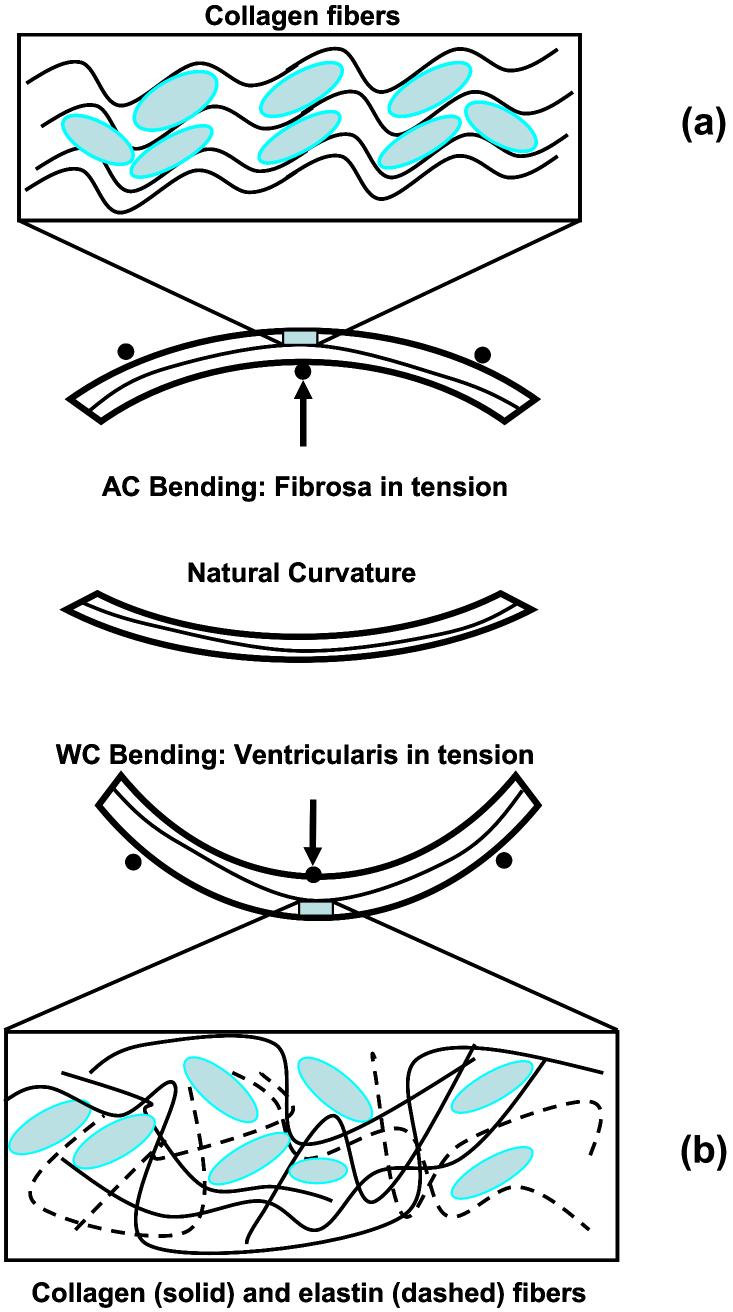

Figure 41. Schematic of AVIC contraction resulting in different layers due to ECM composition: (a) AC bending with AVIC in fibrosa layer anchored by rigid collagen fibers and (b) WC bending with AVIC in ventricularis layer anchored by collagen (solid) and stretchy elastin (dashed) fibers.

5.3.3 Cellular Basal Tonus

The AC_{thap} and WC_{thap} groups revealed no change in effective stiffness after addition of the KCl. This was the anticipated response since thapsigargin is known to inhibit cellular contraction. Exposing the valves to thapsigargin was originally intended to demonstrate that the addition of KCl was effective only on the AVIC population with their inhibition resulting in no changes in stiffness due to cellular contraction (which was the case). More interestingly, however, was the dramatic decrease in leaflet stiffness following treatment with thapsigargin in *both* bending directions (**Figure 39**). A similar *qualitative* response was seen when cultured cells exposed to isoproterenol lost their basal tonus [76]. This decrease in leaflet stiffness for thapsigargin treated samples was greater in both bending directions than the increase in stiffness due to AVIC contraction in the normal samples.

This treatment demonstrates the level of basal tonus of the AVIC population, as their inactivity resulted in a 4-fold ($p=0.001$) and 2-fold ($p=0.036$) decrease in E_{eff} compared to the normal (5 mM KCl) AC and WC flexure testing, respectively. To the authors' knowledge, this is first known quantification of magnitude of AVIC basal tonus at the at the tissue level. Moreover, it is unclear why no directional differences were found with loss of basal tonus. Our results suggest that AVIC basal tonus imparts an overall, uniform contribution to tissue stiffness via a mechanism different from that observed in the contracted state.

5.3.4 Role in Valve Pathology

Clinically, our current findings may shed light on the etiology of degenerative heart valve disease. The characteristic pathologic features of degenerative valve disease, i.e., leaflet fibrosis and calcification with decreases in cellular population and density, may be accelerated by loss of AVIC interstitial cell function, senescence, or death. In a study examining the effects of age-dependent changes in AV leaflet stretch in the radial direction, it was observed that there was a trend with stretch decreasing from birth to the age of 20 years, remaining constant to the age of 40, and then declining with increasing years [47]. These results suggest a declining ability for leaflet regeneration and remodeling with increased age, and are consistent with the concept AVIC functionality is critical to valve homeostasis [80]. While the role of AVIC contraction in leaflet homeostasis is unknown, it can be speculated that it may play some role in facilitating collagen fiber formation and integration into the leaflet ECM. Clearly, ongoing studies are required to elucidate these issues.

It is also unclear if AVIC require *in vivo* strains unique to valvular tissues to maintain their functional characteristics. For example, the resting heart valve duty cycle for the mitral valve has shown that closing occurs in 50 ms, remains closed for 300 ms, reopens in 50 ms, and remains open for 600 ms [131]. While not yet measured for the AV, it is likely loaded in a similar pattern. This indicates that the leaflets are under tension for ~40% of the cardiac cycle. Recently, two different studies showed that porcine aortic leaflets exposed to either constant shear stress [102] or constant static pressure [165] did not maintain the AVIC contractile phenotype after 48 hours. From these works, it was suggested that one of the modes of *in vivo* loading might be necessary in maintaining the contractile phenotype of the AVIC.

5.3.5 Role in TEHV Development

In addition to valvular pathology, the future success of tissue engineered heart valves (TEHV) is likely dependent on the implant's viability and biosynthetic activity. Vascular smooth muscle cells [80, 166], bone marrow derived stem cells [158], and tricuspid valve myofibroblasts obtained from biopsy [167] have been previously suggested as TEHV cell sources. However, it is currently unclear which cell source would be best suited for TEHV success, and there is a need to clarify which cellular endpoints are necessary for proper valve maintenance. Future studies will aim to clarify the loading regimen necessary to maintain AVIC phenotype *in vitro*, which is believed to be a necessary requirement as an aortic TEHV cellular endpoint. Additionally, this testing technique may allow analysis of the intact contractile functionality of AVIC in explanted tissue engineered valves.

5.3.6 Summary

The findings from this work reveal some insights on how the AVIC population can alter native leaflet stiffness at low strain levels experience in bending. These results indicate that changes in AVIC population stiffness can be measured at the tissue level. Further, a significant basal tone was observed and quantified for the first time. It should be emphasized that the mechanical contribution of the AVIC population to the biomechanics of valvular function, while currently unknown, is most likely negligible. However, we speculate that the contractile properties of these cells is likely related to their role in managing ECM formation, and is strongly influence by the local stress environments of the valve leaflet. Regardless of their ultimate role in leaflet function, they obviously serve to maintain homeostasis in native leaflet tissues and thus warrant further investigation.

6.0 IN SITU AORTIC VALVE INTERSTITIAL CELL MICROMECHANICS: CELLULAR OVERLOAD WITH INCREASING STRAIN

Aortic valve (AV) leaflets undergo very large tissue deformations during the cardiac cycle, and most notably significant extension in both the circumferential and radial directions during diastole to prohibit blood regurgitation. The mechanical respons of the AV leaflets varies largely in these directions with very high stretch-low stress in the radial direction with much more modest stretch and higher stress in the circumferential direction [19]. The stiffer response in the circumferential direction is chiefly dictated by the large fibrillar type I collagen that becomes taut at very low strains [20]. In addition to collagen fibers, the AV interstitial cells (AVICs) are also oriented primarily in the circumferential direction [75, 77, 78]. It has been believed for many years that these cells are responsible for the continual renewal and repair of the surrounding ECM [76], and therefore, their function is believed to be paramount for the long term integrity of the AV.

The AVIC phenotype appears to possess characteristics of both fibroblast and smooth muscle cells and is typically referred to as a myofibroblast [75, 76]. Clinical explant studies have implicated the AVIC myofibroblast in various disease pathologies [80, 81, 168] as an activated cell phenotype, possibly contributing to further progression of the disease. Additional in vitro studies have elucidated possible cytokine agents, particularly TGF-β1, which may lead to the AVIC becoming activated [133, 144, 152]; however, there has been no systematic examination of the level of circumferential strain and potential effects on AVIC phenotype and function.

The theory of stress overload of the AV was presented in 2002 by Robicsek et al. [169] and while the theory is highly plausible, little work has been performed since to address this potential contributor to valve disease. Primarily, they theorized that the most likely culprit for degenerative valve disease is increased stress on the AV leaflets due to loss of compliance in the aortic wall. As compliance decreases in the aortic wall, vessel dilation decreases, which inhibits stress transfer from the collagen fibers in the circumferential direction to the highly extensible elastic fibers oriented radially [21, 97]. To further support this theory of stress overload in the circumferential direction, nearly all AV degenerative pathologies originate and perpetuate in fibrosa layer of the leaflet where the circumferentially oriented collagen resides [62].

There is a need to understand the potential biophysical roles that may be played in altering the AVIC phenotype and function in the otherwise healthy AV leaflet from elevated tissue stress. Therefore, we hypothesize that the level of strain applied to a circumferential strip of AV leaflet tissue will modulate the in situ AVIC phenotype and biosynthesis. Moreover, we hypothesize that stress overload (prescribed by strain level) of the AVICs will have a detrimental effect on cellular function and ultimately AV homeostasis. To test these hypotheses, porcine AV leaflet strips were exposed to 3 and 6 day treatments of 0, 10, or 30% strain at 1 Hz. These stretch levels were chosen as 10% is the lower bound of the normal physiologic range (range between 10 and 20%) and 30% is substantially higher (nearly double the average of the normal range). Afterwards, the phenotype of the resident AVICs was quantified along with type I collagen production from the AVICs. Moreover, to further elucidate the micromechanical environment of the AVICs, we subjected additional circumferential strips to 0, 10, and 20% strain and afterwards fixed these tissues in their strained state for examination with small angle light scattering (SALS) and transmission electron microscopy (TEM).

6.1 PROTOCOLS

6.1.1 Bioreactor Design

The tension bioreactor (**Figure 42**) used in this study is similar to the previously described flexure bioreactor used for flexural stimulation of engineered valvular tissue [32, 33]. Cyclic stretch is applied to the samples by an environmentally sealed linear actuator (UltraMotion, Mattitick, NY) which is rigidly coupled to the base of the system and the cross-arm of the bioreactor. The cross-arm is coupled to the actuating arms penetrating each chamber via a hole that is protected with an accordion-style rubber bellow. Each actuating arm has two orthogonal crossbars with exiting holes into which stainless steel pins are inserted. These pins align directly across from the stationary pins to apply uni-directional tension to the specimen. Applied strain and strain rate are controlled with programmable Si Programmer software (Applied Motion Products, Watsonville, CA). The entire device, including lids, pins, and screws can be cold gas sterilized with ethylene oxide.

6.1.2 Tissue preparation

AVs were collected upon sacrifice of young hogs (~10 mos., ~250 lbs.) at a local USDA approved abattoir (Thoma Meat Market, Saxonburg, PA). The entire valve root complex was submerged in PBS and maintained at 4ºC. As reported previously, leaflets were removed and a rectangular strip was dissected from the central portion of the leaflet (15mm x 8mm). The three leaflets (NC=non coronary; LC=left coronary, and RC=right coronary) of the AV were separated into treatment groups. NC leaflets were used as day 0 controls, LC leaflets as static controls, and RC leaflets as strain samples. For each treatment group, n=6 AVs were used.

6.1.3 Treatment configuration

NC strips were snap frozen immediately after dissection and stored at -80ºC. LC strips were each placed in a single well of a 6-well plate. RC strips were threaded with custom made stainless steel springs (8 mm long x 2 mm diameter x 10 turns/cm) on the short axis side of the tissue. The strips were penetrated with the spring at least four times to allow for uniform stress distribution. Tissue strips were then inserted into the tension bioreactor (**Figure 42**) by sliding the springs onto the pins inserted into the floor of the culture well and the actuating arm of the bioreactor. For LC and RC strips, 5 mL of complete media was added (DMEM, 10% FBS, 1% penicillin-streptomycin, and 0.5% fungizone, all from Gibco) and was subsequently changed every 24 hours. RC strips received 10, 20, or 30% strain at 1Hz for either 3 or 6 days. After 3 and 6 days, LC and RC strips were snap frozen and stored at -80ºC.

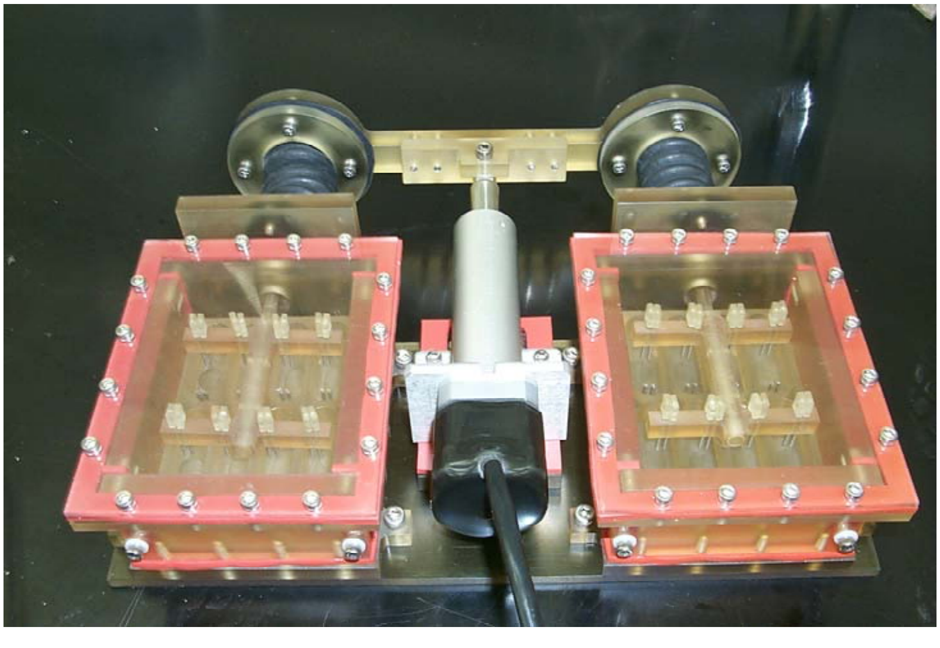

Figure 42. Tension bioreactor used to house and mechanically train AVL strips. Each chamber has 8 wells, which allows 16 samples to receive the same mechanical stimulation simultaneously.

6.1.4 AVIC phenotype and collagen biosynthesis analysis

Samples were thawed, homogenized, and the intra-AVIC proteins analyzed by enzyme-linked immunosorbent assays (ELISAs) for SMA, Hsp47, and CICP as reported previously [132, 134]. In our previous work, it was shown that Hsp47 accurately represents type I collagen production for AVICs [134]. This was validated by an ELISA for type I collagen C-terminal propeptide (CICP, Metra CICP EIA Kit, Quidel Corp.) according to the manufacturer's instructions. Similarly, biologically active TGF-β1 was assayed with the TGF-β1 E_{max}® Immuno-Assay System (Promega Corp.) according to the manufacturer's instructions [152]. To demonstrate that AVIC phenotype and collagen biosynthesis were equivalent between the three leaflets, a set of valves (n=6) was used to form a comparison.

6.1.5 Tissue, cell, and nuclei micromechanical analysis

To elucidate the micromechanics of the AV leaflet to increasing strain and the in situ micromechanical environment of the AVICs, additional leaflets were obtained and dissected as above. RC leaflets were subjected to a single extension of 0, 10, or 20% strain and fixed with either 2.5% Grade I or Grade II (EM grade) gluteraldehyde (Sigma Aldrich, St. Lousi, MO) for 60 min in their strained state. Afterwards, the strips were either analyzed by small angle light scattering (SALS) [146, 170] to determine the change in collagen orientation due to increasing strain or dissected such that AVICs could be viewed in the circumferential-tissue thickness plane with transmission electron microscopy (TEM).

SALS is an effective technique for the microstructural analysis of planar fibrous connective tissues, and we have used it previously for mapping the architecture of leaflets from normal, pressure fixed, and explanted bioprosthetic valves [20, 27, 40]. Briefly, a continuous unpolarized wave laser is passed through the tissue, which scatters light according to the internal planar fiber structure. The resulting angular distribution of scattered light intensity about the laser axis represents the distribution of fiber angles within the beam envelope at the current tissue location. Gathered information includes: 1) preferred fiber direction, 2) distribution skew, and 3) orientation index (OI), which represents 50% of the total number of fibers.

For TEM, tissue specimens were prepared with standard protocol and sectioned at 70 nm. Individual AVICs and their nuclei were imaged at 8-15kx. From these images, the orthogonal major and minor axes of the cell and nucleus were measured (SigmaScan, SYSTAT) and used to calculate aspect ratios as reported previously for AVICs fixed under increasing pressure [84].

6.1.6 Statistics

All ELISA results were normalized to their day 0 values such that changes could be seen with respect to this baseline value; each ELISA data point represents n=6 samples. Comparisons between ratio values were performed with a one-way ANOVA. For cell and nuclear aspect ratios and SALS analysis (OI), comparisons were made with an unpaired Student t-test.

6.2 RESULTS

6.2.1 Changes in SMA, Hsp47, CICP, and TGF-β1 due to strain level

In order to demonstrate that the AVICs from the three leaflets of a given AV are phenotypically and biosynthetically comparable, ELISA values for SMA, Hsp47, CICP, and

TGF-β1 from each leaflet were analyzed (**Figure 43**). As expected, there was no significant difference between leaflets with respect to any of the proteins or cytokine analyzed in this study.

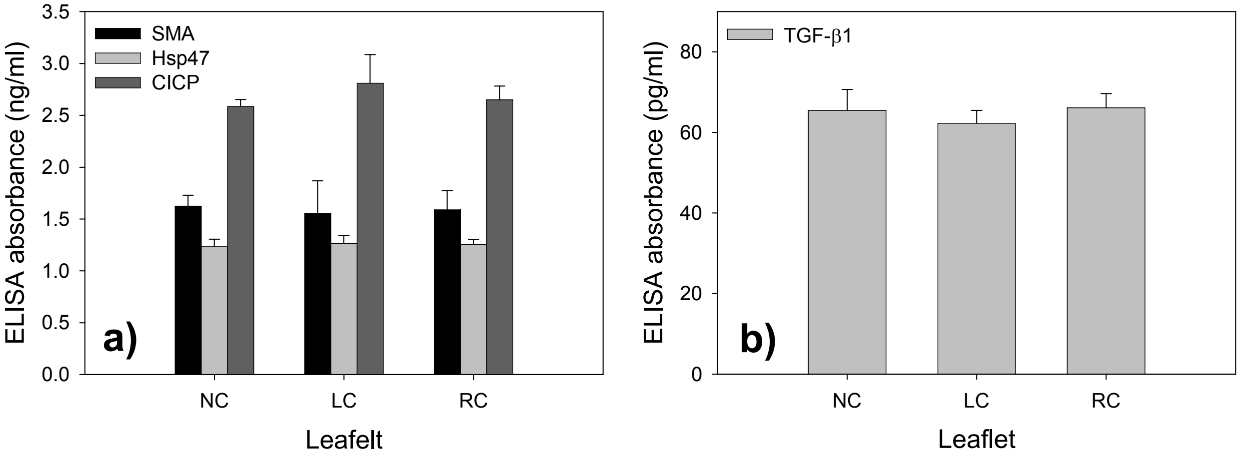

Figure 43. a) ELISA absorbance values for SMA, Hsp47, and CICP for the three leaflets of n=6 porcine AVs. b) ELISA values for TGF-β1 from the same AVs. These results reveal that the phenotype, biosynthesis, and cytokine levels are consistent for the AVICs of the three AV leaflets.

As there was no difference between the three leaflets with respect to the proteins/cytokine measured in this study (**Figure 43**), it was deemed appropriate to normalize changes at 3 and 6 days to the day 0 controls (NC leaflets). For SMA, there was no significant difference at either 3 or 6 days for any of the strain protocols (**Figure 44a**). There was a decrease of SMA in the static samples at 3 and 6 days, but they were not significant. Tissues treated with 10 and 30% strain had nearly identical SMA values at 3 and 6 days and neither of these were different from day 0 values. For Hsp47, there was a significant decrease (+, **Figure 44b**) at 3 and 6 days for both 30% strain and the static group compared to the 10% strain treatment which was nearly unity at both time points. CICP was analyzed here to confirm any differences observed with Hsp47 as this would represent collagen actually synthesized and delivered outside of the cell whereas Hsp47 represents a surrogate for collagen synthesis within the cell. Here, we see that while there is a difference for 30% strain compared to 10% strain with respect to Hsp47, no such difference is apparent for CICP (**Figure 44c**). Like Hsp47, CICP was significantly lower for the static group at day 6 compared to both 10 and 30% strain (#, **Figure 44c**). TGF-β1 was not different for any treatments at any time point (**Figure 44d**).

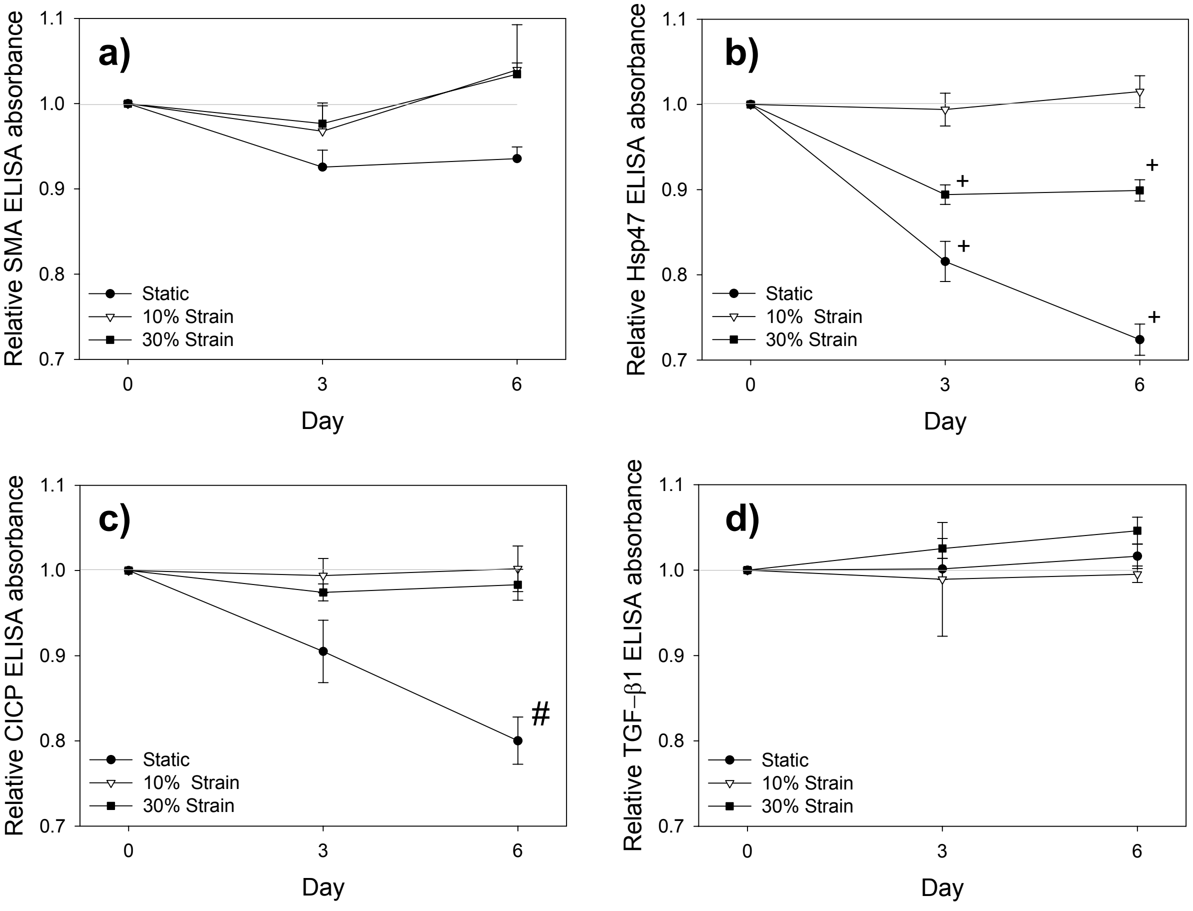

Figure 44. ELISA absorbance values for a) SMA, b) Hsp47, c) CICP, and d) TGF-β1at 0, 3, and 6 days exposed to static culture or cyclic strain of 10 or 30%. Drawn gray line represents unity. +, significantly less ($p<0.05$) than 10% strain at that time point. #, significantly less ($p<0.05$) than 10 and 30% strain at that time point.

6.2.2 AVIC deformation under circumferential tissue strain

To appreciate the micromechanical environment of the AVIC, additional leaflets were strained and held at 0, 10, and 20% strain and, after fixation, analyzed with TEM (**Figure 45**) and SALS (**Figure 46**). TEM images of single AVICs were analyzed such that the aspect ratio (major axis length/minor axis length) of the entire cell and nucleus were calculated. Using SALS, the distribution of the collagen orientation (normalized orientation index, NOI=[(90-OI)/90]*100) was calculated [171]. OI represents 50% of the fiber distribution for a given scattering of light at a point in the tissue (250 μm diameter region). Therefore, as NOI increases from 0 to 100, the fiber distribution peak becomes narrower, representing more collagen alignment.

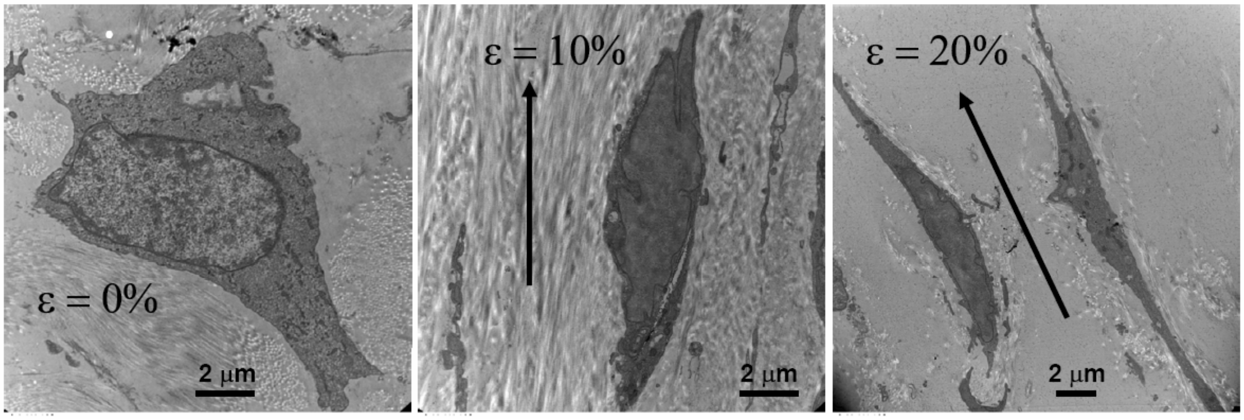

Figure 45. TEM images of AVICs at 0, 10, and 20% strain. Drawn arrows show orientation of circumferential strain.

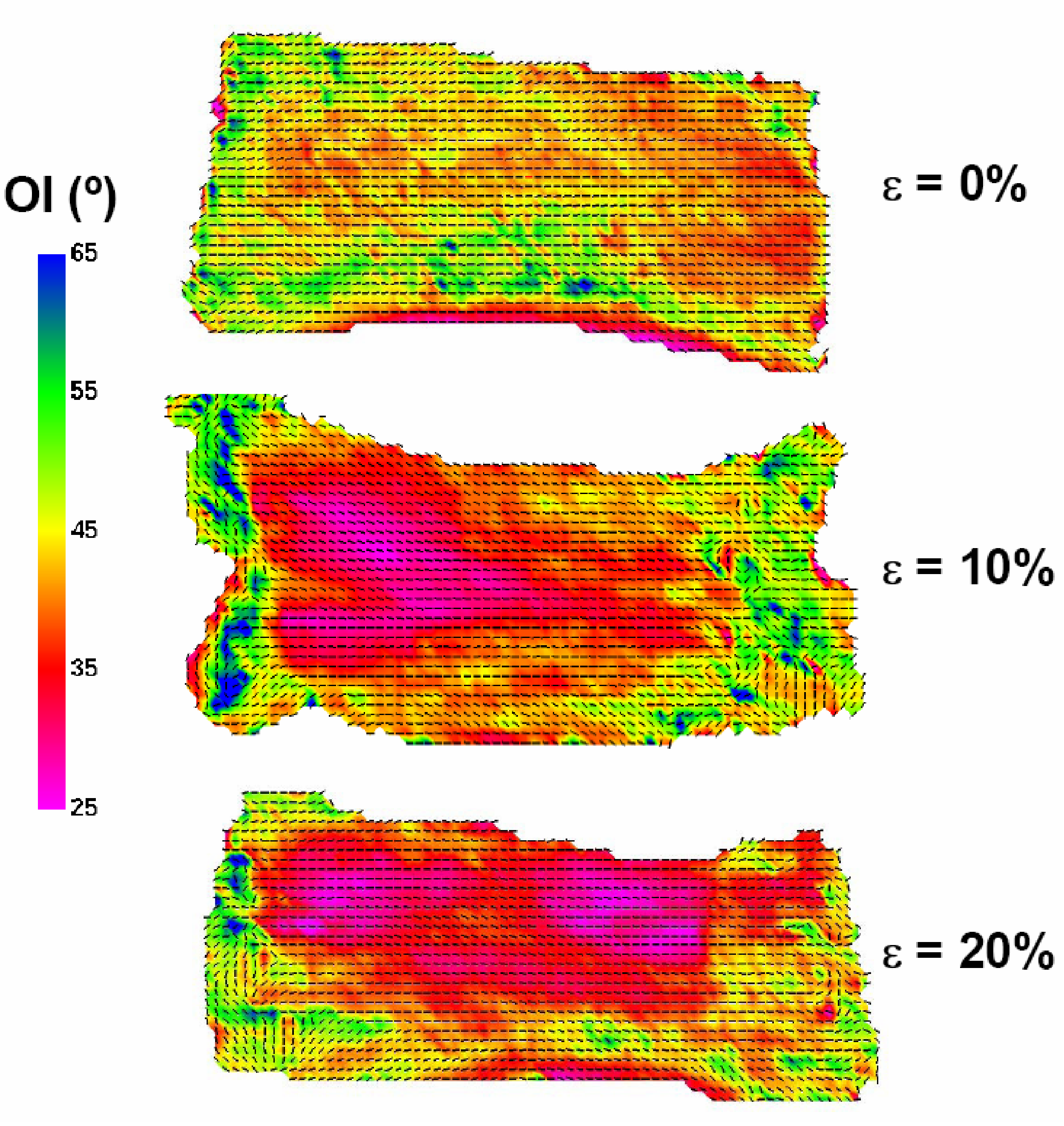

Figure 46. SALS images of circumferential strips of AV tissue under 0, 10, and 20% stain. OI color scale on left shows areas of pink as highly aligned and areas of blue as less aligned.

As found previously, with AVs fixed under increasing diastolic pressure [84], NOI increased appreciably with increasing strain (**Figure 47a**). NOI at 10 and 20% strains are significantly greater ($p<0.01$) than 0% strain. The fact that there is no change in NOI from 10 to

20% strain demonstrate that 10% strain is sufficient to largely orient the fibrillar collagen and subsequent strains result in elongation of the fibers (**Figure 47c**). The cell and nucleus aspect ratio increase together with increasing strain (**Figure 47b,d**), aspect ratios were significantly greater ($p<0.05$) for the both the cell and nucleus at 20% compared to 0 and 10%. This finding demonstrates that the nucleus is indeed a reliable cellular strain gage when examining H & E images, as preformed previously [84].

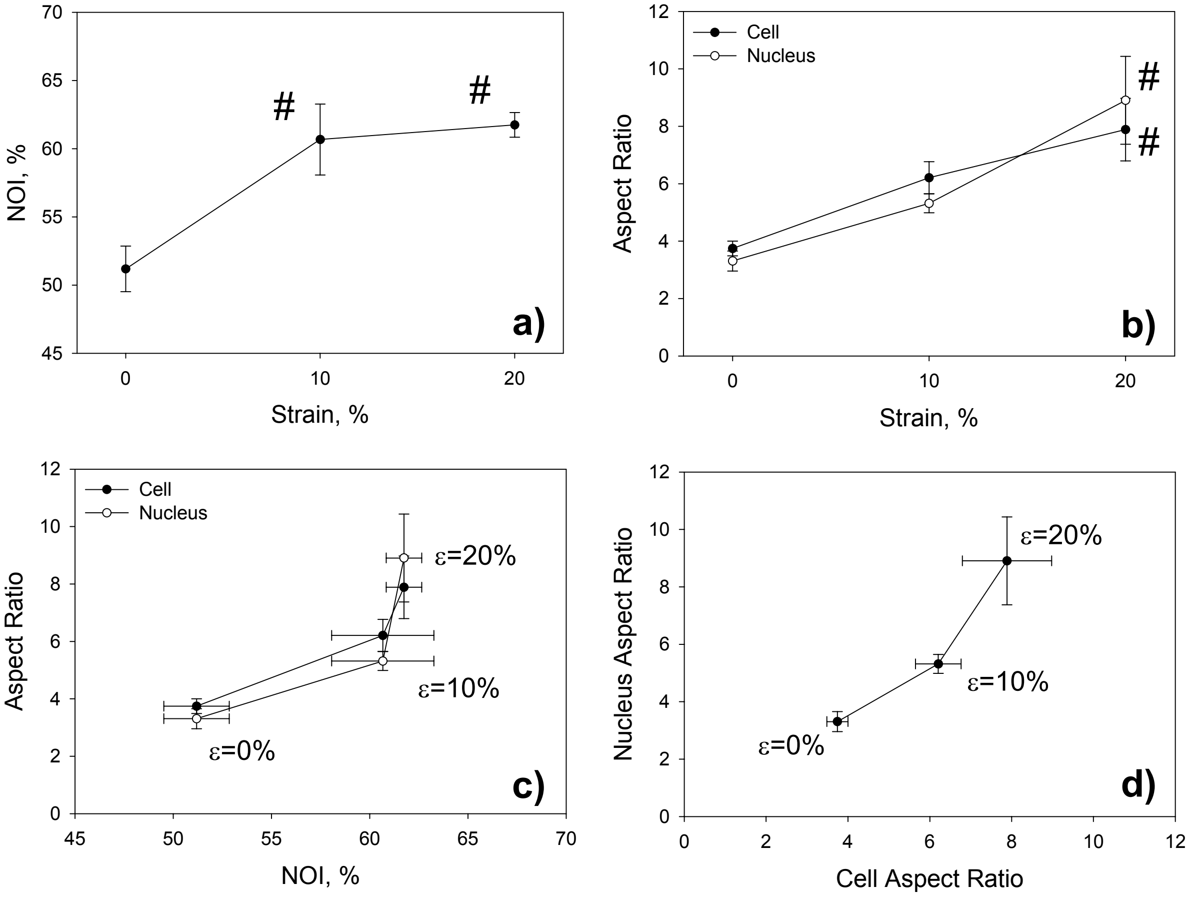

Figure 47. a) NOI versus strain, b) Aspect ratio versus strain, c) Aspect ratio versus NOI, and d) Nucleus aspect ratio versus Cell aspect ratio. #, significantly greater than 0% strain.

6.3 DISCUSSION

6.3.1 Effects of strain level on AVIC deformation, phenotype, and function

The goal of this study was to examine both the micromechanical environment of the AVIC under varying levels of circumferential strain and probe the hypothesis that biophysical mechanisms can lead to AVIC dysfunction. As expected, the AVIC and nuclei deformed in a very predictable manner with increasing circumferential strains. This was not surprising given our previous findings of changes in tissue stiffness due to AVIC contraction and relaxation [29] which highlighted the tight AVIC-ECM binding within the AV tissue.

The effect of 10% cyclic strain on the AVICs was beneficial for AVIC function compared to static culture at both 3 and 6 days as it maintained the day 0 levels of SMA, Hsp47, and CICP. There was no change in TGF-β1 from any treatments, at any time. 30% cyclic strain was chosen as it represents a substantial increase from what is thought to be the normal physiologic strain range which persists during diastolic function. From what is observed in diseased AV explants (fibrosis and calcification in the fibrosa layer), there was great interest in examining the AVIC response to cyclic strain in the circumferential direction, and it was hypothesized that excessive strain may overload the AVICs, leading to dysfunction. Within the time frame examined here, this turned out not to be the case. In fact, 30% strain had no effect on SMA or CICP compared to 10% strain, indicating that the higher strain did not cause AVICs to become more contractile or produce more collagen. There was a difference in Hsp47 with 30% strain, but it was actually decreased compared to 10%, which is counterintuitive based on what is thought about mechano-sensitive cells and their response to increased strains.

Changes in Hsp47 have been observed previously in smooth muscle cells that were exposed to excessive heat (42ºC) or oxidized LDL without a subsequent change in collagen production [123]. These states are thought to represent non-physiologic cases that were initiated *in vitro* and therefore are not the norm for typical collagen biosynthesis in a healthy tissue. Therefore, this finding is doubly confounding: primarily, one would not suspect that increased strain would lead to decreased collagen production (Hsp47) and secondly, besides the cases mentioned above we have not observed an instance with the AVIC where Hsp47 and CICP are not essentially in tandem. Hence, while this work may be somewhat preliminary with regard to duration and strain levels examined, it appears from first blush that excessive strain does not alter the AVIC phenotype nor affect collagen biosynthesis. The mechanism that leads to the decrease in Hsp47 for the 30% strain treatment is not known and further studies need to be completed to elucidate this.

The precise mechanism by which AVICs sense and adapt their surrounding micromechanical environment is currently unknown. It is assumed that they undergo large deformations during diastole which lasts about 300 ms. From the viscoelastic data that was presented in Chapter 3, it seems reasonable to assume that the AVICs deform elastically and proceed to nearly triple their aspect ratio at 20% strain during this short time frame. While aspect ratios of 30% strain were not analyzed here, it is likely that they will continue along the linear path similar to the 10 and 20% samples and result in an aspect ratio around 11 or 12. If this turns out to be the case and the ELISA results shown above are considered, it would appear that the AVIC does not modify either phenotype or function even when its aspect ratio deformation doubles, as in the case of going from 10% strain to 30% strain. Therefore, further experiments need to be performed to test the hypothesis of cellular overload possibly by modifying the setup such that biaxial loading is applied to the sample. While it has not been considered in detail previously, there is need to understand AVIC deformation response to radial loading as well.

6.3.2 AVIC micromechanics

Examination of the micromechanics of AVICs under circumferential strain was highly desirable as it allowed us to test our previous knowledge regarding AVIC deformation under increasing transvalvular pressures [84]. While the direct correlation between the uniaxial deformation of the AV strips used here and an AV under diastolic loading is not trivial, there is good evidence that normal diastolic pressure generates 10-20% circumferential strain. The biaxial response of the AV leaflet during diastole additionally includes a much larger strain in the radial direction that certainly contributes to the collagen fiber kinematics and resulting orientation due to loading. However, as the fibrillar collagen runs circumferentially with the AV leaflet, it was believed that this loading direction is likely more crucial in the mechanobiological function of the AVICs. Hence, AVIC response to circumferential strain was focused on in this study and the normal range of physiologic loading was considered.

AVIC micromechanics under increasing circumferential strain appear to be largely linear; however, from what is known about type I collagen within the AV leaflet, this response is not entirely clear. Likely, there is a very low range of tissue strain that may not result in cellular deformation as the collagen becomes uncrimped and does not carry an appreciable load. Conversely, this may not matter and any elongation of collagen fibers (from uncrimping) could cause cellular deformations as the relative compliant cells are attached to the crimped fibers via focal adhesions. There is a need to examine low increments to understand how the cells deform at the beginning of diastole.

6.3.3 Summary

The goal of this work was to examine the effect of circumferential strain on the AVIC micromechanics and potential for excessive strain causing cellular dysfunction. As anticipated, the AVIC response to increasing strain was nearly linear and the cells, once again, revealed the tight binding to the surrounding ECM. Primarily, the aspect ratio of the AVICs appears to more than double during diastole; future studies should use this result as a directive for mechanobiological studies. While the results regarding 30% strain were somewhat unexpected and imply that excessive strain does not alter AVIC function, we suspect that there is more complexity to the theory of stress overload that could be explained here and further studies should be designed accordingly.

7.0 SYNERGISTIC EFFECTS OF CYCLIC TENSION AND TRANSFORMING GROWTH FACTOR-β1 ON THE AORTIC VALVE INTERSTITIAL CELL

Aortic valve leaflets (AVLs) are unique tissues that are both supple and strong, allowing them to perform their primary function of unidirectional blood flow. Their suppleness is required for efficient opening and closing, while their compliance and strength permit apposition to withstand blood-imposed transvalvular pressure when the valve is closed. The ability to perform these passive responses is severely compromised by degenerative disease conditions wherein the leaflets become either calcified and/or fibrotic. Both conditions result in stiffening of the leaflets which simultaneously decreases their opening and closing efficacy, and may shorten the leaflets leading to insufficiency [62].

The mechanisms by which AVLs maintain their structural and functional homeostasis is presently unclear, and although the role of the aortic valve interstitial cells (AVICs) is believed to be crucial, it is not known if their biosynthetic response is driven primarily by mechanical, biochemical, or a synergistic combination of both mechanisms. Valve interstitial cells (VICs) have been recognized for many years as a heterogeneous population of fibroblasts, secretory and contractile smooth muscle cells, and myofibroblasts, aptly named due to expression of both fibroblast and smooth muscle cell markers, primarily smooth muscle α-actin (SMA) [75-78, 81]. Using micropipette aspiration, we have recently shown that isolated ovine VICs from the left side of the heart were significantly stiffer than the right side VICs [132]. Moreover, the mitral and aortic VICs were not only stiffer but also produced significantly more type I collagen, as determined by the surrogate, heat shock protein 47 (Hsp47). Hsp47 levels correlated well with cellular SMA among all VIC populations, which revealed a first-order approximation of their mechano-dependent biosynthesis. This finding implies that VICs are phenotypically and functionally tuned to actively remodel the ECM due to the synthetic demands necessary for normal tissue homeostasis.

The modulating environmental factors controlling AVIC contractility are uncertain. Additionally, it is unclear how mechanotransduction from the global and multi-modal stresses (i.e. planar tension, flexure, and shear stress) on AVLs translate to the cell and sub-cellular levels. Infiltration of neutral lipid and inflammatory cells is thought to initiate AVL calcification [156], and it is interesting to note that inflammatory cells (macrophages) are an excellent source of many growth factors and cytokines, notably transforming growth factor beta-1 (TGF-β1) [172]. This is of importance as TGF-β1 has been demonstrated to effectively alter the AVIC phenotype from a quiescent fibroblast to an activated and contractile myofibroblast in vitro [144, 152]. In vivo, this phenotypic shift is apparent when comparing VICs from normal, healthy valves with those from developing, diseased, and remodeling valves [81, 168, 173].

Therefore, we hypothesize that both cyclic, circumferential tension and TGF-β1 are modulating factors for the in situ AVIC phenotype and resulting biosynthetic state; hence, each were examined independently and in concert to determine their resulting isolated and synergistic effects. This was accomplished by exposing circumferential AVL tissue strips to extended tissue cultures under the following four scenarios and afterwards assaying AVIC contractile and synthetic proteins, bioactive TGF-β1, and performing standard histology for ECM composition:

1) Cyclic tension (Tension)

2) No loading with exogenously added TGF-β1 (TGF)

3) Neither loading nor exogenously added TGF-β1 (Null)

4) Cyclic tension with exogenously added TGF-β1 (Tension+TGF)

7.1 PROTOCOL

7.1.1 Tissue Preparation

Porcine hearts were excised from young hogs (~10 mos., ~250 lbs.) at a local USDA approved abattoir (Thoma Meat Mkt., Saxonburg, PA); for each treatment group four hearts were used. Intact AVs were excised on site and placed in preservation media (HypoThermosol HTS-FRS, BioLife Solutions, Binghamton, NY) at 4°C to assure maximal cell survival during transport [29]. Individual AVLs were excised in the lab and separated into left (LC), right (RC), and non coronary (NC) groups (**Figure 48a**). Each AVL was then trimmed such that a tissue strip was formed measuring 20 mm circumferentially and 8 mm radially (**Figure 48b**). An attempt was made to keep the endothelial cells viable by limited handling.

7.1.2 Treatment Configuration

Tissue strips from the LC and RC groups were prepared to be inserted into the tension bioreactor shown in the previous chapter (**Figure 42**). In order to couple the tissue strips and the posts of the bioreactor, the tissue was threaded on both 8 mm ends with stainless steel springs (1 cm long x 2 mm diameter x 5 turns/cm, **Figure 48c**) as reported previously for development of engineered heart valve tissues [174]. Each end of the tissue was penetrated at least four times by the spring, allowing a good stress distribution along the short axis of the tissue during loading.

Tissue strips were then inserted into the tension bioreactor by sliding the springs onto the pins inserted into the floor of the culture well and the actuating arm of the bioreactor (**Figure 48d**). To each well, 7mL of complete media was added (DMEM, 10% FBS, 1% penicillin-streptomycin, and 0.5% fungizone, all from Gibco) and was subsequently changed every 24 hours.

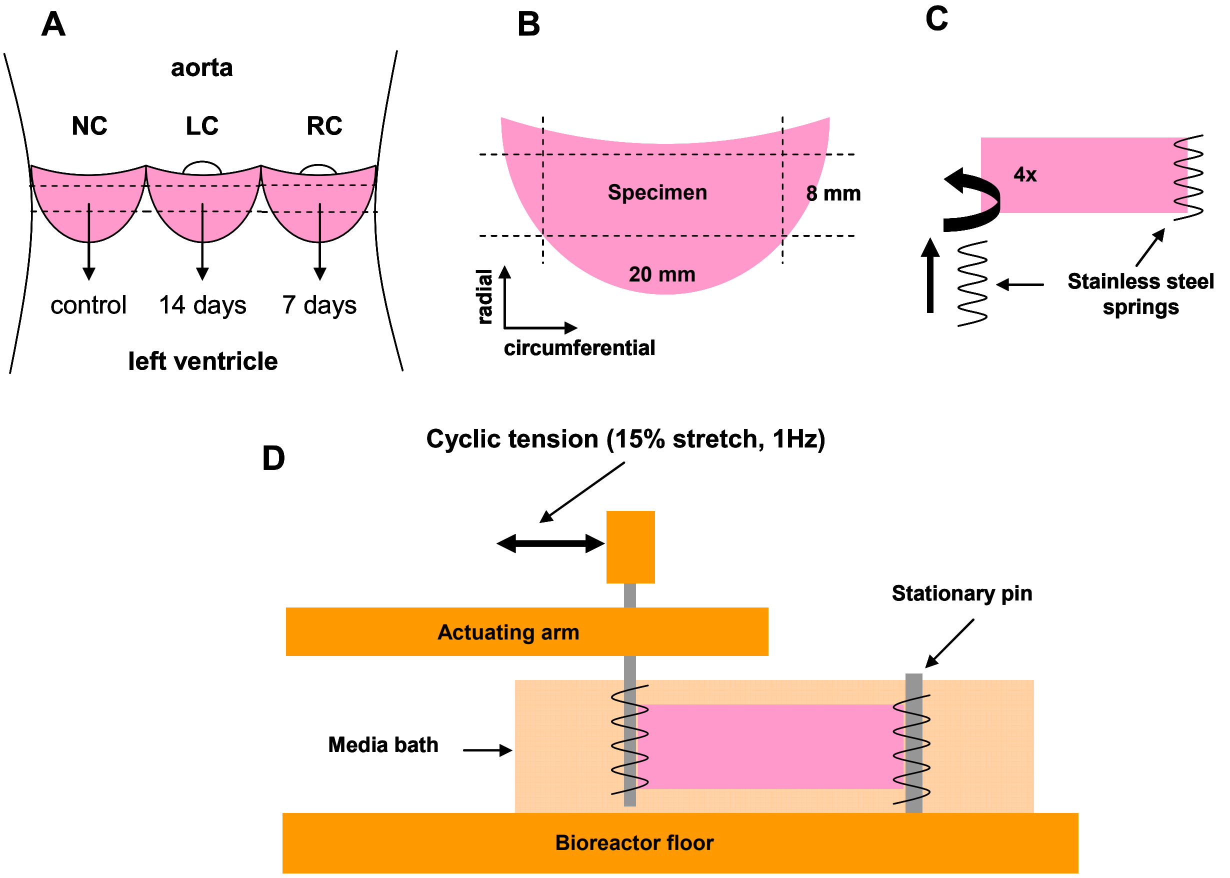

Figure 48. Schematic of AVL strip preparation. A, Opened aortic root with leaflets shown. Each leaflet (NC, RC, and LC) was designated for specific treatment durations for all groups. B, Sample preparation from dissected leaflet to attain a circumferential AVL strip measuring (20 x 8 mm). C, Threading of stainless steel springs into both tissue ends; at least four puncture sites in the tissue were used to achieve a uniform stress distribution across the width of the sample. D, Side view of an AVL strip in the tension bioreactor. The actuating arm is coupled to the linear actuator of the system to apply 15% stretch to the sample.

For groups receiving biologically active TGF-β1 (0.5 ng/mL, T5050, Sigma) [152] media was prepared as 10x stock (5 mL aliquots), frozen (-20°C), and thawed for use daily to ensure that the growth factor remained active over the subsequent 24 hours. For groups receiving cyclic tension, the linear actuator was programmed to apply ~15% stretch to the tissue at 1Hz. Groups receiving no cyclic tension were mounted into the bioreactor with the motor inactive and 0% stretch applied (tissues were slightly slack). Immediately after the LC and RC groups were loaded into the bioreactor, the NC samples were snap frozen in liquid nitrogen (-196°C) and stored at –80°C to serve as day 0 controls of AVIC function and tissue morphology. RC strips were exposed to protocols listed previously for 7 days and LC strips for 14 days (**Figure 48a**). After each treatment, tissues were removed from the bioreactor and frozen as with the day 0 samples.

7.1.3 Cell and Tissue Analysis

Samples were thawed and the center 2 mm of the tissue, along the radial axis, was removed and fixed in 10% buffered formalin for standard histology. Sections were then paraffin-embedded, sectioned at 10μm, and stained with Movat's pentachrome stain for ECM composition and distribution analysis. The average thickness of each leaflet was digitally calculated from the histology slides (SigmaScan, SYSTAT) to determine if there was any appreciable compression of the specimens during treatment. The remaining tissue was homogenized and the intra-AVIC proteins analyzed by enzyme-linked immunosorbent assays (ELISAs) for SMA and Hsp47 as reported previously [132]. Hsp47, a molecular chaperone located in the endoplasmic reticulum, has been shown to facilitate proper secretion of type I collagen in multiple cell types [122, 123, 130], and has also been found to nearly eliminate proper collagen production in Hsp47$^{-/-}$ cells [175, 176]. Moreover, it has been demonstrated that selectively transfecting smooth muscle cells with a retrovirus containing Hsp47 cDNA resulted in increases of both intra- and extracellular steady state type I collagen production, while Northern blots of total RNA showed a tandem increase in both Hsp47 and procollagen [123]. Hence, Hsp47 was deemed a suitable surrogate for type I collagen in this study; however, to validate the accuracy of Hsp47, all samples were additionally assayed by an ELISA for type I collagen C-terminal propeptide (CICP, Metra CICP EIA Kit, Quidel Corp.) according to the manufacturer's instructions. Similarly, biologically active TGF-β1 was assayed with the TGF-β1 E_{max}® Immuno-Assay System (Promega Corp.) according to the manufacturer's instructions [152].

As it is not possible to demarcate the cell type variability within the tissue, we assumed that the AVIC population is on a continuum which ranges from fibroblasts to myofibroblasts to smooth muscle cells. Therefore, all assays herein are lumped quantifications of the cell population. Based on previous work [51, 80, 81, 168, 173], there is strong support that the myofibroblast is highly responsible for active valvular tissue remodeling and is very prevalent in many valvular pathologies.

7.1.4 Statistics

ELISA values, thickness measurements, and bioactive TGF-β1 values are reported as mean ± standard error (SEM). For statistical comparison, all ELISAs and bioactive TGF-β1 were analyzed with a repeated measures two-way ANOVA for day and treatment group. Post-hoc pair wise comparisons were performed with the Tukey test. Thickness measurements were compared with ANOVA within each treatment group. All differences were deemed statistically significant for p<0.05.

7.2 RESULTS

All biochemical assay results are found in **Table 5** (mean ± SEM). It was found that for all assays (Hsp47, SMA, CICP, and Bioactive TGF-β1) there was a significant difference (p<0.001) for time, treatment, and their interaction. Statistical comparisons that follow were preformed with the Tukey test.

Table 5. Raw values (mean ± SEM) for each assay

mean ± SEM n=4	Day	SMA (ng/ml)	Hsp47 (ng/ml)	CICP (ng/ml)	Bioactive TGF-β1 (pg/ml)
Null	**0**	1.65 ± 0.04	1.34 ± 0.03	2.74 ± 0.07	46.78 ± 1.67
	7	1.53 ± 0.03	1.25 ± 0.04	2.54 ± 0.07	52.43 ± 2.09
	14	1.15 ± 0.02	0.96 ± 0.02	2.12 ± 0.02	47.20 ± 1.64
Tension	**0**	1.62 ± 0.05	1.16 ± 0.01	2.29 ± 0.10	52.20 ± 1.28
	7	1.57 ± 0.03	1.51 ± 0.02	2.95 ± 0.23	66.86 ± 3.16
	14	1.82 ± 0.04	1.52 ± 0.04	2.98 ± 0.09	63.30 ± 1.09
TGF	**0**	1.65 ± 0.02	1.41 ± 0.02	3.04 ± 0.13	50.23 ± 2.33
	7	1.81 ± 0.02	1.73 ± 0.03	3.50 ± 0.15	117.50 ± 5.56
	14	1.96 ± 0.03	2.03 ± 0.04	4.23 ± 0.04	95.25 ± 1.70
Tension+TGF	**0**	1.58 ± 0.02	1.30 ± 0.06	3.14 ± 0.12	55.43 ± 1.88
	7	3.02 ± 0.05	3.42 ± 0.12	7.29 ± 0.19	621.25 ± 8.69
	14	3.87 ± 0.04	4.30 ± 0.07	8.72 ± 0.28	647.00 ± 8.13

7.2.1 SMA and Hsp47 Quantification

ELISA absorbance values for SMA (Fig. 3A) and Hsp47 (Fig. 3B) reveal very similar trends for each treatment over the duration of the experiment. All SMA data points are significantly different (p<0.05) ***except*** the following: no difference between any groups at day 0; no difference between Null and Tension at day 7; and no difference between day 0 and 7 for the Tension group (**Figure 49a**). The Tension+TGF group was significantly greater (p<0.001) than all other groups at both days 7 and 14. All Hsp47 data points are significantly different ($p<0.05$) ***except*** the following: no difference between any groups at day 0 except between TGF and Tension ($p=0.006$); no difference between day 7 and 14 for the Tension group (**Figure 49b**). The Tension+TGF group was significantly greater ($p<0.001$) than all other groups at days 7 and 14.

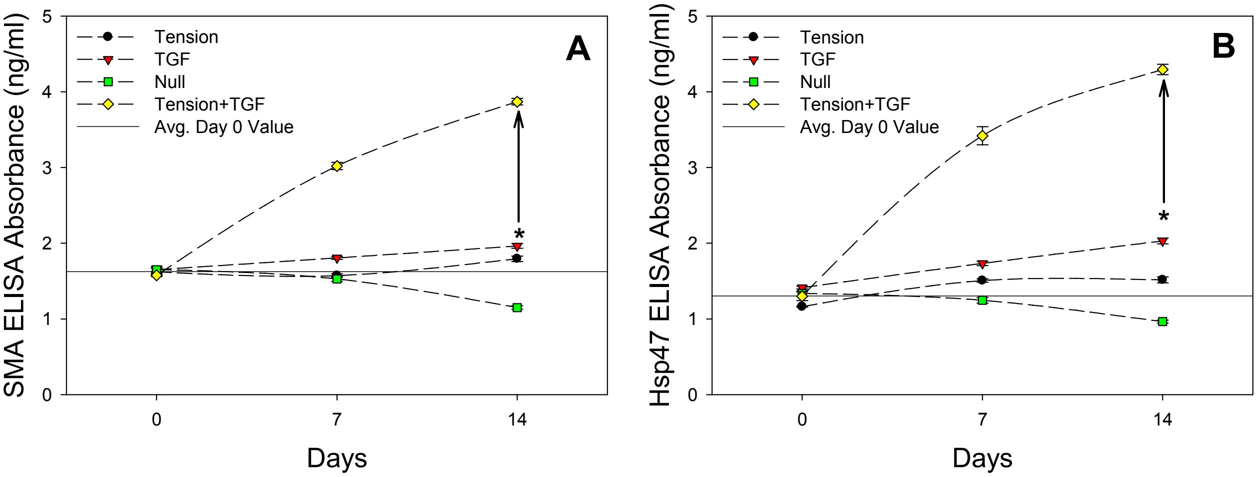

Figure 49. A, SMA ELISA results (mean ± SEM). Tension+TGF group significantly greater ($p<0.001$) than all other groups at 7 and 14 days. B, Hsp47 ELISA results (mean ± SEM). Tension+TGF group significantly greater ($p<0.001$) than all other groups at 7 and 14 days. Drawn asterisk (*) shows sum of Tension and TGF results individually at 14 days and drawn vertical line represents the difference between this sum and the Tension+TGF group. As a reference, the drawn horizontal line represents the average day 0 value of all groups.

7.2.2 CICP Quantification

While Hsp47 expression has been shown to be highly correlated with type I collagen biosynthesis [122, 123, 130, 175, 176], it was confirmed here by the use of a CICP ELISA (**Figure 50**). All CICP data points are significantly different ($p<0.05$) ***except*** the following: no difference between Tension and Null groups or TGF and Null groups on day 0; no difference between day 0 and day 7 or day 7 and day 14 for the Null group; no difference between day 7 and 14 for the Tension group; and no difference between day 0 and 7 for the TGF group. As with

Hsp47 (**Figure 49b**), CICP values were significantly greater (p<0.001) for the Tension+TGF group at both 7 and 14 days, compared to all other groups (**Figure 50**). Therefore, throughout the remainder of this manuscript, only Hsp47 will be discussed when referring to collagen biosynthesis, as the present result validates that increases in Hsp47 expression suitably represent increased type I collagen synthesis for AVICs. The drawn asterisk (*) on each graph in **Figure 49** and **Figure 50** represents the cumulative effects of Tension and TGF at day 14 with the vertical arrow representing the difference between this value and the Tension+TGF group, which is considered the synergistic response of the two stimuli.

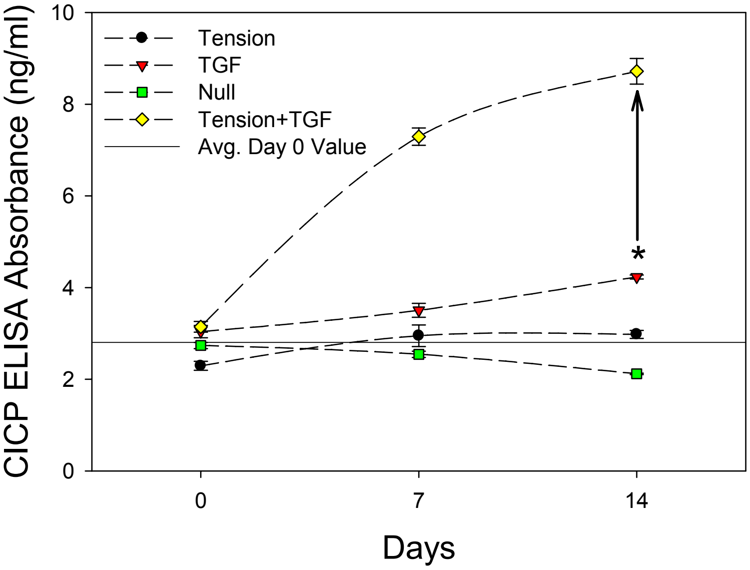

Figure 50. CICP ELISA results (mean ± SEM). Tension+TGF group significantly greater (p<0.001) than all other groups at 7 and 14 days. The CICP results demonstrate that Hsp47 is suitable surrogate for type I collagen synthesis as their trends are nearly identical. Drawn asterisk (*) shows sum of Tension and TGF results individually at 14 days and drawn vertical line represents the difference between this sum and the Tension+TGF group. As a reference, the drawn horizontal line represents the average day 0 value of all groups.

7.2.3 Bioactive TGF-β1 Quantification

All bioactive TGF-β1 data points are significantly different (p<0.05) ***except*** the following: no difference between any groups on day 0; no difference between Tension and Null groups on day 7; no difference between day 0, 7, or 14 for Null group; and no difference between day 0, 7, or 14 for Tension group (**Figure 51**). The Tension+TGF group was significantly greater ($p<0.001$) than all other groups at both days 7 and 14.

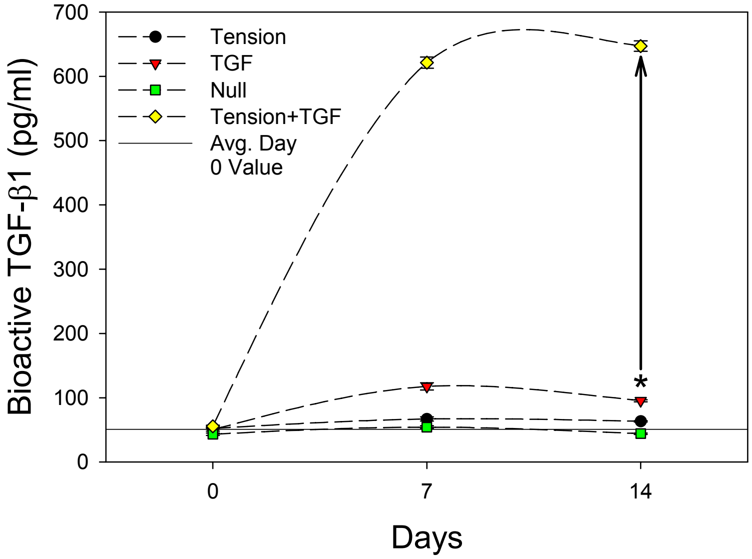

Figure 51. Bioactive TGF (mean ± SEM) was statistically greater ($p<0.001$) for the Tension+TGF group compared to all other groups at 7 and 14 days. Drawn asterisk (*) shows sum of Tension and TGF results individually at 14 days and drawn vertical line represents the difference between this sum and the Tension+TGF group. As a reference, the drawn horizontal line represents the average day 0 value of all groups.

7.2.4 Ratio Change due to 14 Day Treatment

Normalized results at day 14 (ratio of day 14/day 0) revealed a dramatic response for the Tension+TGF group; SMA, Hsp47, CICP, and bioactive TGF-β1 (**Figure 52**) were significantly greater ($p<0.001$, shown as # on **Figure 52**) compared to all other groups. For the Null group, SMA, Hsp47, and CICP were all significantly less ($p<0.05$, shown as ^) at day 14 compared to day 0 (drawn line at unity represents day 0 values). For both Tension and TGF groups, SMA, Hsp47, CICP, and bioactive TGF-b1 were significantly greater ($p<0.05$, shown as +) at day 14 compared to day 0.

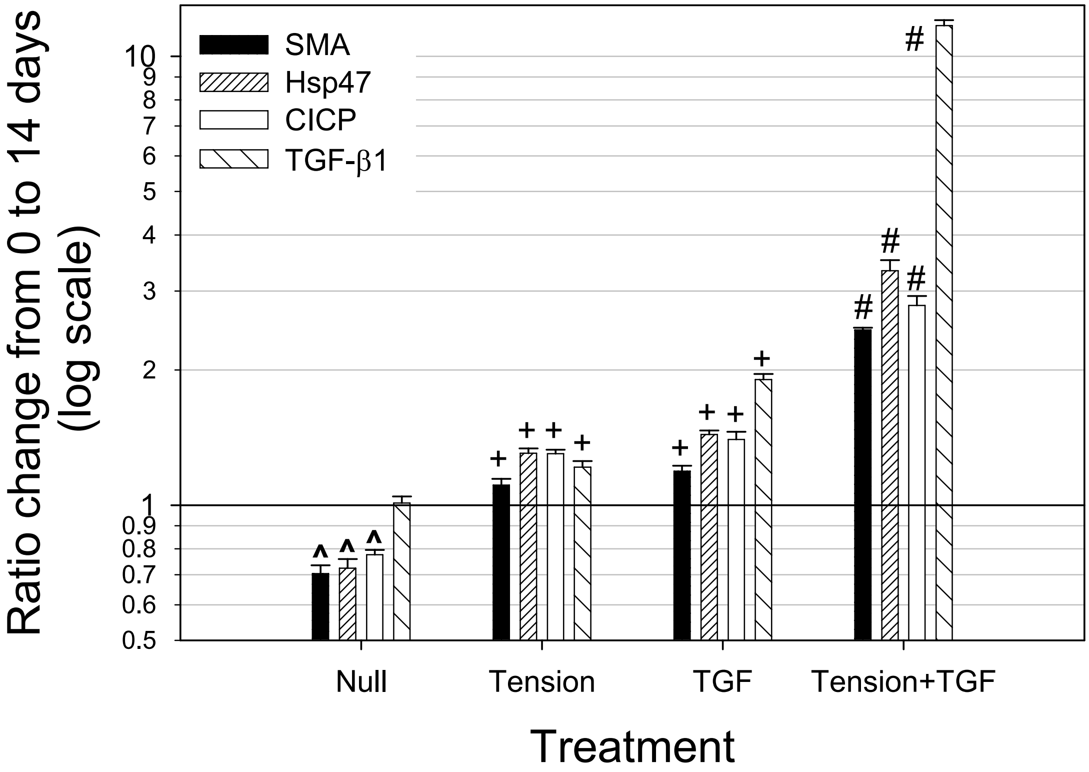

Figure 52. Ratio change from 0 to 14 days (i.e. day 14/day 0) (mean ± SEM). Drawn line at unity represents day 0 values; ^ denotes significantly less ($p<0.05$) than unity, + denotes significantly greater ($p>0.05$) than unity, and # denotes significantly greater ($p<0.001$) than all other groups. NOTE: LOG SCALE.

7.2.5 Histology of AVL Strips

With Movat's pentachrome stain (**Figure 53**), ECM components are distinguished as proteoglycans (bluish-green), collagen (yellow), and elastin (dark violet); AVIC nuclei are dark red. All day 0 samples were similar with a distinct tri-layered architecture (fibrosa (F), composed of collagen; spongiosa (S), composed of proteoglycans; ventricularis (V), composed of elastin; **Figure 53a**). Only 14 day samples are shown (**Figure 53b-e**) as changes in the 7 day samples were not as distinctive.

Null samples (**Figure 53b**) appeared to have little or no proteoglycans in the spongiosa layer. Moreover, elastin fibers in the ventricularis layer were less pronounced than at day 0. Tension samples (**Figure 53c**) showed the tri-layered structure seen at day 0. TGF samples (**Figure 53d**) appeared to be similar to Null samples with few proteoglycans evident in the spongiosa layer. However, unlike the Null samples, TGF samples did have a clear ventricularis layer with numerous elastin fibers. Finally, Tension+TGF samples (**Figure 53e**) did not have an apparent spongiosa layer, but had elastin fibers making up nearly half of the thickness of the leaflets. In all samples, AVIC nuclei were present and evenly dispersed throughout the thickness of the tissue. Thickness changes between groups at any time point were not statistically different (**Table 6**).

Table 6. AVL thickness values (mean ± SEM)

mean ± SEM n=4	Day	Thickness (μm)
Null	0	405 ± 38
	7	365 ± 49
	14	377 ± 33
Tension	0	417 ± 17
	7	342 ± 48
	14	365 ± 14
TGF	0	407 ± 38
	7	352 ± 36
	14	403 ± 64
Tension+TGF	0	385 ± 33
	7	357 ± 36
	14	390 ± 45

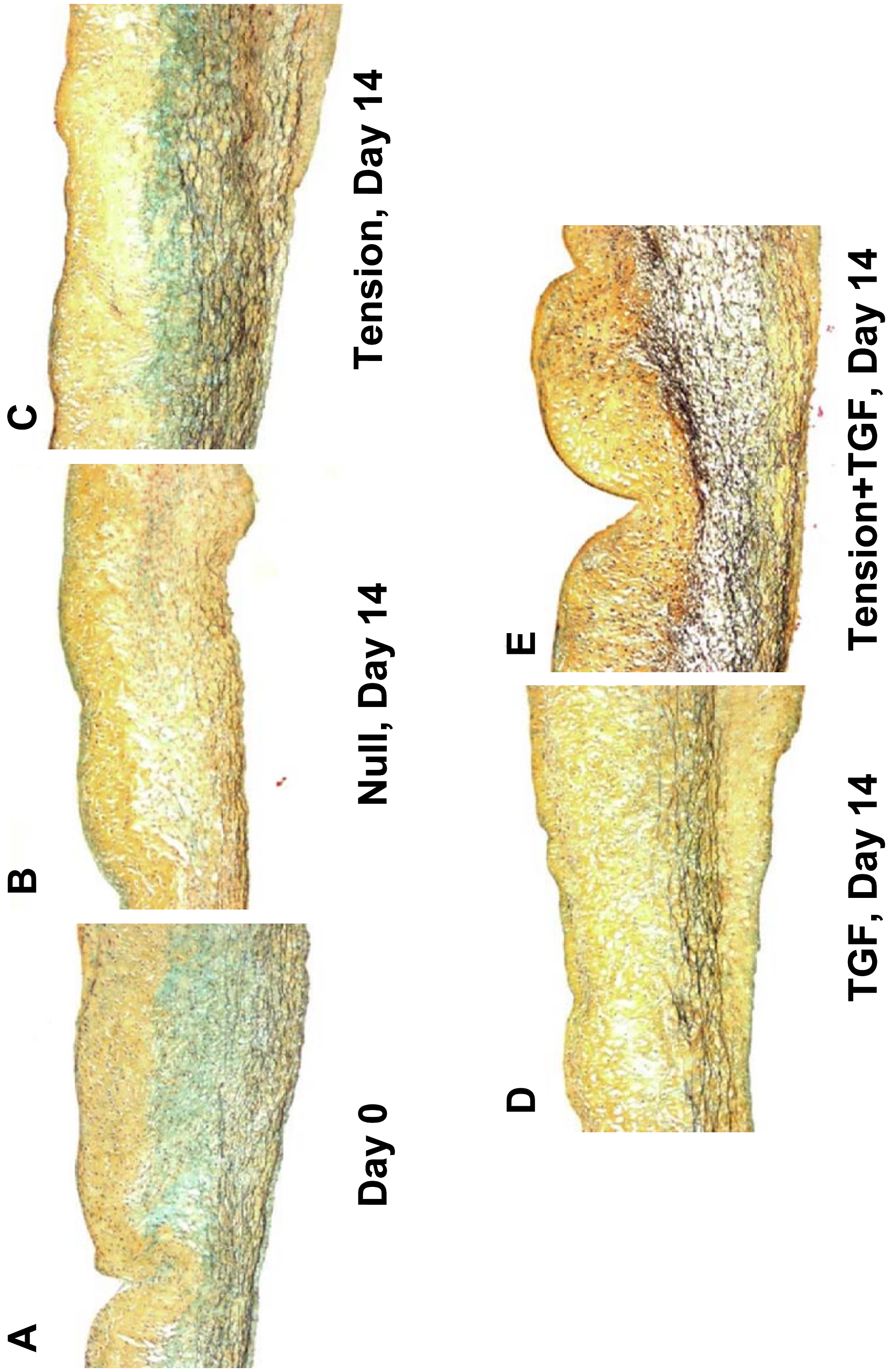

Figure 53. Movat's pentachrome staining of the middle portion of treatment strips at day 0 and 14 days. A, Healthy porcine AVL (day 0). Note the distinct tri-layered structure (fibrosa (F): collagen (yellow, top); spongiosa (S): proteoglycans (bluish green, middle); ventricularis (V): elastin (dark violet fibers, bottom)). B, Null group at 14 days with no apparent proteoglycans and diminshed elastin fibers. C, Tension group at 14 days with similar ECM composition to day 0 (A), but more intense elastin fibers. D, TGF group at 14 days with no apparent proteoglycans and slightly diminished elastin fibers. E, Tension+TGF group at 14 days with no apparent protoeglycans, but intense elastin fibers in the central portion of the leaflet.

7.3 DISCUSSION

7.3.1 AVIC Physiology: SMA and Hsp47 Correlates

The overarching goal of this study was to determine the effects of cyclic tension and TGF-β1 on the in situ AVIC phenotype and biosynthetic function. To accomplish this, circumferential AVL strips were exposed to isolated and combined biomechanical and biochemical treatments for up to 14 days in vitro. Effective changes were determined by quantifying the contractile (SMA) and collagen biosynthetic (Hsp47, confirmed with CICP) proteins of the AVIC population and examining histology of the AVLs.

As we previously found that SMA and Hsp47 were well correlated between isolated ovine VICs of the four different heart valve leaflets [132], we were interested if this remained the case with in situ AVICs under different stimuli. Indeed, the results from this study further support the observation that VICs are highly sensitive to their environment, as SMA and Hsp47 trends were very similar for each treatment group (**Figure 49a, b**). The mechanobiological consequence of this is that VICs are not only well tuned to their mechanical and biochemical environment, but are capable of adaptive cytoskeletal remodeling and resulting biosynthetic response, which likely serves to retain homeostasis within the tissue.

7.3.2 AVIC Mediated-Pathology: Synergistic Effects of Tension+TGF

It is our opinion that the most interesting finding from this study was the profound, synergistic effect of Tension+TGF on SMA (**Figure 49a**) and Hsp47 (**Figure 49b**) levels of the AVICs. While changes resulted from other treatments, their effects were not as substantial as those seen in the combined group. The effect of TGF-β1, in the presence of applied cyclic tension, to dramatically increase the intracellular SMA and Hsp47 levels reveals an important finding. Here, we demonstrate the ability to effectuate an altered AVIC state in the presence of TGF-β1, which would be analogous to TGF-β1-producing, infiltrating macrophages under quasi-normal AVL biomechanical function in vivo.

The effectiveness of added bioactive TGF-β1 was apparent in the TGF group (**Figure 51**). However, the mechanism behind the substantial increase in bioactive TGF-β1 for the Tension+TGF group is not clear, as Tension alone revealed minimal differences in bioactive TGF-β1 at 7 or 14 days. While this sensitivity to TGF-β1 has been shown previously for AVICs in culture [144, 152, 177], it has yet, until now, to be demonstrated with AVICs in situ. After two weeks of the Tension+TGF treatment, the AVIC population was nearly 2.5-fold more contractile (by SMA quantification) and was producing ~3-times as much type I collage (by Hsp47 and CICP quantification) compared to day 0 (**Figure 51**).

The ramifications of this finding serve to directly implicate the AVIC as a contributor to AVL degenerative pathologies. Since cyclic tension can never be relieved in AVLs in-vivo, the introduction of TGF-β1 (e.g. by macrophage infiltration) would likely lead to a similar response in vivo that was observed here. The chronic effects of hyper-contractile and hyper-collagen producing AVICs are not entirely clear at the present time as this study was only conducted over a two week period; however, if TGF-β1 levels such as these are achieved in vivo over a period of months or years, the resulting state of the AVL architecture would likely no longer resemble that of healthy tissue. Additionally, while Tension alone had little effect on the ECM architecture compared to day 0 controls (**Figure 53a, c**), TGF was similar to Null with a loss of the spongiosa; however, there was still an apparent layer of elastin. The combination of

Tension+TGF (**Figure 53e**) resulted in loss of the spongiosa layer with a substantial increase in elastin. Therefore, while elastin was not directly quantified in this study, it appears to be macroscopically conserved by the AVICs in the presence of TGF-β1 and further examination of this will be necessary in the future.

7.3.3 AVIC Homeostasis: Sensitivity to TGF-β1 and the Role of Cyclic Tension

The general myofibroblast phenotype found elsewhere in the body is normally identified by the presence of SMA, which has been shown to be upregulated in the presence of TGF-β1 [90]. The efficacy of TGF-β1 is dependent on the co-localization of fibronectin (FN) splice variant ED-A-FN in the surrounding ECM [172]. However, it has been shown that the presence of both TGF-β1 and ED-A-FN were not sufficient to maintain the contractile phenotype of rat dermal myofibroblasts when mechanical tension was released from the tissue [93]. Hence, we speculated from the outset of this work that Tension alone would be able to maintain the in vivo AVIC protein levels, and that TGF alone would not be effective in this maintenance. This turned out not to be the case as TGF alone actually resulted in comparable or greater SMA and Hsp47 levels than Tension alone. The consequence of this finding reveals the sensitivity of the AVIC to surrounding levels of cytokines in the absence of applied mechanical stimuli. Though an interesting finding, this situation does not occur in vivo for AVLs.

During normal in vivo function, AVLs are exposed to cyclic flexure (during opening and closing), tension (when closed), and shear from passing blood (when opened), with tension dominating 60% of the cardiac cycle. Therefore, the effects of cyclic tension were thought to be a major contributor in AVIC mechanobiological function. Previously, static pressure [165] and constant shear [102] of AVLs has been unable to maintain the SMA+ AVIC phenotype; hence, we sought to examine the cellular response due to circumferential cyclic tension in the physiologic range. As expected, SMA and Hsp47 levels of the Tension group at day 14 most resembled those of day 0 compared to the other treatment groups. Moreover, the histological results (**Figure 53**) reveal that the Tension group at 14 days was most similar to the day 0 controls with respect to ECM composition and architecture. This finding implies that under normal physiologic conditions, mechanical stimulation (particularly planar tension during diastole) is a key contributor to AVIC phenotypic modulation and resulting biosynthesis. Additionally, loss of proteoglycans in the spongiosa region of groups not receiving mechanical stimulation was not expected, as tension was believed to likely compress this region; however, it appears from the histology that these proteoglycans either dissociated on their own, the non-stimulated AVICs enzymatically digested them, or the AVICs were not able to actively synthesize new proteoglycans in the absence of applied tension.

The Null treatment resulted in concomitant decreases in all proteins assayed (**Figures 49 and 50**) and loss of the tri-layered ECM architecture (**Figure 53b**). This indicates that AVICs require mechanical stimulation or cytokines to remain biosynthetically active and normal. Though data points were only obtained up to two weeks, there is reason to believe that further decreases in both protein levels would occur at longer times. This finding is believed to be a directive of pre-implant mechanical conditioning that will likely be needed for a tissue engineered heart valve. As this was an exemplary tissue, with proper ECM architecture, cell-ECM connectivity, and cell-cell communication, the loss of in vivo-like qualities of the AVICs in the absence of mechanical stimulation further supports the need for proper conditioning of an engineered tissue prior to implantation.

7.3.4 Study Rationale and Limitations

In the present study, AV leaflets used for each treatment group at 0, 7, and 14 days came from the same valves. Chiefly, we assumed that the range of SMA and Hsp47 levels between the leaflets of the same AV were small compared to the changes measured in this study due to applied treatments. This was based on results from our previous study where we quantified these proteins from each leaflet of two AVs [132] and found the range of protein levels to be fairly small (Hsp47=1.163 ± 0.047 ng/ml; SMA=1.638 ± 0.024 ng/ml; n=6). Thus, this experimental design allowed us to use a single leaflet from each valve (NC leaflet) essentially as its own control, so that changes at 7 and 14 days in the RC and LC leaflets resulted from the applied treatments.

The small differences between the means of any day 0 groups are believed to be a result of collecting specimens on different days from the abattoir. Indeed, consistent with this assumption was the observation in the current study that variation in the Hsp47 and SMA values for all day 0 means (**Figure 49**) was very small. Because it was necessary to use slaughterhouse animals for this type of study, it was not possible to control variables such as diet, weight, and overall health of the animals (nor, screen these protein levels *a priori*); therefore, day 0 differences are believed to be due to valve-to-valve variability of the animals collected on different days. Moreover, due to the destructive nature of the assays, it was not possible to do repeated measures analysis with these samples. Therefore, with the above considerations, the experimental design and statistical comparison were deemed appropriate for the goals of the present study. Finally, changes resulting from each applied treatments over time was the focus of this work and differences for the Tension+TGF group, due to synergism, were far more substantial compared to all other groups, including those at day 0.

The results and interpretation presented here are predicated on the circumferential cyclic tension applied to the samples, and 15% stretch is within the normal physiologic range [19]. We have recently shown that AVICs undergo profound nuclear deformations during diastolic loading [84] and implicitly assumed that the main effect of tissue strain on AVICs is to induce cellular deformations to elicit key biological responses. In this previous study [84], we demonstrated that these cellular deformations occur at peak diastolic loading, where the circumferential strains are approximately 10% to 20% strain [178]. Thus, application of 15% strains to circumferentially oriented strips was a suitable approximation to the in vivo mechanical milieu. Moreover, the method of attachment of the tissue to the bioreactor actually is considered strip biaxial and not uniaxial [49], which is more physiologic because the strain in the radial direction is held at ~0%. While the strain level used in this study was within the physiologic range, the strain rate used to achieve this level is far below that found in vivo. Currently, we have begun to examine high strain rate, tissue-level mechanics of heart valve leaflets [39], and plan on examining these effects on AVIC function in the near future, while also incorporating load measurement due to applied strain for more advanced biomechanical analyses.

Although AVIC survival was not directly quantified in this study, it has been previously demonstrated that extended static cultures of heart valve tissues contained predominantly viable VICs throughout the leaflet well past 30 days [179]. Additionally, an attempt was made to maintain an intact endothelium on the AVL strips with limited handling; however, examination of endothelial cells was not the focus of this study and their state was not assayed at any point. While the interaction between the AVICs and endothelial cells likely plays a key role in valve physiology and resulting pathologies, their interaction was beyond the scope of this study. Well controlled experiments are currently being planned to address this important topic.

7.3.5 Summary

This study was the first to examine the combined effects of cyclic tension and TGF-β1 on the AVIC contractile phenotype and resulting collagen biosynthesis. As in previous studies, TGF-β1 had an impact on AVICs in the absence of mechanical stimulation; however, this was the first examination of in situ AVIC response. Moreover, we demonstrated the ability to elicit an activated AVIC phenotype in the combined presence of Tension+TGF, which is extremely relevant for the genesis and possible perpetuation of AVL degenerative pathologies such as calcification and fibrosis. It is believed that results from this study aid in understanding the means by which AVICs maintain homeostasis, the etiology of certain degenerative AVL pathologies, and the development of protocols used to condition engineered valvular tissues.

8.0 SUMMARY AND CONCLUSIONS

8.1.1 Major findings from this work

The goal of this work was to elucidate the complex mechanobiologic function of the AVIC with respect to its biomechanical environment, plastic phenotype, and biosynthetic capabilities. To accomplish this, we examined the central hypothesis that the AVIC is a unique cell with a plastic phenotype that is modulated due to certain environmental factors and that is modulation is important in the homeostasis of AV leaflet tissue. This hypothesis was examined via five aims that are recalled below for the benefit of the reader. From these aims, many insights were gained and, indeed, the body of knowledge of AVIC mechanobiology was appropriately added to. The primary findings from each of the five specific aims can be summarized belwo.

1. **Determine the correlation between VIC stiffness and biosynthesis in all heart valves.**
2. **Determine the tissue remodeling potential of AVICs in comparison to PVICs *in vitro*.**
3. **Determine AVIC-ECM connectivity and biomechanical contribution of the contractile AVIC to leaflet bending stiffness *in situ*.**
4. **Determine the *in situ* micromechanical environment of the AVIC under varying degrees of circumferential strain and the possible effects of cellular stress overload.**

5. **Determine the independent and synergistic effects of cyclic tension and TGF-β1 on the AVIC *in situ*.**

From Aim 1, it was found that he left side valves (MV and AV) have interstitial cells that are significantly stiffer, contain more cytoskeletal SMA, and produce more type I collagen. Additionally, it was found that the level of SMA and type I collagen production are highly correlated, suggesting that all VICs are mechano-sensitive cells such that they appropriately modulate their level of SMA in order to synthesize the appropriate level of structural collagen. This study served to form a firm foundation and reference from which the further studies are based.

Results from Aim 2 studies further highlighted this finding of left side VICs being stiffer and containing more SMA. This was accomplished by comparing PVICs and AVICs with respect to cell stiffness (with AFM) and remodeling potential via a collagen gel contraction protocol. With identical treatment, AVICs were much stiffer when seeded in a monolayer configuration and effectively contracted the collagen gels much faster. As the internal cytoskeleton generates the necessary forces to resist deformation and elicit contraction, these results again reveal that the AVIC has a more substantial cytoskeleton, and therefore, is capable of greater tissue remodeling.

Aim 3 represented a transition from single cell, *in vitro* experiments to *in situ* experiments. Here, the ability of the AVICs to contract and relax, due to the internal myofibroblastic cytoskeleton, was examined by examining the bending stiffness of AV leaflets before and after addition of KCl and thapsigargin, respectively. It was found that the AVICs can generate different levels of contraction depending on the surrounding ECM which was probed by bending the leaflets in different layers. While showing that the cellular contraction of AVICs does not contribute to tissue level mechanics, this study revealed the intimate binding of the AVICs and the various ECM components of the leaflet tissue.

Aim 4 was envisioned from the outset to be a seminal study in AVIC mechanobiology; however, the results were somewhat unremarkable and increasing circumferential strain did not appear to generate cellular overload. There was a significant decrease in the molecular chaperone Hsp47, which is a surrogate for type I collagen production, but this was not confirmed by CICP. Though excessive strain (30%) in the circumferential direction did elicit a change in Hsp47, this decrease was counter-intuitive as previous findings have shown an increase in Hsp47 due to heat treatment (42ºC) and excessive oxidized-LDL. Therefore, within the short duration of treatment used here, it appears that excessive strain does not overload the AVICs and they are able to effectively maintain normal cytoskeletal and biosynthetic levels.

Finally, studies from Aim 5 revealed a very significant and synergistic effect of TGF-β1 in the presence of cyclic strain on the *in situ* AVIC. This study was the first to examine the effects of TGF-β1 on intact AVICs in a quasi-physiologic environment. Results from this study represent the most clinically relevant work presented here. Essentially, dysfunction of AVICs was initiated with the addition of TGF-β1 such that the cell population was 3x more contractile and producing 3x more collagen than in normal conditions. Therefore, this final study represents a directive for future mechanobiologic studies of the AVIC that highlights the need to understand how elevated cytokine levels arise in the AV and the subsequent cascade of events that follow.

8.1.2 AVIC phenotype and function to maintain tissue homeostasis

Native AV leaflet architecture is tri-layered with distinct ECM components in each layer though the AVIC population appears to be evenly dispersed and present through the thickness. This specialized and highly evolved architecture demonstrates that while they appear phenotypically similar despite their location through the thickness, the AVICs effectively synthesize and degrade the surrounding and different ECM components that make up constituent layers. Although the ventricularis (containing elastin) and spongiosa (containing glycosaminoglycans) layers were not the ECM components which were the focus of this work, their appropriate maintenance is likely as critical as that of the type I collagen of the fibrosa layer.

It has been shown here and by others that the AVIC is sufficiently bound to the surrounding ECM such that it can generate tissue-level forces due to contraction and relaxation. This measurable quality is a direct reflection of the mechano-sensitive apparatus used by the AVIC to effectively modulate its internal cytoskeleton and resulting biosynthetic output depending on the state of the surrounding tissue. One component of this apparatus not explored here is the focal adhesion where the cell-ECM junction and integrins are found. Just as the cytoskeleton is crucial, this extracellular anchorage is crucial for mechanotransduction and should be appropriately investigated in due course. Moreover, and likely most importantly, the internal workings of the AVIC have not, to our knowledge, been explored in any detail and these elements certainly hold the greatest wealth of information for understanding the mechanobiology of the AVIC.

8.1.3 Role of AVIC phenotype and biosynthesis in AV pathologies

The results from all studies shown here summarily and further demonstrate that the AVIC is dynamic and unique cell with potential for phenotypic modulation that is predicated on environmental factors. As these cells are responsible for the synthesis of new proteins and degradation of old or damaged ECM proteins, their continued performance is crucial to the long term stability of the valvular tissue. Further, their dysfunction is likely paramount for the etiology of age-related, degenerative valve disease. As shown in **Figure 12**, there are multiple environmental factors with potential to alter the intracellular machinery and function of the AVICs, but we speculated from the outset that the local mechanical environment would be the primary modulator and that cytokines would be secondary. During the *in situ* portion of this work (Aims 4 and 5), it became evident that this was not necessarily the case. Though it appears that the dynamic mechanical environment surrounding the AVICs is necessary to elicit dysfunction, it was the addition of TGF-β1 that synergistically resulted in altered cell function and tissue architecture.

It appears obvious that the phenotype of the resident AVIC population is a direct indication of the state of the tissue and may be a forewarning for future tissue dysfunction during instance when the myofibroblast phenotype is not transient but persistent for long periods of time. Though these studies were short in duration, our results indicate that circumferential stretch alone does not significantly alter the AVIC phenotype or collagen biosynthesis. Hence, the primary question that arises at the conclusion of this work is “which environmental factor(s), whether physiologic stresses imposed on the tissue or circulating biomolecules/cells, effectively alter the AVIC phenotype such that it becomes an activated myofibroblast?” In short, we speculate that the future burden of proof appears to be laid upon the circulating factors.

8.1.4 Future directions

To begin to address the question of the precise mechanisms that lead to elevated cytokine levels within the AV, future studies should focus on potential initiators of AV sclerosis that result from circulating factors in the blood and their penetration via the AV endothelial cells. Primarily, it is believed that AV endothelial cell adhesion molecules (CAM) expression initiates leukocyte adhesion, which in turn results in leukocyte infiltration, potentially initiating a cascade of events resulting in AV sclerosis. Although the role of CAMs in macrophage adhesion and infiltration in atherosclerosis in blood vessels is well established, the role of CAMs in contributing to sclerosis of the AV is less clear. To date, the precise mechanisms which regulate CAM expression in AV endothelial cells are unknown. From studies in the vasculature, it is clear that both biochemical triggers and biophysical conditions, such as altered shear flow, contribute to upregulation of cell adhesion molecules and macrophage infiltration in the vessel wall. Therefore, future work will likely investigate AV endothelial cell CAM expression and probe the possibility that this expression is a function of one or more of the following: aortic-side fluid mechanics; increased tissue deformation of the AV due to hypertension; and elevated lipid levels in the circulating blood.

Additionally, changes in AVICs over a lifetime is a largely unexplored area that could reveal a potential mechanism for degenerative aortic stenosis alternative to the inflammatory cell or lipid hypothesis described by Otto and others [61, 62]. We suspect that the AVICs do indeed change their function over the lifetime of the individual and dysfunction seen later in life may be do to senescence or loss of a key cellular attribute necessary for proper synthesis or degradation. Or, another possibility is the AVICs inability to effectively modulate its phenotype with increasing age. Under normal circumstances, the AVIC may become 'activated' when need be and then revert back to a quiescent phenotype; however, if this ability to revert is lost and the AVIC becomes a constitutive myofibroblast, this could potential have a cascade-like effect for the whole tissue. The question of AVIC proliferation during one's lifetime has yet to be addressed as well, and clarifying how the AVIC adapts to its environment during different periods adulthood is an area that would certainly aid in distilling down to the mechanism(s) responsible for degenerative valve disease.

Ultimately, we would like to connect the organ-scale simulations to evaluate our understanding of AVIC mechano-transduction. To this end, it would be beneficial to develop an AVIC phenotypic/biosynthetic model linked to organ-level deformations. In the AVL, physiologic loading during diastole predominately results in ECM compaction as the collagen fibers become uncrimped and taut. From this ECM compaction, significant AVIC deformations have been observed with increasing pressures. Even a phenomenological model could thus simulate the AVIC population with mechanical inputs (quantified by the deformation of the AVIC nuclei) and cytokine levels. It could then be possible to predict the phenotypic and biosynthetic response of AVICs after repeated loading cycles. Moreover, if this predictive model could be realized, it could be further used to address levels of hypertension, hyperlipidemia, and potential other sources that may serve to alter AVIC function.

BIBLOGRAPHY

1. Otto, C.M., *Clinical practice. Evaluation and management of chronic mitral regurgitation.* N Engl J Med, 2001. **345**(10): p. 740-6.

2. Reul, H. and N. Talukder, *Heart valve mechanics*, in *The Heart*. 1989, McGraw Hill.

3. Kilner, P.J., et al., *Helical and retrograde secondary flow patterns in the aortic arch studied by three-directional magnetic resonance velocity mapping.* Circulation, 1993. **88**(5 Pt 1): p. 2235-47.

4. Ormiston, J.A., et al., *Size and motion of the mitral valve annulus in man. I. A two-dimensional echocardiographic method and findings in normal subjects.* Circulation, 1981. **64**(1): p. 113-20.

5. Bellhouse, B.J. and F.H. Bellhouse, *Fluid mechanics of the mitral valve.* Nature, 1969. **224**: p. 615-618.

6. Otsuji, Y., et al., *Insights from three-dimensional echocardiography into the mechanism of functional mitral regurgitation: direct in vivo demonstration of altered leaflet tethering geometry.* Circulation, 1997. **96**(6): p. 1999-2008.

7. Schwammenthal, E., et al., *Dynamics of mitral regurgitant flow and orifice area. Physiologic application of the proximal flow convergence method: clinical data and experimental testing.* Circulation, 1994. **90**(1): p. 307-22.

8. Ming, L. and H.K. Zhen, *Study of the closing mechanism of natural heart valves.* Applied Mathematics and Mechanics, 1986. **17**(10).

9. Hartiala, J.J., et al., *Velocity-encoded cine MRI in the evaluation of left ventricular diastolic function: measurement of mitral valve and pulmonary vein flow velocities and flow volume across the mitral valve.* Am Heart J, 1993. **125**(4): p. 1054-66.

10. Arts, T., et al., *Stresses in the closed mitral valve: a model study.* J Biomech, 1983. **16**(7): p. 539-47.

11. Kunzelman, K.S., M.S. Reimink, and R.P. Cochran, *Flexible versus rigid ring annuloplasty for mitral valve annular dilatation: a finite element model.* J Heart Valve Dis, 1998. **7**(1): p. 108-16.

12. Kunzelman, K.S., et al., *Finite element analysis of the mitral valve.* J Heart Valve Dis, 1993. **2**(3): p. 326-40.

13. Kunzelman, K.S., et al., *Anatomic basis for mitral valve modelling.* J Heart Valve Dis, 1994. **3**(5): p. 491-6.

14. Thubrikar, M., et al., *Analysis of the design and dynamics of aortic bioprostheses in vivo.* J Thorac Cardiovasc Surg, 1982. **84**(2): p. 282-90.

15. Thubrikar, M.J., et al., *Stress analysis of porcine bioprosthetic heart valves in vivo.* J Biomed Mater Res, 1982. **16**(6): p. 811-26.

16. Thubrikar, M., et al., *Interpretation of aortic root angiography in dogs and in humans.* Cardiovasc Res, 1982. **16**(1): p. 16-21.

17. Thubrikar, M.J., J. Aouad, and S.P. Nolan, *Comparison of the in vivo and in vitro mechanical properties of aortic valve leaflets.* J Thorac Cardiovasc Surg, 1986. **92**(1): p. 29-36.

18. Smith, D.B., et al., *Surface geometric analysis of anatomic structures using biquintic finite element interpolation.* Ann Biomed Eng, 2000. **28**(6): p. 598-611.

19. Billiar, K.L. and M.S. Sacks, *Biaxial mechanical properties of the natural and glutaraldehyde treated aortic valve cusp--Part I: Experimental results.* Journal of Biomechanical Engineering, 2000a. **122**(1): p. 23-30.

20. Sacks, M.S., D.B. Smith, and E.D. Hiester, *The aortic valve microstructure: effects of transvalvular pressure.* Journal of Biomedical Materials Research, 1998. **41**(1): p. 131-41.

21. Vesely, I., *The role of elastin in aortic valve mechanics.* Journal of Biomechanics, 1998. **31**(2): p. 115-123.

22. Gerosa, G., et al., *Aortic valve replacement with pulmonary homografts. Early experience.* J Thorac Cardiovasc Surg, 1994. **107**(2): p. 424-36; discussion 436-7.

23. Guyton, A.C., Hall, J.E., *Textbook of Medical Physiology*. 9 ed. 1996: W.B. Saunders Company.

24. Christie, G.W. and B.G. Barratt-Boyes, *Mechanical properties of porcine pulmonary valve leaflets: how do they differ from aortic leaflets?* Ann Thorac Surg, 1995. **60**(2 Suppl): p. S195-9.

25. Christie, G.W. and B.G. Barratt-Boyes, *Biaxial mechanical properties of explanted aortic allograft leaflets.* Ann Thorac Surg, 1995. **60**(2 Suppl): p. S160-4.

26. Christie, G.W. and B.G. Barratt-Boyes, *Age-dependent changes in the radial stretch of human aortic valve leaflets determined by biaxial testing.* Ann Thorac Surg, 1995. **60**(2 Suppl): p. S156-8; discussion S159.

27. Sacks, M.S., D.B. Smith, and E.D. Hiester, *A small angle light scattering device for planar connective tissue microstructural analysis.* Ann Biomed Eng, 1997. **25**(4): p. 678-89.

28. Gloeckner, D.C., K.L. Billiar, and M.S. Sacks, *Effects of mechanical fatigue on the bending properties of the porcine bioprosthetic heart valve.* Asaio J, 1999. **45**(1): p. 59-63.

29. Merryman, W.D., et al., *The effects of cellular contraction on aortic valve leaflet flexural stiffness.* J Biomech, 2006. **39**(1): p. 88-96.

30. Billiar, K.L. and M.S. Sacks, *Biaxial mechanical properties of the native and glutaraldehyde-treated aortic valve cusp: Part II--A structural constitutive model.* Journal of Biomechanical Engineering, 2000b. **122**(4): p. 327-35.

31. Sacks, M.S., *Incorporation of experimentally-derived fiber orientation into a structural constitutive model for planar collagenous tissues.* J Biomech Eng, 2003. **125**(2): p. 280-7.

32. Engelmayr, G.C., Jr., et al., *The independent role of cyclic flexure in the early in vitro development of an engineered heart valve tissue.* Biomaterials, 2005. **26**(2): p. 175-87.

33. Engelmayr, G.C., et al., *A novel bioreactor for the dynamic flexural stimulation of tissue engineered heart valve biomaterials.* Biomaterials, 2003. **24**(14): p. 2523-32.

34. Sacks, M.S. and C.J. Chuong, *Orthotropic mechanical properties of chemically treated bovine pericardium.* Ann Biomed Eng, 1998. **26**(5): p. 892-902.

35. Sacks, M.S., *Biaxial mechanical evaluation of planar biological materials.* Journal of Elasticity, 2000. **61**: p. 199-246.

36. Sacks, M.S., *A method for planar biaxial mechanical testing that includes in-plane shear.* J Biomech Eng, 1999. **121**(5): p. 551-5.

37. Sun, W., M.J. Scott, and M.S. Sacks, *Effects of boundary conditions on the planar biaxial mechanical propreties of soft tissues.* ASME Journal of Biomechanical Engineering, in-press.

38. Grashow, J.S., et al., *Planar biaxial creep and stress relaxation of the mitral valve anterior leaflet.* Ann Biomed Eng, 2006a. **34**(10): p. 1509-18.

39. Grashow, J.S., A.P. Yoganathan, and M.S. Sacks, *Biaxial stress-stretch behavior of the mitral valve anterior leaflet at physiologic strain rates.* Ann Biomed Eng, 2006b. **34**(2): p. 315-25.

40. Sacks, M.S. and F.J. Schoen, *Collagen fiber disruption occurs independent of calcification in clinically explanted bioprosthetic heart valves.* J Biomed Mater Res, 2002. **62**(3): p. 359-71.

41. Lee, J.M., D.W. Courtman, and D.R. Boughner, *The glutaraldehyde-stablized porcine aortic valve xenograft. I. Tensile viscoelastic properties of the fresh leaflet material.* Journal of Biomedical Materials Research, 1984. **18**: p. 61-77.

42. Lee, J.M., D.R. Boughner, and D.W. Courtman, *The glutaraldehyde-stabilized porcine aortic valve xenograft. II. Effect of fixation with or without pressure on the tensile viscoelastic properties of the leaflet material.* Journal of Biomedical Materials Research, 1984. **18**: p. 79-98.

43. Vesely, I. and R. Noseworthy, *Micromechanics of the fibrosa and the ventricularis in aortic valve leaflets.* Journal of Biomechanics, 1992. **25**(1): p. 101-113.

44. Broom, N. and G.W. Christie, *The Structure/Function Relationship of Fresh and Gluteraldehyde-Fixed Aortic Valve Leaflets*, in *Cardiac Bioprosthesis*, L.H. Cohn and V. Gallucci, Editors. 1982, Yorke Medical Books: New York. p. 477-491.

45. Christie, G.W., *Anatomy of aortic heart valve leaflets: the influence of glutaraldehyde fixation on function.* European Journal of Cardio-Thoracic Surgery, 1992. **6**: p. S25-S33.

46. Mayne, A.S., et al., *An assessment of the mechanical properties of leaflets from four second- generation porcine bioprostheses with biaxial testing techniques [see comments].* J Thorac Cardiovasc Surg, 1989. **98**(2): p. 170-80.

47. Christie, G.W. and B.G. Barratt-Boyes, *Age-Dependent Changes in the Radial Stretch of Human Aortic Valve Leaflets Determined by Biaxial Stretching.* Annals of Thoracic Surgery, 1995. **60**: p. S156-159.

48. Brossollet, L.J. and R.P. Vito, *An alternate formulation of blood vessel mechanics and the meaning of the in vivo property.* J Biomech, 1995. **28**(6): p. 679-87.

49. Stella, J. and M.S. Sacks, *On the biaxial mechanical properties of the layers of the aortic valve leaflet.* Journal of Biomechanial Engineering, in-press.

50. Schoen, F.J., *Pathology of heart valve substitution with mechanical and tissue prostheses*, in *Cardiovascular Pathology*, M.D. Silver, A.I. Gotlieb, and F.J. Schoen, Editors. 2001, Livingstone: New York.

51. Rabkin-Aikawa, E., et al., *Clinical pulmonary autograft valves: pathologic evidence of adaptive remodeling in the aortic site.* J Thorac Cardiovasc Surg, 2004. **128**(4): p. 552-61.

52. Thom, T., et al., *Heart disease and stroke statistics--2006 update: a report from the American Heart Association Statistics Committee and Stroke Statistics Subcommittee.* Circulation, 2006. **113**(6): p. e85-151.

53. Otto, C.M., *Valvular Heart Disease*. 2nd ed. 2004, Philadelphia: Saunders.

54. Stewart, B.F., et al., *Clinical factors associated with calcific aortic valve disease. Cardiovascular Health Study.* J Am Coll Cardiol, 1997. **29**(3): p. 630-4.

55. Cosmi, J.E., et al., *The risk of the development of aortic stenosis in patients with "benign" aortic valve thickening.* Arch Intern Med, 2002. **162**(20): p. 2345-7.

56. Faggiano, P., et al., *Progression of aortic valve sclerosis to aortic stenosis.* Am J Cardiol, 2003. **91**(1): p. 99-101.

57. Otto, C.M., et al., *Association of aortic-valve sclerosis with cardiovascular mortality and morbidity in the elderly.* N Engl J Med, 1999. **341**(3): p. 142-7.

58. Olsen, M.H., et al., *Aortic valve sclerosis relates to cardiovascular events in patients with hypertension (a LIFE substudy).* Am J Cardiol, 2005. **95**(1): p. 132-6.

59. Agmon, Y., et al., *Aortic valve sclerosis and aortic atherosclerosis: different manifestations of the same disease? Insights from a population-based study.* J Am Coll Cardiol, 2001. **38**(3): p. 827-34.

60. Mohler, E.R., et al., *Development and progression of aortic valve stenosis: atherosclerosis risk factors--a causal relationship? A clinical morphologic study.* Clin Cardiol, 1991. **14**(12): p. 995-9.

61. O'Brien, K.D., *Pathogenesis of calcific aortic valve disease: a disease process comes of age (and a good deal more).* Arterioscler Thromb Vasc Biol, 2006. **26**(8): p. 1721-8.

62. Otto, C.M., et al., *Characterization of the early lesion of 'degenerative' valvular aortic stenosis. Histological and immunohistochemical studies.* Circulation, 1994. **90**(2): p. 844-53.

63. Olsson, M., M. Rosenqvist, and J. Nilsson, *Expression of HLA-DR antigen and smooth muscle cell differentiation markers by valvular fibroblasts in degenerative aortic stenosis.* J Am Coll Cardiol, 1994. **24**(7): p. 1664-71.

64. Olsson, M., et al., *Accumulation of T lymphocytes and expression of interleukin-2 receptors in nonrheumatic stenotic aortic valves.* J Am Coll Cardiol, 1994. **23**(5): p. 1162-70.

65. Walton, K.W., N. Williamson, and A.G. Johnson, *The pathogenesis of atherosclerosis of the mitral and aortic valves.* J Pathol, 1970. **101**(3): p. 205-20.

66. O'Brien, K.D., et al., *Apolipoproteins B, (a), and E accumulate in the morphologically early lesion of 'degenerative' valvular aortic stenosis.* Arterioscler Thromb Vasc Biol, 1996. **16**(4): p. 523-32.

67. O'Brien, K.D., et al., *Association of angiotensin-converting enzyme with low-density lipoprotein in aortic valvular lesions and in human plasma.* Circulation, 2002. **106**(17): p. 2224-30.

68. Butcher, J.T., et al., *Unique morphology and focal adhesion development of valvular endothelial cells in static and fluid flow environments.* Arterioscler Thromb Vasc Biol, 2004. **24**(8): p. 1429-34.

69. Butcher, J.T. and R.M. Nerem, *Porcine aortic valve interstitial cells in three-dimensional culture: comparison of phenotype with aortic smooth muscle cells.* J Heart Valve Dis, 2004. **13**(3): p. 478-85; discussion 485-6.

70. Deck, J.D., *Endothelial cell orientation on aortic valve leaflets.* Cardiovasc Res, 1986. **20**(10): p. 760-7.

71. Leask, R.L., N. Jain, and J. Butany, *Endothelium and valvular diseases of the heart.* Microsc Res Tech, 2003. **60**(2): p. 129-37.

72. Marron, K., et al., *Innervation of human atrioventricular and arterial valves.* Circulation, 1996. **94**(3): p. 368-75.

73. Davies, P.F., *Mechanisms involved in endothelial responses to hemodynamic forces.* Atherosclerosis, 1997. **131 Suppl**: p. S15-7.

74. Davies, P.F. and S.C. Tripathi, *Mechanical stress mechanisms and the cell. An endothelial paradigm.* Circ Res, 1993. **72**(2): p. 239-45.

75. Filip, D.A., A. Radu, and M. Simionescu, *Interstitial cells of the heart valve possess characteristics similar to smooth muscle cells.* Circulation Research, 1986. **59**(3): p. 310-320.

76. Messier, R.H., Jr., et al., *Dual structural and functional phenotypes of the porcine aortic valve interstitial population: characteristics of the leaflet myofibroblast.* Journal of Surgical Research, 1994. **57**(1): p. 1-21.

77. Taylor, P.M., et al., *The cardiac valve interstitial cell.* International Journal of Biochemistry and Cell Biology, 2003. **35**(2): p. 113-8.

78. Mulholland, D.L. and A.I. Gotlieb, *Cell biology of valvular interstitial cells.* Canadian Journal of Cardiology, 1996. **12**(3): p. 231-6.

79. Bairati, A. and S. DeBiasi, *Presence of a smooth muscle system in aortic valve leaflets.* Anatomy and Embryology, 1981. **161**(3): p. 329-40.

80. Rabkin, E., et al., *Evolution of cell phenotype and extracellular matrix in tissue-engineered heart valves during in-vitro maturation and in-vivo remodeling.* Journal of Heart Valve Disease, 2002. **11**(3): p. 308-14; discussion 314.

81. Rabkin-Aikawa, E., et al., *Dynamic and reversible changes of interstitial cell phenotype during remodeling of cardiac valves.* J Heart Valve Dis, 2004. **13**(5): p. 841-7.

82. Chester, A.H., et al. *Specific regional and direcrtional contractile response of aortic cusp tissue-Relevance to valve function.* in *Second Biennial Meeting of the Society for Heart Valve Disease*. 2003. Paris.

83. Guyton, A.C., *Textbook of Medical Physiology*. 5th ed. 1976, Philadelphia: W.B. Saunders Company.

84. Huang, H.-Y.S., J. Liao, and M.S. Sacks, *Effects of transvalvular pressure on aortic valve interstitial cell nuclear aspect ratio.* Journal of Biomechanial Engineering, in-press.

85. Tomasek, J.J., et al., *Myofibroblasts and mechano-regulation of connective tissue remodelling.* Nat Rev Mol Cell Biol, 2002. **3**(5): p. 349-63.

86. Gabbiani, G., G.B. Ryan, and G. Majno, *Presence of modified fibroblasts in granulation tissue and their role in wound contracture.* Experientia, 1971. **27**: p. 549-550.

87. Serini, G. and G. Gabbiani, *Mechanisms of myofibroblast activity and phenotypic modulation.* Exp Cell Res, 1999. **250**(2): p. 273-83.

88. Darby, I., O. Skalli, and G. Gabbiani, *Alpha-smooth muscle actin is transiently expressed by myofibroblasts during experimental wound healing.* Lab Invest, 1990. **63**(1): p. 21-9.

89. Skalli, O., et al., *A monoclonal antibody against alpha-smooth muscle actin: a new probe for smooth muscle differentiation.* J Cell Biol, 1986. **103**(6 Pt 2): p. 2787-96.

90. Desmouliere, A., et al., *Transforming growth factor-beta 1 induces alpha-smooth muscle actin expression in granulation tissue myofibroblasts and in quiescent and growing cultured fibroblasts.* J Cell Biol, 1993. **122**(1): p. 103-11.

91. Grinnell, F., *Fibroblasts, myofibroblasts, and wound contraction.* J Cell Biol, 1994. **124**(4): p. 401-4.

92. Harris, A.K., D. Stopak, and P. Wild, *Fibroblast traction as a mechanism for collagen morphogenesis.* Nature, 1981. **290**(5803): p. 249-51.

93. Hinz, B., et al., *Mechanical tension controls granulation tissue contractile activity and myofibroblast differentiation.* Am J Pathol, 2001. **159**(3): p. 1009-20.

94. Filip, D.A., A. Radu, and M. Simionescu, *Interstitial cells of the heart valves possess characteristics similar to smooth muscle cells.* Circ Res, 1986. **59**(3): p. 310-20.

95. Taylor, P.M., et al., *The cardiac valve interstitial cell.* Int J Biochem Cell Biol, 2003. **35**(2): p. 113-8.

96. McDonald, P.C., et al., *The challenge of defining normality for human mitral and aortic valves: geometrical and compositional analysis.* Cardiovascular Pathology, 2002. **11**(4): p. 193-209.

97. Schoen, F., *Aortic valve structure-function correlations: Role of elastic fibers no longer a stretch of the imagination.* Journal of Heart Valve Disease, 1997. **6**: p. 1-6.

98. Mori, Y., R.I. Bashey, and A. Angrist, *The in vitro biosynthesis of collagen in bovine heart valves.* Biochemical Medicine, 1967. **1**: p. 295.

99. Henney, A.M., D.J. Parker, and M.J. Davies, *Collagen biosynthesis in normal and abnormal human heart valves.* Cardiovasc Res, 1982. **16**(11): p. 624-30.

100. Kershaw, J.D., et al., *Specific regional and directional contractile responses of aortic cusp tissue.* J Heart Valve Dis, 2004. **13**(5): p. 798-803.

101. Hafizi, S., et al., *Mitogenic and secretory responses of human valve interstitial cells to vasoactive agents.* Journal of Heart Valve Disease, 2000. **9**(3): p. 454-8.

102. Weston, M.W. and A.P. Yoganathan, *Biosynthetic activity in heart valve leaflets in response to in vitro flow environments.* Annals of Biomedical Engineering, 2001. **29**(9): p. 752-63.

103. Roy, A., N.J. Brand, and M.H. Yacoub, *Molecular characterization of interstitial cells isolated from human heart valves.* Journal of Heart Valve Disease, 2000. **9**(3): p. 459-64; discussion 464-5.

104. Guilak, F., et al., *Viscoelastic properties of intervertebral disc cells. Identification of two biomechanically distinct cell populations.PG - 2475-83.* Spine, 1999. **24**(23).

105. Schmid-Schonbein, G.W., et al., *Passive mechanical properties of human leukocytes.* Biophys J, 1981. **36**(1): p. 243-56.

106. Sato, M., et al., *Application of the micropipette technique to the measurement of cultured porcine aortic endothelial cell viscoelastic properties.* J Biomech Eng, 1990. **112**(3): p. 263-8.

107. Dong, C., R. Skalak, and K.L. Sung, *Cytoplasmic rheology of passive neutrophils.* Biorheology, 1991. **28**(6): p. 557-67.

108. Hochmuth, R.M., *Micropipette aspiration of living cells.* J Biomech, 2000. **33**(1): p. 15-22.

109. Evans, E. and A. Yeung, *Apparent viscosity and cortical tension of blood granulocytes determined by micropipet aspiration.* Biophys J, 1989. **56**(1): p. 151-60.

110. Trickey, W.R., T.P. Vail, and F. Guilak, *The role of the cytoskeleton in the viscoelastic properties of human articular chondrocytes.* J Orthop Res, 2004. **22**(1): p. 131-9.

111. Evans, E.A. and R.M. Hochmuth, *A solid-liquid composite model of the red cell membrane.* J Membr Biol, 1977. **30**(4): p. 351-62.

112. Evans, E.A. and R.M. Hochmuth, *Membrane viscoplastic flow.* Biophys J, 1976. **16**(1): p. 13-26.

113. Evans, E.A. and R.M. Hochmuth, *Membrane viscoelasticity.* Biophys J, 1976. **16**(1): p. 1-11.

114. Hochmuth, R.M., P.R. Worthy, and E.A. Evans, *Red cell extensional recovery and the determination of membrane viscosity.* Biophys J, 1979. **26**(1): p. 101-14.

115. Hochmuth, R.M., E.A. Evans, and D.F. Colvard, *Viscosity of human red cell membrane in plastic flow.* Microvasc Res, 1976. **11**(2): p. 155-9.

116. Sato, M., M.J. Levesque, and R.M. Nerem, *Micropipette aspiration of cultured bovine aortic endothelial cells exposed to shear stress.* Arteriosclerosis, 1987. **7**(3): p. 276-86.

117. Sato, M., M.J. Levesque, and R.M. Nerem, *An application of the micropipette technique to the measurement of the mechanical properties of cultured bovine aortic endothelial cells.* J Biomech Eng, 1987. **109**(1): p. 27-34.

118. Levesque, M.J., et al., *Correlation of endothelial cell shape and wall shear stress in a stenosed dog aorta.* Arteriosclerosis, 1986. **6**(2): p. 220-9.

119. Theret, D.P., et al., *The application of a homogeneous half-space model in the analysis of endothelial cell micropipette measurements.* J Biomech Eng, 1988. **110**(3): p. 190-9.

120. Love, A.E.H., *The stress produced in a semi-infinite solid by pressureon part of the boundary.* Philosophical Transactions of the Royal Society of London, Series A, 1929. **228**: p. 377-420.

121. Collins, W.D., *On the solution of some axisymmetricboundary value problems by means of integral equations VIII. Potential problems for a circular annulus.* Proc Edinburgh Math Soc, 1963. **13**: p. 235-46.

122. Tasab, M., M.R. Batten, and N.J. Bulleid, *Hsp47: a molecular chaperone that interacts with and stabilizes correctly-folded procollagen.* Embo J, 2000. **19**(10): p. 2204-11.

123. Rocnik, E.F., et al., *Functional linkage between the endoplasmic reticulum protein Hsp47 and procollagen expression in human vascular smooth muscle cells.* J Biol Chem, 2002. **277**(41): p. 38571-8.

124. Guilak, F. and V.C. Mow, *The mechanical environment of the chondrocyte: a biphasic finite element model of cell-matrix interactions in articular cartilage.PG - 1663-73.* J Biomech, 2000. **33**(12).

125. Iyengar, A.K.S., et al., *Dynamic in vitro quantification of bioprosthetic heart valve leaflet motion using structured light projection.* Ann Biomed Eng, 2001. **29**(11): p. 963-73.

126. Berry, D.P., et al., *Human wound contraction: collagen organization, fibroblasts, and myofibroblasts.* Plast Reconstr Surg, 1998. **102**(1): p. 124-31; discussion 132-4.

127. Ehrlich, H.P., G.M. Allison, and M. Leggett, *The myofibroblast, cadherin, alpha smooth muscle actin and the collagen effect.* Cell Biochem Funct, 2004.

128. Li, S., et al., *Vascular smooth muscle cells orchestrate the assembly of type I collagen via alpha2beta1 integrin, RhoA, and fibronectin polymerization.* Am J Pathol, 2003. **163**(3): p. 1045-56.

129. Yperman, J., et al., *Molecular and functional characterization of ovine cardiac valve-derived interstitial cells in primary isolates and cultures.* Tissue Eng, 2004. **10**(9-10): p. 1368-75.

130. Sauk, J.J., N. Nikitakis, and H. Siavash, *Hsp47 a novel collagen binding serpin chaperone, autoantigen and therapeutic target.* Front Biosci, 2005. **10**: p. 107-18.

131. Sacks, M.S., et al., *Surface strains in the anterior leaflet of the functioning mitral valve.* Annals of Biomedical Engineering, 2002. **30**(10): p. 1281-90.

132. Merryman, W.D., et al., *Correlation between heart valve interstitial cell stiffness and transvalvular pressure: implications for collagen biosynthesis.* Am J Physiol Heart Circ Physiol, 2006. **290**(1): p. H224-31.

133. Merryman, W.D., et al., *Differences in tissue remodeling potential of the aortic and pulmonary heart valve interstitial cells.* Tissue Engineering, in-press.

134. Merryman, W.D., et al., *Synergistic effects of cyclic tension and transforming growth factor beta1 on the aortic valve myofibroblast.* Cardiovascular Pathology, in-press.

135. Wineman, A.S. and K.R. Rajagopal, *Mechanical Response of Polymers* 2000, Cambridge, 2000: Cambridge University Press. 328.

136. Press, W.H., et al., *Numerical Receipes in C.* 1988, Cambridge: Cambridge University Press. 735.

137. Thubrikar, M.J., J.L. Heckman, and S.P. Nolan, *High speed cine-radiographic study of aortic valve leaflet motion.* J Heart Valve Dis, 1993. **2**(6): p. 653-61.

138. Huang, H.-Y.S., J. Liao, and M.S. Sacks, *Effects of transvalvular pressure on aortic valve interstitial cell nuclear aspect ratio.* Annals of Biomedical Engineering, accepted.

139. Chester, A.H., M. Misfeld, and M.H. Yacoub, *Receptor-mediated contraction of aortic valve leaflets.* Journal of Heart Valve Disease, 2000. **9**(2): p. 250-4; discussion 254-5.

140. Taylor, P.M., S.P. Allen, and M.H. Yacoub, *Phenotypic and functional characterization of interstitial cells from human heart valves, pericardium and skin.* Journal of Heart Valve Disease, 2000. **9**(1): p. 150-8.

141. Schoen, F.J. and R.J. Levy, *Calcification of tissue heart valve substitutes: progress toward understanding and prevention.* Ann Thorac Surg, 2005. **79**(3): p. 1072-80.

142. Jian, B., et al., *Progression of aortic valve stenosis: TGF-beta1 is present in calcified aortic valve cusps and promotes aortic valve interstitial cell calcification via apoptosis.* Ann Thorac Surg, 2003. **75**(2): p. 457-65; discussion 465-6.

143. Jian, B., et al., *Serotonin mechanisms in heart valve disease I: serotonin-induced up-regulation of transforming growth factor-beta1 via G-protein signal transduction in aortic valve interstitial cells.* Am J Pathol, 2002. **161**(6): p. 2111-21.

144. Walker, G.A., et al., *Valvular myofibroblast activation by transforming growth factor-beta: implications for pathological extracellular matrix remodeling in heart valve disease.* Circ Res, 2004. **95**(3): p. 253-60.

145. Taylor, P.M., et al., *Human cardiac valve interstitial cells in collagen sponge: a biological three-dimensional matrix for tissue engineering.* Journal of Heart Valve Disease, 2002. **11**(3): p. 298-306; discussion 306-7.

146. Merryman, W.D., et al., *Defining biomechanical endpoints for tissue engineered heart valve leaflets from native leaflet properties.* Progress in Pediatric Cardiology, 2006. **21**(2): p. 153-60.

147. Della Rocca, F., et al., *Cell composition of the human pulmonary valve: a comparative study with the aortic valve--the VESALIO Project. Vitalitate Exornatum Succedaneum Aorticum labore Ingegnoso Obtinebitur.* Annals of Thoracic Surgery, 2000. **70**(5): p. 1594-600.

148. Mathur, A.B., et al., *Endothelial, cardiac muscle and skeletal muscle exhibit different viscous and elastic properties as determined by atomic force microscopy.* J Biomech, 2001. **34**(12): p. 1545-53.

149. Costa, K.D. and F.C. Yin, *Analysis of indentation: implications for measuring mechanical properties with atomic force microscopy.* J Biomech Eng, 1999. **121**(5): p. 462-71.

150. Kasas, S., et al., *Superficial and deep changes of cellular mechanical properties following cytoskeleton disassembly.* Cell Motil Cytoskeleton, 2005. **62**(2): p. 124-32.

151. Bell, E., B. Ivarsson, and C. Merrill, *Production of a tissue-like structure by contraction of collagen lattices by human fibroblasts of different proliferative potential in vitro.* Proc Natl Acad Sci U S A, 1979. **76**(3): p. 1274-8.

152. Cushing, M.C., J.T. Liao, and K.S. Anseth, *Activation of valvular interstitial cells is mediated by transforming growth factor-beta1 interactions with matrix molecules.* Matrix Biol, 2005. **24**(6): p. 428-37.

153. Na, S., et al., *On atomic force microscopy and the constitutive behavior of living cells.* Biomech Model Mechanobiol, 2004. **3**(2): p. 75-84.

154. Fu, P., et al., *Effects of basic fibroblast growth factor and transforming growth factor-beta on maturation of human pediatric aortic cell culture for tissue engineering of cardiovascular structures.* Asaio J, 2004. **50**(1): p. 9-14.

155. Peters, T., et al., *Wound-healing defect of CD18(-/-) mice due to a decrease in TGF-beta(1) and myofibroblast differentiation.* Embo J, 2005.

156. Edwards, J.E., *Calcific aortic stenosis: pathologic features.* Mayo Clin Proc, 1961. **36**: p. 444-51.

157. Perry, T.E., et al., *Peripheral blood as a cell source for tissue engineering heart valves.* Surgical Forum, 2001. **LII**: p. 99-101.

158. Perry, T.E., et al., *Thoracic Surgery Directors Association Award. Bone marrow as a cell source for tissue engineering heart valves.* Annals of Thoracic Surgery, 2003. **75**(3): p. 761-7; discussion 767.

159. Kadner, A., et al., *A new source for cardiovascular tissue engineering: human bone marrow stromal cells.* Eur J Cardiothorac Surg, 2002. **21**(6): p. 1055-60.

160. Sales, V.L., et al., *Transforming growth factor-beta1 modulates extracellular matrix production, proliferation, and apoptosis of endothelial progenitor cells in tissue-engineering scaffolds.* Circulation, 2006. **114**(1 Suppl): p. I193-9.

161. Sacks, M.S. and D.B. Smith, *Effects of accelerated testing on porcine bioprosthetic heart valve fiber architecture.* Biomaterials, 1998. **19**(11-12): p. 1027-1036.

162. Scott, M. and I. Vesely, *Aortic valve cusp microstructure: The role of elastin.* Annals of Thoracic Surgery, 1995. **60**: p. S391-S394.

163. Sugimoto, H., K. Shimada, and M.S. Sacks, *Dynamic Geometry of the native aortic heart valve leaflet.* Journal of Biomechanical Engineering, accepted.

164. Mirnajafi, A., et al., *The effects of collagen fiber orientation on the flexural properties of pericardial heterograft biomaterials.* Biomaterials, 2005. **26**(7): p. 795-804.

165. Xing, Y., et al., *Effects of constant static pressure on the biological properties of porcine aortic valve leaflets.* Annals of Biomedical Engineering, 2004. **32**(4): p. 555-562.

166. Shinoka, T., *Tissue engineered heart valves: autologous cell seeding on biodegradable polymer scaffold.* Artificial Organs, 2002. **26**(5): p. 402-6.

167. Maish, M.S., et al., *Tricuspid valve biopsy: A potential source of cardiac myofibroblast cells for tissue-engineered cardiac valves.* Journal of Heart Valve Disease, 2003. **12**: p. 264-269.

168. Rabkin, E., et al., *Activated interstitial myofibroblasts express catabolic enzymes and mediate matrix remodeling in myxomatous heart valves.* Circulation, 2001. **104**(21): p. 2525-32.

169. Robicsek, F., M.J. Thubrikar, and A.A. Fokin, *Cause of degenerative disease of the trileaflet aortic valve: review of subject and presentation of a new theory.* Ann Thorac Surg, 2002. **73**(4): p. 1346-54.

170. Sacks, M.S., *Small-angle light scattering methods for soft connective tissue structural analysis.* Encyclopedia of Biomaterials and Biomedical Engineering, 2004.

171. Gilbert, T.W., et al., *Fiber kinematics of small intestinal submucosa under biaxial and uniaxial stretch.* J Biomech Eng, 2006. **128**(6): p. 890-8.

172. Peters, T., et al., *Wound-healing defect of CD18(-/-) mice due to a decrease in TGF-beta1 and myofibroblast differentiation.* Embo J, 2005. **24**(19): p. 3400-10.

173. Aikawa, E., et al., *Human semilunar cardiac valve remodeling by activated cells from fetus to adult: implications for postnatal adaptation, pathology, and tissue engineering.* Circulation, 2006. **113**(10): p. 1344-52.

174. Engelmayr, G.C., Jr., et al., *Cyclic flexure and laminar flow synergistically accelerate mesenchymal stem cell-mediated engineered tissue formation: Implications for engineered heart valve tissues.* Biomaterials, 2006. **27**(36): p. 6083-95.

175. Ishida, Y., et al., *Type I Collagen in Hsp47-null Cells Is Aggregated in ER and Deficient in N-Propeptide Processing and Fibrillogenesis.* Mol Biol Cell, 2006.

176. Nagai, N., et al., *Embryonic lethality of molecular chaperone hsp47 knockout mice is associated with defects in collagen biosynthesis.* J Cell Biol, 2000. **150**(6): p. 1499-506.

177. Mohler, E.R., 3rd, et al., *Identification and characterization of calcifying valve cells from human and canine aortic valves.* J Heart Valve Dis, 1999. **8**(3): p. 254-60.

178. Adamczyk, M.M. and I. Vesely, *Characteristics of compressive strains in porcine aortic valves cusps.* J Heart Valve Dis, 2002. **11**(1): p. 75-83.

179. Allison, D.D., et al., *Cell viability mapping within long-term heart valve organ cultures.* J Heart Valve Dis, 2004. **13**(2): p. 290-6.